CMS-SUS-16-033

Search for supersymmetry in multijet events with missing transverse momentum in proton-proton collisions at 13 TeV

The CMS Collaboration*

Abstract

A search for supersymmetry is presented based on multijet events with large missing transverse momentum produced in proton-proton collisions at a center-of-mass energy of $\sqrt{s} = 13\,\text{TeV}$. The data, corresponding to an integrated luminosity of $35.9\,\text{fb}^{-1}$, were collected with the CMS detector at the CERN LHC in 2016. The analysis utilizes four-dimensional exclusive search regions defined in terms of the number of jets, the number of tagged bottom quark jets, the scalar sum of jet transverse momenta, and the magnitude of the vector sum of jet transverse momenta. No evidence for a significant excess of events is observed relative to the expectation from the standard model. Limits on the cross sections for the pair production of gluinos and squarks are derived in the context of simplified models. Assuming the lightest supersymmetric particle to be a weakly interacting neutralino, 95% confidence level lower limits on the gluino mass as large as 1800 to 1960 GeV are derived, and on the squark mass as large as 960 to 1390 GeV, depending on the production and decay scenario.

*See Appendix C for the list of collaboration members

arXiv:1704.07781v2 [hep-ex] 31 Aug 2017

1 Introduction

The standard model (SM) of particle physics describes many aspects of weak, electromagnetic, and strong interactions. However, it requires fine tuning [1] to explain the observed value of the Higgs boson mass [2], and it does not provide an explanation for dark matter. Supersymmetry (SUSY) [3–10], a widely studied extension of the SM, potentially solves these problems through the introduction of a new particle, called a superpartner, for each SM particle, with a spin that differs from that of its SM counterpart by a half unit. Additional Higgs bosons and their superpartners are also introduced. The superpartners of quarks and gluons are squarks $\widetilde{q}$ and gluinos $\widetilde{g}$, respectively, while neutralinos $\widetilde{\chi}^0$ and charginos $\widetilde{\chi}^\pm$ are mixtures of the superpartners of the Higgs and electroweak gauge bosons. Provided that the masses of gluinos, top squarks, and bottom squarks are no heavier than a few TeV, SUSY can resolve the fine-tuning problem [1, 11–13]. Furthermore, in R-parity [14] conserving SUSY models, the lightest SUSY particle (LSP) is stable and might interact only weakly, thus representing a dark matter candidate.

In this paper, we present a search for squarks and gluinos produced in proton-proton (pp) collisions at $\sqrt{s} = 13$ TeV. Squark and gluino production have large potential cross sections in pp collisions, thus motivating this search. The study is performed in the multijet final state, i.e., the visible elements consist solely of jets. Other $\sqrt{s} = 13$ TeV inclusive multijet SUSY searches are presented in Refs. [15–20]. We assume the conservation of R-parity, meaning that the squarks and gluinos are produced in pairs. The events are characterized by the presence of jets and undetected, or "missing," transverse momentum, where the missing transverse momentum arises from the weakly interacting and unobserved LSPs. The data, corresponding to an integrated luminosity of 35.9 fb^{-1}, were collected in 2016 with the CMS detector at the CERN LHC. The analysis is performed in four-dimensional exclusive regions in the number of jets N_{jet}, the number of tagged bottom quark jets $N_{\text{b-jet}}$, the scalar sum H_T of the transverse momenta p_T of jets, and the magnitude H_T^{miss} of the vector p_T sum of jets. The number of observed events in each region is compared with the expected number of SM events to search for excesses in the data.

The study is an extension of that presented in Ref. [17], using improved analysis techniques and around 16 times more data. Relative to Ref. [17], the following principal modifications have been made. Firstly, the search intervals in N_{jet} and H_T are given by $N_{\text{jet}} \geq 2$ and $H_T > 300$ GeV, compared with $N_{\text{jet}} \geq 4$ and $H_T > 500$ GeV in Ref. [17]. Inclusion of events with $N_{\text{jet}} = 2$ and 3 increases the sensitivity to squark pair production. The lower threshold in H_T provides better sensitivity to scenarios with small mass differences between the LSP and the squark or gluino. Secondly, the rebalance-and-smear technique [21, 22] is introduced as a complementary means to evaluate the quantum chromodynamics (QCD) background, namely the background from SM events with multijet final states produced exclusively through the strong interaction. Thirdly, the search interval in H_T^{miss} is given by $H_T^{\text{miss}} > 300$ GeV, rather than the previous $H_T^{\text{miss}} > 200$ GeV, in order to reserve the QCD-dominated $250 < H_T^{\text{miss}} < 300$ GeV region for a QCD background control sample in data. A final principal change is that finer segmentation than in Ref. [17] is used to define exclusive intervals in H_T and H_T^{miss}, to profit from the increased sensitivity afforded by the larger data sample.

Gluino and squark pair production are studied in the context of simplified models [23–26]. For all models considered, the lightest neutralino $\widetilde{\chi}_1^0$ is the LSP. For gluino pair production, the T1tttt, T1bbbb, T1qqqq, T1tbtb, and T5qqqqVV [27] simplified models are considered, defined as follows. In the T1tttt scenario [Fig. 1 (upper left)], each gluino decays to a top quark-antiquark ($t\bar{t}$) pair and the $\widetilde{\chi}_1^0$. The T1bbbb and T1qqqq scenarios are the same as the T1tttt
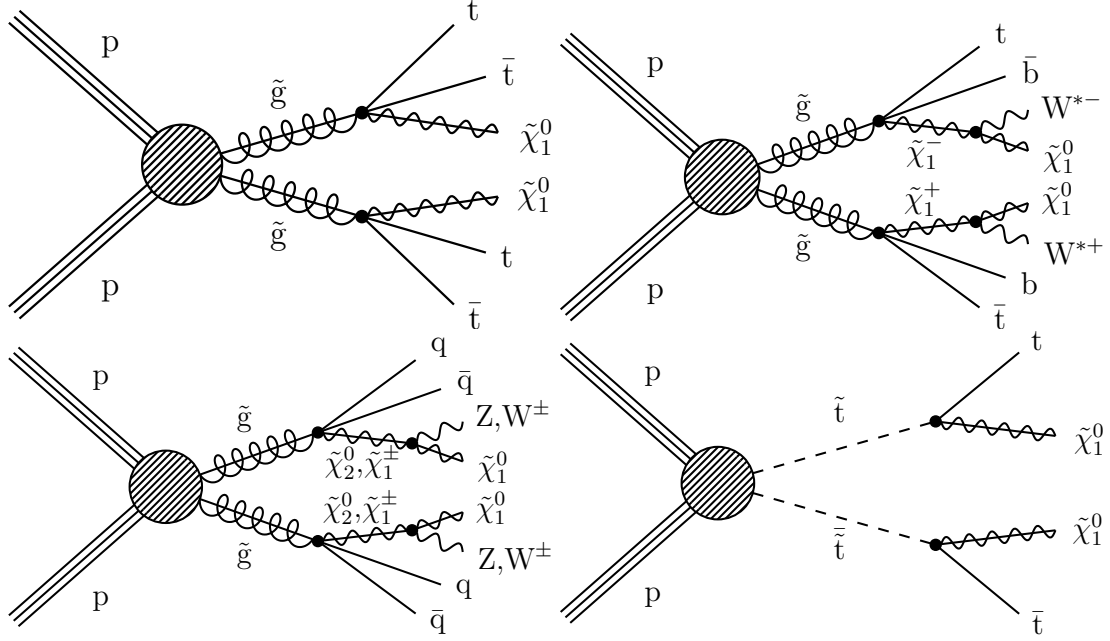
Figure 1: Example Feynman diagrams for the simplified model signal scenarios considered in this study: the (upper left) T1tttt, (upper right) T1tbtb, (lower left) T5qqqqVV, and (lower right) T2tt scenarios. In the T5qqqqVV model, the flavors of the quark q and antiquark $\overline{q}$ differ from each other if the gluino $\widetilde{g}$ decays as $\widetilde{g} \to q\overline{q}\widetilde{\chi}_1^{\pm}$, where $\widetilde{\chi}_1^{\pm}$ is the lightest chargino.

scenario except with the $t\overline{t}$ pairs replaced by bottom quark-antiquark ($b\overline{b}$) or light-flavored (u, d, s, c) quark-antiquark ($q\overline{q}$) pairs, respectively. In the T1tbtb scenario [Fig. 1 (upper right)], each gluino decays either as $\widetilde{g} \to \overline{t}b\widetilde{\chi}_1^{+}$ or as its charge conjugate, each with 50% probability, where $\widetilde{\chi}_1^{\pm}$ denotes the lightest chargino. The $\widetilde{\chi}_1^{\pm}$ is assumed to be nearly degenerate in mass with the $\widetilde{\chi}_1^0$, representing the expected situation should the $\widetilde{\chi}_1^{\pm}$ and $\widetilde{\chi}_1^0$ appear within the same SU(2) multiplet [26]. The chargino subsequently decays to the $\widetilde{\chi}_1^0$ and to an off-shell W boson (W^*). In the T5qqqqVV scenario [Fig. 1 (lower left)], each gluino decays to a light-flavored $q\overline{q}$ pair and either to the next-to-lightest neutralino $\widetilde{\chi}_2^0$ or to the $\widetilde{\chi}_1^{\pm}$. The probability for the decay to proceed via the $\widetilde{\chi}_2^0$, $\widetilde{\chi}_1^{+}$, or $\widetilde{\chi}_1^{-}$ is 1/3 for each possibility. The $\widetilde{\chi}_2^0$ ($\widetilde{\chi}_1^{\pm}$) subsequently decays to the $\widetilde{\chi}_1^0$ and to an on- or off-shell Z ($W^{\pm}$) boson.

We also consider models in which more than one of the decays $\widetilde{g} \to t\overline{t}\widetilde{\chi}_1^0$, $\widetilde{g} \to b\overline{b}\widetilde{\chi}_1^0$, and $\widetilde{g} \to \overline{t}b\widetilde{\chi}_1^{+}$ (or its charge conjugate) can occur [26]. Taken together, these scenarios reduce the model dependence of the assumptions for gluino decay to third-generation particles. Specifically, we consider the following three mixed scenarios, with the respective branching fractions in parentheses:

- $\widetilde{g} \to \overline{t}b\widetilde{\chi}_1^{+}$ (25%), $\widetilde{g} \to t\overline{b}\widetilde{\chi}_1^{-}$ (25%), $\widetilde{g} \to t\overline{t}\widetilde{\chi}_1^0$ (50%);
- $\widetilde{g} \to \overline{t}b\widetilde{\chi}_1^{+}$ (25%), $\widetilde{g} \to t\overline{b}\widetilde{\chi}_1^{-}$ (25%), $\widetilde{g} \to b\overline{b}\widetilde{\chi}_1^0$ (50%);
- $\widetilde{g} \to \overline{t}b\widetilde{\chi}_1^{+}$ (25%), $\widetilde{g} \to t\overline{b}\widetilde{\chi}_1^{-}$ (25%), $\widetilde{g} \to t\overline{t}\widetilde{\chi}_1^0$ (25%), $\widetilde{g} \to b\overline{b}\widetilde{\chi}_1^0$ (25%).

For squark-antisquark production, three simplified models are considered, denoted T2tt, T2bb, and T2qq. In the T2tt scenario [Fig. 1 (lower right)], top squark-antisquark production is followed by the decay of each squark to a top quark and the $\widetilde{\chi}_1^0$. The T2bb and T2qq scenarios are the same as the T2tt scenario except with bottom squarks and quarks, or light-flavored squarks and quarks, respectively, in place of the top squarks and quarks.

Supersymmetric particles not participating in the respective reaction are assumed to have infi-

nite mass. All considered SUSY particles are taken to decay promptly.

Background from SM processes arises from events with a top quark (either $t\bar{t}$ events or events with a single top quark), events with jets and an on- or off-shell W or Z boson (W+jets and Z+jets events, respectively), and QCD events. Top quark and W+jets events can exhibit significant H_T^{miss} and thus contribute to the background if a W boson decays to a neutrino and an undetected or out-of-acceptance charged lepton. Similarly, Z+jets events can exhibit significant H_T^{miss} if the Z boson decays to two neutrinos. Significant H_T^{miss} in QCD events is mostly the consequence of mismeasured jet p_T, but it can also arise if an event contains a charm or bottom quark that decays semileptonically. Note that $t\bar{t}$ events in which both top quarks decay hadronically are indistinguishable in our analysis from QCD events and are accounted for in the evaluation of the QCD background. Because the cross section is small compared to that for QCD events, all-hadronic $t\bar{t}$ events comprise only a small (sub-percent level) component of the evaluated QCD background.

2 Detector and trigger

A detailed description of the CMS detector, along with a definition of the coordinate system and pertinent kinematic variables, is given in Ref. [28]. Briefly, a cylindrical superconducting solenoid with an inner diameter of 6 m provides a 3.8 T axial magnetic field. Within the cylindrical volume are a silicon pixel and strip tracker, a lead tungstate crystal electromagnetic calorimeter (ECAL), and a brass and scintillator hadron calorimeter (HCAL). The tracking detectors cover the pseudorapidity range $|\eta| < 2.5$. The ECAL and HCAL, each composed of a barrel and two endcap sections, cover $|\eta| < 3.0$. Forward calorimeters extend the coverage to $3.0 < |\eta| < 5.0$. Muons are measured within $|\eta| < 2.4$ by gas-ionization detectors embedded in the steel flux-return yoke outside the solenoid. The detector is nearly hermetic, permitting accurate measurements of H_T^{miss}.

The CMS trigger is described in Ref. [29]. For this analysis, signal event candidates were recorded by requiring H_T^{miss} at the trigger level to exceed a threshold that varied between 100 and 120 GeV depending on the LHC instantaneous luminosity. The efficiency of this trigger, which exceeds 98% following application of the event selection criteria described below, is measured in data and is taken into account in the analysis. Additional triggers, requiring the presence of charged leptons, photons, or minimum values of H_T, are used to select samples employed in the evaluation of backgrounds, as described below.

3 Event reconstruction

Individual particles are reconstructed with the CMS particle-flow (PF) algorithm [30], which identifies them as photons, charged hadrons, neutral hadrons, electrons, or muons. To improve the quality of electron candidates [31], additional criteria are imposed on the ECAL shower shape and on the ratio of associated energies in the HCAL and ECAL. Analogously, for muon candidates [32], more stringent requirements are imposed on the matching between silicon-tracker and muon-detector track segments. Electron and muon candidates are restricted to $|\eta| < 2.5$ and < 2.4, respectively.

The reconstructed vertex with the largest value of summed physics-object p_T^2 is taken to be the primary pp interaction vertex. The physics objects are the objects returned by a jet finding algorithm [33, 34] applied to all charged tracks associated with the vertex, plus the corresponding associated missing transverse momentum. The primary vertex is required to lie within 24 cm

of the center of the detector in the direction along the beam axis and within 2 cm in the plane transverse to that axis. Charged-particle tracks associated with vertices other than the primary vertex are removed.

To suppress jets erroneously identified as leptons and genuine leptons from hadron decays, electron and muon candidates are subjected to an isolation requirement. The isolation criterion is based on the variable I, which is the scalar p_T sum of charged hadron, neutral hadron, and photon PF candidates within a cone of radius $\sqrt{(\Delta\phi)^2 + (\Delta\eta)^2}$ around the lepton direction, divided by the lepton p_T, where ϕ is the azimuthal angle. The expected contributions of neutral particles from extraneous pp interactions (pileup) are subtracted [35]. The radius of the cone is 0.2 for lepton $p_T < 50\,\text{GeV}$, $10\,\text{GeV}/p_T$ for $50 \le p_T \le 200\,\text{GeV}$, and 0.05 for $p_T > 200\,\text{GeV}$. The decrease in cone size with increasing lepton p_T accounts for the increased collimation of the decay products from the lepton's parent particle as the Lorentz boost of the parent particle increases [36]. The isolation requirement is $I < 0.1\,(0.2)$ for electrons (muons).

Charged-particle tracks not identified as an isolated electron or muon, including PF electrons and muons not so identified, are subjected to a track isolation requirement. To be identified as an isolated track, the scalar p_T sum of all other charged-particle tracks within a cone of radius 0.3 around the track direction, divided by the track p_T, must be less than 0.2 if the track is identified as a PF electron or muon and less than 0.1 otherwise. Isolated tracks are required to satisfy $|\eta| < 2.4$.

Jets are defined by clustering PF candidates using the anti-k_T jet algorithm [33, 34] with a distance parameter of 0.4. Jet quality criteria [37] are imposed to eliminate jets from spurious sources such as electronics noise. The jet energies are corrected for the nonlinear response of the detector [38] and to account for the expected contributions of neutral particles from pileup [35]. Jets are required to have $p_T > 30\,\text{GeV}$.

The identification of bottom quark jets (b jets) is performed by applying the combined secondary vertex algorithm (CSVv2) at the medium working point [39] to the selected jet sample. The signal efficiency for b jets with $p_T \approx 30\,\text{GeV}$ is 55%. The corresponding misidentification probability for gluon and light-flavored (charm) quark jets is 1.6 (12)%.

4 Event selection and search regions

Events considered as signal candidates are required to satisfy:

- $N_\text{jet} \ge 2$, where jets must appear within $|\eta| < 2.4$;
- $H_T > 300\,\text{GeV}$, with H_T the scalar p_T sum of jets with $|\eta| < 2.4$;
- $H_T^\text{miss} > 300\,\text{GeV}$, where H_T^miss is the magnitude of $\vec{H}_T^\text{miss}$, the negative of the vector p_T sum of jets with $|\eta| < 5$; an extended η range is used to calculate H_T^miss so that it better represents the total missing transverse momentum in an event;
- no identified, isolated electron or muon candidate with $p_T > 10\,\text{GeV}$;
- no isolated track with $m_T < 100\,\text{GeV}$ and $p_T > 10\,\text{GeV}$ ($p_T > 5\,\text{GeV}$ if the track is identified as a PF electron or muon), where m_T is the transverse mass [40] formed from the $\vec{p}_T^\text{miss}$ and isolated-track p_T vector, with $\vec{p}_T^\text{miss}$ the negative of the vector p_T sum of all PF objects;
- $\Delta\phi_{H_T^\text{miss},j_i} > 0.5$ for the two highest p_T jets j_1 and j_2, with $\Delta\phi_{H_T^\text{miss},j_i}$ the azimuthal angle between $\vec{H}_T^\text{miss}$ and the p_T vector of jet j_i; if $N_\text{jet} \ge 3$, then, in addition, $\Delta\phi_{H_T^\text{miss},j_3} > 0.3$ for the third highest p_T jet j_3; if $N_\text{jet} \ge 4$, then, yet in addition, $\Delta\phi_{H_T^\text{miss},j_4} > 0.3$ for the

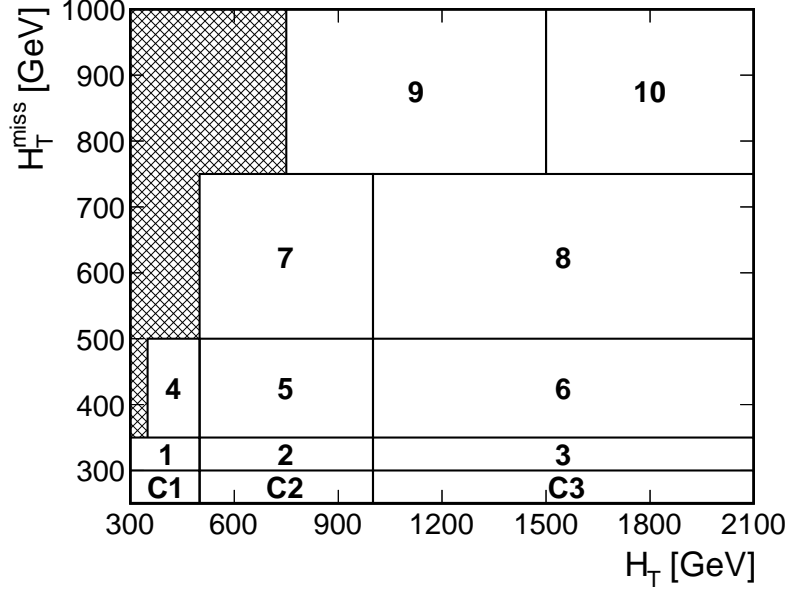Figure 2: Schematic illustration of the 10 kinematic search intervals in the H_T^{miss} versus H_T plane. Intervals 1 and 4 are discarded for $N_{jet} \geq 7$. The intervals labeled C1, C2, and C3 are control regions used to evaluate the QCD background. The rightmost and topmost bins are unbounded, extending to $H_T = \infty$ and $H_T^{miss} = \infty$, respectively.

fourth highest p_T jet j_4; all considered jets must have $|\eta| < 2.4$.

In addition, anomalous events with reconstruction failures or that arise from noise or beam halo interactions are removed [41]. A breakdown of the efficiency at different stages of the selection process for representative signal models is given in Tables A.1 and A.2 of Appendix A.

The isolated-track veto requirement suppresses events with a hadronically decaying τ lepton, or with an isolated electron or muon not identified as such; the m_T requirement restricts the isolated-track veto to situations consistent with W boson decay. The selection criteria on $\Delta\phi_{H_T^{miss},j_i}$ suppress background from QCD events, for which $\vec{H}_T^{miss}$ is usually aligned along a jet direction.

The search is performed in four-dimensional exclusive regions of N_{jet}, $N_{b\text{-}jet}$, H_T, and H_T^{miss}. The search intervals in N_{jet} and $N_{b\text{-}jet}$ are:

- N_{jet}: 2, 3–4, 5–6, 7–8, ≥ 9;
- $N_{b\text{-}jet}$: 0, 1, 2, ≥ 3.

Intervals with $N_{b\text{-}jet} \geq 3$ and $N_{jet} = 2$ are discarded since there are no entries. For H_T and H_T^{miss}, 10 kinematic intervals are defined, as specified in Table 1 and illustrated in Fig. 2. Events with both small H_T and large H_T^{miss} are not considered (see the hatched area in Fig. 2) because such events are likely to arise from mismeasurement. For $N_{jet} \geq 7$, the kinematic intervals labeled 1 and 4 are discarded because of the small number of events. The total number of search regions is 174.

The intervals labeled C1, C2, and C3 in Fig. 2 are control regions defined by $250 < H_T^{miss} < 300\,\text{GeV}$, with the same boundaries in H_T as kinematic intervals 1, 2, and 3, respectively. These regions are used in the method to estimate the QCD background described in Section 7.3.2.

Table 1: Definition of the search intervals in the H_T^{miss} and H_T variables. Intervals 1 and 4 are discarded for $N_{jet} \geq 7$.

Interval	H_T^{miss} [GeV]	H_T [GeV]
1	300–350	300–500
2	300–350	500–1000
3	300–350	>1000
4	350–500	350–500
5	350–500	500–1000
6	350–500	>1000
7	500–750	500–1000
8	500–750	>1000
9	>750	750–1500
10	>750	>1500

5   Simulated event samples

To evaluate the background, we mostly rely on data control regions, as discussed in Section 7. Samples of simulated SM events are used to validate the analysis procedures and for some secondary aspects of the background estimation. The SM production of t$\bar{t}$, W+jets, Z+jets, γ+jets, and QCD events is simulated using the MADGRAPH5_aMC@NLO 2.2.2 [42, 43] event generator at leading order (LO). The t$\bar{t}$ events are generated with up to three additional partons in the matrix element calculations, while up to four additional partons can be present for W+jets, Z+jets, and γ+jets events. Single top quark events produced through the s channel, diboson events such as WW, ZZ, and ZH production, where H is a Higgs boson, and rare events such as t$\bar{t}$W, t$\bar{t}$Z, and WWZ production, are generated with this same program [42, 44] at next-to-leading (NLO) order, except that WW events in which both W bosons decay leptonically are generated using the POWHEG v2.0 [45–49] program at NLO. The same POWHEG generator is used to describe single top quark events produced through the t and tW channels. The detector response is modeled with the GEANT4 [50] suite of programs. Normalization of the simulated background samples is performed using the most accurate cross section calculations available [42, 48, 49, 51–59], which generally correspond to NLO or next-to-NLO precision.

Samples of simulated signal events are generated at LO using the MADGRAPH5_aMC@NLO program. Up to two additional partons are included in the matrix element calculation. The production cross sections are determined with NLO plus next-to-leading logarithmic (NLL) accuracy [60–64]. Events with gluino (squark) pair production are generated for a range of gluino $m_{\tilde{g}}$ (squark $m_{\tilde{q}}$) and LSP $m_{\tilde{\chi}_1^0}$ mass values, with $m_{\tilde{\chi}_1^0} < m_{\tilde{g}}$ ($m_{\tilde{\chi}_1^0} < m_{\tilde{q}}$). The ranges of mass considered vary according to the model but are generally from around 600 to 2200 GeV for $m_{\tilde{g}}$, 200 to 1700 GeV for $m_{\tilde{q}}$, and 0 to 1200 GeV for $m_{\tilde{\chi}_1^0}$ (see the results shown in Section 8 for more detail). For the T1tbtb model, the mass of the intermediate $\tilde{\chi}_1^\pm$ state is taken to be $m_{\tilde{\chi}_1^0} + 5$ GeV, while for the T5qqqqVV model, the masses of the intermediate $\tilde{\chi}_2^0$ and $\tilde{\chi}_1^\pm$ are given by the mean of $m_{\tilde{\chi}_1^0}$ and $m_{\tilde{g}}$. The gluinos and squarks decay according to phase space [65]. To render the computational requirements manageable, the detector response is described using the CMS fast simulation [66, 67], which yields consistent results with the GEANT4-based simulation, except that we apply a correction of 1% to account for differences in the efficiency of the jet quality requirements [37], corrections of 5–12% to account for differences in the b jet tagging efficiency, and corrections of 0–14% to account for differences in the modeling of H_T and H_T^{miss}.

For simulated samples generated at LO (NLO), the NNPDF3.0LO [68] (NNPDF3.0NLO [68])

Table 2: Systematic uncertainties in the yield of signal events, averaged over all search regions. The variations correspond to different signal models and choices for the SUSY particle masses. Results reported as 0.0 correspond to values less than 0.05%. "Mixed T1" refers to the mixed models of gluino decays to heavy squarks described in the introduction.

Item	Relative uncertainty (%)
Trigger efficiency	$0.2 - 2.8$
Jet quality requirements	1.0
Initial-state radiation	$0.0 - 14$
Renormalization and factorization scales	$0.0 - 6.2$
Jet energy scale	$0.0 - 7.7$
Jet energy resolution	$0.0 - 4.2$
Statistical uncertainty of MC samples	$1.5 - 30$
H_T and H_T^{miss} modeling	$0.0 - 13$
Pileup	$0.2 - 5.5$
Isolated-lepton & isolated-track vetoes	2.0
(T1tttt, T1tbtb, mixed T1, T5qqqqVV, and T2tt models)	
Integrated luminosity	2.5
Total	$3.9 - 34$

parton distribution functions (PDFs) are used. Parton showering and hadronization are described by the PYTHIA 8.205 [65] program for all samples.

To improve the description of initial-state radiation (ISR), we compare the MADGRAPH prediction to data in a control region enriched in $t\bar{t}$ events: two leptons (ee, $\mu\mu$, or eμ) and two tagged b jets are required. The number of all other jets in the event is denoted N_{jet}^{ISR}. The correction factor is derived as a function of N_{jet}^{ISR}, with a central value ranging from 0.92 for $N_{jet}^{ISR} = 1$ to 0.51 for $N_{jet}^{ISR} \geq 6$. These corrections are applied to simulated $t\bar{t}$ and signal events. From studies with a single-lepton data control sample, dominated by $t\bar{t}$ events, the associated systematic uncertainty is taken to be 20% of the correction for $t\bar{t}$ events and 50% of the correction for signal events, where the larger uncertainty in the latter case accounts for possible differences between $t\bar{t}$ and signal event production.

6 Signal systematic uncertainties

Systematic uncertainties in the signal event yield are listed in Table 2. To evaluate the uncertainty associated with the renormalization (μ_R) and factorization (μ_F) scales, each scale is varied independently by a factor of 2.0 and 0.5 [69, 70]. The uncertainties associated with μ_R, μ_F, and ISR, integrated over all search regions, typically lie below 0.1% but can be as large as the maximum values noted in Table 2 for $\Delta m \approx 0$, where Δm is the difference between the gluino or squark mass and the sum of the masses of the particles into which it decays. For example, for the T1tttt model, Δm is given by $\Delta m = m_{\widetilde{g}} - (m_{\widetilde{\chi}_1^0} + 2m_{top})$, with m_{top} the top quark mass. The uncertainties associated with the jet energy scale and jet energy resolution are evaluated as a function of jet p_T and η. An uncertainty in the event yield associated with pileup is evaluated based on the observed distribution of the number N_{vtx} of reconstructed vertices, and on the selection efficiency and its uncertainty determined from simulation as a function of N_{vtx}. The isolated-lepton and isolated-track vetoes have a minimal impact on the T1bbbb, T1qqqq, T2bb, and T2qq models because events in these models rarely contain an isolated lepton. Thus, the associated uncertainty is negligible ($\lesssim 0.1\%$). The systematic uncertainty in the determination

of the integrated luminosity is 2.5% [71].

Systematic uncertainties in the signal predictions associated with the b jet tagging and misidentification efficiencies are also evaluated. These uncertainties do not affect the signal yield but can potentially alter the shape of signal distributions. The systematic uncertainties associated with the trigger, μ_R, μ_F, ISR, jet energy scale, jet energy resolution, statistical precision in the event samples, and H_T^{miss} modeling can also affect the shapes of the signal distributions. We account for these potential changes in shape, i.e., migration of events between search regions, in the limit-setting procedure described in Section 8.

7 Background evaluation

The evaluation of background is primarily based on data control regions (CRs). Signal events, if present, could populate the CRs, an effect known as signal contamination. The impact of signal contamination is evaluated as described in Section 8. Signal contamination is negligible for all CRs except those used to evaluate the top quark and W+jets background (Section 7.1). It is nonnegligible only for the models that can produce an isolated track or lepton, viz., the T1tttt, T1tbtb, T5qqqqVV, and T2tt models, and the mixed models of gluino decays to heavy squarks described in the introduction.

7.1 Background from top quark and W+jets events

The background from the SM production of $t\bar{t}$, single top quark, and W+jets events originates from W bosons that decay leptonically to yield a neutrino and a charged lepton. If the charged lepton is an electron or muon, including those from τ lepton decay, it is called a "lost" lepton. A lost lepton arises if an electron or muon lies outside the analysis acceptance, is not reconstructed, or is not isolated, and thus is not vetoed by the requirements of Section 4. The other possibility is that the charged lepton is a hadronically decaying τ lepton, denoted "τ_h."

7.1.1 Lost-lepton background

The procedure used to evaluate the lost-lepton background is described in Ref. [17] (see also Refs. [21, 22, 72]). Briefly, single-lepton CRs are selected using the standard trigger and selection criteria, except with the electron and muon vetoes inverted and the isolated-track veto not applied. Exactly one isolated electron or muon must be present. In addition, the transverse mass m_T formed from the $\vec{p}_T^{\,miss}$ and lepton $\vec{p}_T$ is required to satisfy $m_T < 100\,\text{GeV}$: this requirement is effective at identifying SM events, while reducing potential signal contamination. The T1tttt (T1tbtb, T5qqqqVV, T2tt) signal contamination in the resulting CRs is generally negligible ($\lesssim 0.1\%$), but it can be as large as 30–50% (25–60%, 2–15%, 5–50%) for large values of N_{jet}, $N_{b\text{-jet}}$, H_T, and/or H_T^{miss}, depending on $m_{\tilde{g}}$ or $m_{\tilde{q}}$ and $m_{\tilde{\chi}_1^0}$. Similar results to the T1tbtb model are obtained for the mixed models of gluino decay to heavy squarks.

Each CR event is entered into one of the 174 search regions with a weight that represents the probability for a lost-lepton event to appear with the corresponding values of H_T, H_T^{miss}, N_{jet}, and $N_{b\text{-jet}}$. The weights are determined from the $t\bar{t}$, W+jets, single top quark, and rare process simulations through evaluation of the efficiency of the lepton acceptance, lepton reconstruction, lepton isolation, isolated-track, and m_T requirements. Corrections are applied to account for the purity of the CR, the contributions of dilepton events to the signal regions and CR, and efficiency differences with respect to data. More details are provided in Ref. [17]. The efficiencies are determined as a function of H_T, H_T^{miss}, N_{jet}, $N_{b\text{-jet}}$, lepton p_T and η, and other kinematic variables. Improvements relative to Ref. [17] are that we now use $N_{b\text{-jet}}$ and lepton η to help

characterize the efficiencies, and the efficiency of the isolated-track veto is now determined separately for lost-lepton events that fail the acceptance, reconstruction, or isolation requirements. Previously, only a single overall isolated-track veto efficiency was evaluated (as a function of search region) when constructing the weights.

The weighted distributions of the search variables, summed over the events in the CRs, define the lost-lepton background prediction. The procedure is performed separately for the single-electron and single-muon CRs, both of which are used to predict the total lost-lepton background, i.e., the background due both to lost electrons and to lost muons. The two predictions yield consistent results and are averaged, with correlations in the uncertainties taken into account, to obtain the final lost-lepton background estimate. The method is checked with a closure test, namely by determining the ability of the method, applied to simulated event samples, to predict correctly the true number of background events. The results of this test are shown in Fig. 3.
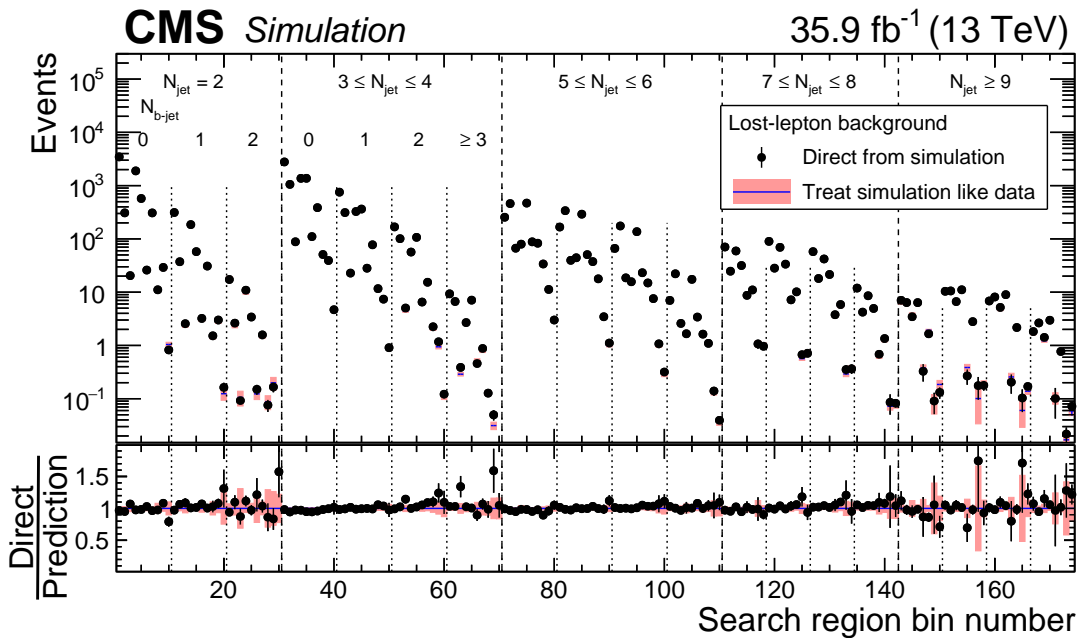
Figure 3: The lost-lepton background in the 174 search regions of the analysis as determined directly from $t\bar{t}$, single top quark, W+jets, diboson, and rare-event simulation (points, with statistical uncertainties) and as predicted by applying the lost-lepton background determination procedure to simulated electron and muon control samples (histograms, with statistical uncertainties). The results in the lower panel are obtained through bin-by-bin division of the results in the upper panel, including the uncertainties, by the central values of the "predicted" results. The 10 results (8 results for $N_{jet} \geq 7$) within each region delineated by vertical dashed lines correspond sequentially to the 10 (8) kinematic intervals of H_T and H_T^{miss} indicated in Table 1 and Fig. 2.

The dominant uncertainty in the lost-lepton background prediction is statistical, due to the limited number of CR events. As a systematic uncertainty, we take the larger of the observed nonclosure and the statistical uncertainty in the nonclosure, for each search region, where "nonclosure" refers to the bin-by-bin difference between the solid points and histogram in Fig. 3. Additional systematic uncertainties are evaluated as described in Ref. [17] and account for potential differences between the data and simulation for the lepton acceptance, lepton reconstruction efficiency, lepton isolation efficiency, isolated-track efficiency, m_T selection efficiency, dilepton contributions, and purity of the CRs.

7.1.2 Hadronically decaying τ lepton background

To evaluate the top quark and W+jets background due to τ_h events, a CR event sample is selected using a trigger that requires either at least one isolated muon candidate with $p_T > 24\,\text{GeV}$, or at least one isolated muon candidate with $p_T > 15\,\text{GeV}$ in conjunction with $H_T > 500\,\text{GeV}$. The reason a special trigger is used, and not the standard one, is that the τ_h background determination method requires there not be a selection requirement on missing transverse momentum, as is explained below. The selected events are required to contain exactly one identified muon with $|\eta| < 2.1$. The p_T of the muon candidate must exceed $20\,\text{GeV}$, or $25\,\text{GeV}$ if $H_T < 500\,\text{GeV}$. The fraction of T1tttt (T1tbtb, T5qqqqVV, T2tt) events in the CR due to signal contamination is generally $\lesssim 0.1\%$, but can be as large as 5–22% (1–20%, 1–15%, 1–40%) for large values of N_{jet}, $N_{\text{b-jet}}$, H_T, and/or H_T^{miss}, depending on $m_{\tilde{g}}$ or $m_{\tilde{q}}$ and $m_{\tilde{\chi}_1^0}$, with similar results to the T1tbtb model for the mixed models of gluino decay to heavy squarks.

The τ_h background is determined using the method described in Ref. [17] (see also Refs. [21, 22, 72]). It makes use of the similarity between μ+jets and τ_h+jets events aside from the detector response to the μ or τ_h. In each CR event, the muon p_T is smeared through random sampling of τ_h response functions derived from simulation of single $W \to \tau_h \nu_\tau$ decay events. This differs from Ref. [17], in which $W \to \tau_h \nu_\tau$ decays in simulated $t\bar{t}$ and W+jets events were used to derive the response functions. The change was made in order to reduce the risk of contamination in the response functions from nearby non-τ_h-related particles; note that the CR already includes the effects from the underlying event and nearby jets. The response functions express the expected visible-p_T distribution of a τ_h candidate as a function of the true τ lepton p_T, taken to be the measured muon p_T in the CR event. Following the smearing, the values of H_T, H_T^{miss}, N_{jet}, and $N_{\text{b-jet}}$ are calculated for the CR event, and the selection criteria of Section 4 are applied. Note that CR events with relatively low values of H_T^{miss} can be promoted, after smearing, to have H_T^{miss} values above the nominal threshold, and thus appear in the τ_h background prediction. It is for this reason that the CR is selected using a trigger without a requirement on missing transverse momentum: to avoid possible H_T^{miss} bias. The probability for a τ_h jet to be erroneously identified as a b jet is taken into account. Corrections are applied to account for the trigger efficiency, the acceptance and efficiency of the μ selection, and the ratio of branching fractions $\mathcal{B}(W \to \tau_h \nu)/\mathcal{B}(W \to \mu \nu) = 0.65$ [73]. The resulting event yield provides the τ_h background estimate. The method is validated with a closure test, whose results are shown in Fig. 4.

Systematic uncertainties are assigned based on the level of nonclosure, as described for the lost-lepton background. In addition, systematic uncertainties are evaluated for the muon reconstruction, isolation, and acceptance efficiencies, for the response functions, and for the misidentification rate of τ_h jets as b jets. The dominant source of uncertainty, as for the lost-lepton background, is from the limited statistical precision of the CR sample.

7.2 Background from $Z \to \nu\bar{\nu}$ events

The evaluation of background from SM Z+jets events with $Z \to \nu\bar{\nu}$ is based on CR samples of γ+jets events, and of Z+jets events with $Z \to \ell^+\ell^-$ ($\ell = $ e, μ). The photon in the γ+jets events and the $\ell^+\ell^-$ pair in the $Z \to \ell^+\ell^-$ events are removed from the event in order to emulate missing transverse momentum. The γ+jets and $Z \to \ell^+\ell^-$ events are then subjected to the same selection criteria as in the standard analysis, with corrections applied to account for differences in acceptance with respect to the $Z(\to \nu\bar{\nu})$+jets process. The use of γ+jets events exploits the similarity between Z boson and direct photon production in pp collisions, where "direct" refers to a photon produced through the Compton scattering ($qg \to q\gamma$) or annihilation ($q\bar{q} \to g\gamma$) process.
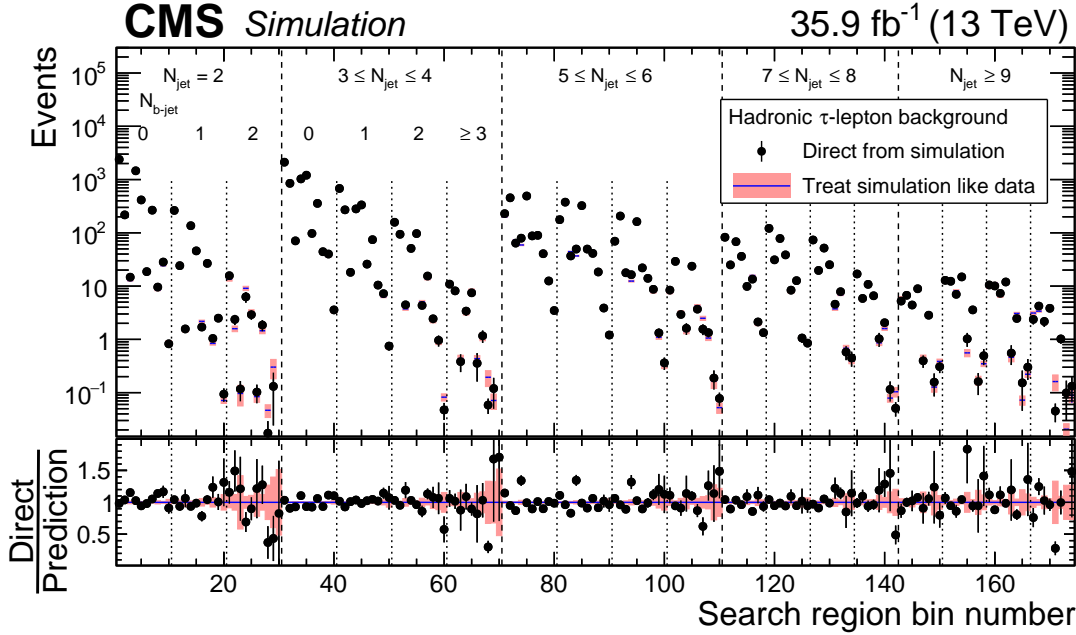
Figure 4: The background from hadronically decaying τ leptons in the 174 search regions of the analysis as determined directly from $t\bar{t}$, single top quark, and W+jets simulation (points, with statistical uncertainties) and as predicted by applying the hadronically decaying τ lepton background determination procedure to a simulated muon control sample (histograms, with statistical uncertainties). The results in the lower panel are obtained through bin-by-bin division of the results in the upper panel, including the uncertainties, by the central values of the "predicted" results. The labeling of the bin numbers is the same as in Fig. 3.

The method is an extension of that described in Ref. [17]. Briefly, the relatively copious γ+jets events are used to evaluate the background in the 46 search regions with $N_{\text{b-jet}} = 0$. We do not use γ+jets events for the $N_{\text{b-jet}} > 0$ search regions to avoid reliance on the theoretical modeling of γ+jets versus Z+jets production with bottom quarks. The less abundant $Z \to \ell^+\ell^-$ events are used to validate and calibrate the $N_{\text{b-jet}} = 0$ results, as described below, and to extrapolate to the $N_{\text{b-jet}} > 0$ search regions. For this extrapolation, the $Z \to \ell^+\ell^-$ data are integrated over H_{T} and $H_{\text{T}}^{\text{miss}}$ because of the limited number of events.

The $Z \to \ell^+\ell^-$ CR sample is selected using a combination of triggers that requires either i) at least one isolated electron or muon with $p_{\text{T}} > 15\,\text{GeV}$, and either $H_{\text{T}} > 350$ or $400\,\text{GeV}$ depending on the LHC instantaneous luminosity, ii) at least one electron with either $p_{\text{T}} > 105$ or $115\,\text{GeV}$ depending on the instantaneous luminosity, iii) at least one muon with $p_{\text{T}} > 50\,\text{GeV}$, or iv) at least one isolated electron (muon) with $p_{\text{T}} > 27\,(24)\,\text{GeV}$. The events are required to contain exactly one e^+e^- or one $\mu^+\mu^-$ pair with an invariant mass within $15\,\text{GeV}$ of the nominal Z boson mass, with the constituents of the pair identified using the same criteria for isolated electrons and muons as in the standard analysis. The p_{T} of the lepton pair must exceed $200\,\text{GeV}$. To ensure that the $Z \to \ell^+\ell^-$ and γ+jets CRs are independent, a veto is applied to events containing an identified photon.

The γ+jets CR sample is selected with a trigger that requires a photon candidate with $p_{\text{T}} > 175\,\text{GeV}$. Events are retained if they contain exactly one well-identified isolated photon with $p_{\text{T}} > 200\,\text{GeV}$. The photon isolation criteria require the pileup-corrected energy within a cone of radius 0.3 around the photon direction, excluding the energy carried by the photon candidate itself, to satisfy upper bounds that depend on the p_{T} and η of the photon, and are determined

separately for the contributions of electromagnetic, charged hadronic, and neutral hadronic energy. About 85% of the events in the resulting sample are estimated to contain a direct photon, while the remaining events either contain a fragmentation photon, i.e., emitted as initial- or final-state radiation or during the hadronization process, or a nonprompt photon, i.e., from unstable hadron decay. A fit to the photon isolation variable is performed as a function of H_T^{miss} to determine the photon purity β_γ, defined as the fraction of events in the γ+jets CR with a direct or fragmentation photon (these two types of photons are experimentally indistinguishable and together are referred to as "prompt").

The estimated number $N_{Z \to \nu\bar{\nu}}^{\text{pred}}$ of $Z(\to \nu\bar{\nu})$+jets background events contributing to each $N_{\text{b-jet}} = 0$ search region is given by:

$$N_{Z \to \nu\bar{\nu}}^{\text{pred}} \Big|_{N_{\text{b-jet}}=0} = \rho \mathcal{R}_{Z \to \nu\bar{\nu}/\gamma}^{\text{sim}} \mathcal{F}_{\text{dir}}^{\text{sim}} \beta_\gamma N_\gamma^{\text{obs}} / \mathcal{C}_{\text{data/sim}}^\gamma, \tag{1}$$

where N_γ^{obs} is the number of events in the corresponding N_{jet}, H_T, and H_T^{miss} bin of the γ+jets CR, β_γ is the fraction that are prompt, $\mathcal{F}_{\text{dir}}^{\text{sim}}$ is the fraction of prompt photons that are also direct (evaluated from simulation), and $\mathcal{R}_{Z \to \nu\bar{\nu}/\gamma}^{\text{sim}}$ is the ratio from simulation of the number of $Z(\to \nu\bar{\nu})$+jets events to the number of direct-photon γ+jets events, with the direct photon term obtained from an LO MADGRAPH5_aMC@NLO calculation. The $\mathcal{C}_{\text{data/sim}}^\gamma$ factors are corrections to the simulation that account for efficiency differences in photon reconstruction with respect to data.

The ρ factor in Eq. (1) is determined from $Z \to \ell^+\ell^-$ data and is used to account for potential differences between simulation and data in the $\mathcal{R}_{Z \to \nu\bar{\nu}/\gamma}$ ratio, such as those that might be present because of missing higher-order corrections in the simulated γ+jets term. It is given by:

$$\rho = \frac{\left\langle \mathcal{R}_{Z \to \ell^+\ell^-/\gamma}^{\text{obs}} \right\rangle}{\left\langle \mathcal{R}_{Z \to \ell^+\ell^-/\gamma}^{\text{sim}} \right\rangle} = \frac{\sum N_{Z \to \ell^+\ell^-}^{\text{obs}}}{\sum N_{Z \to \ell^+\ell^-}^{\text{sim}}} \frac{\sum N_\gamma^{\text{sim}}}{\sum N_\gamma^{\text{obs}}} \frac{\left\langle \beta_{\ell\ell}^{\text{data}} \right\rangle}{\left\langle \mathcal{C}_{\text{data/sim}}^{\ell\ell} \right\rangle} \frac{\left\langle \mathcal{C}_{\text{data/sim}}^\gamma \right\rangle}{\left\langle \mathcal{F}_{\text{dir}}^{\text{sim}} \beta_\gamma \right\rangle}, \tag{2}$$

with $N_{Z \to \ell^+\ell^-}^{\text{obs}}$, $N_{Z \to \ell^+\ell^-}^{\text{sim}}$, and N_γ^{sim} the numbers of events in the indicated CRs, with the simulated samples normalized to the integrated luminosity of the data. The sums and averages span the search regions. The $\beta_{\ell\ell}^{\text{data}}$ factors represent the purity of the $Z \to \ell^+\ell^-$ CR, obtained from fits to the measured lepton-pair mass distributions, while $\mathcal{C}_{\text{data/sim}}^{\ell\ell}$ are corrections to account for data-versus-simulation differences in lepton reconstruction efficiencies. While the $Z \to \ell^+\ell^-$ sample is too small to allow a meaningful measurement of ρ in each search region, we examine the projections of ρ in each dimension. We find a modest dependence on H_T and on the correlated variable N_{jet}. Based on the observed empirical result $\rho(H_T) = 0.91 + \left(9.6 \times 10^{-5} \, \text{GeV}^{-1}\right) \min(H_T, 900 \, \text{GeV})$, we apply a weight to each simulated γ+jets event entering the evaluation of ρ and $\mathcal{R}_{Z \to \nu\bar{\nu}/\gamma}$. Following this weighting, the projections of ρ in the N_{jet}, H_T, and H_T^{miss} dimensions are consistent with a constant value of 1.00, with uncertainties deduced from linear fits to the projections that vary with these variables between 2 and 13%.

For search regions with $N_{\text{b-jet}} > 0$, the $Z \to \nu\bar{\nu}$ background estimate is:

$$\left(N_{Z \to \nu\bar{\nu}}^{\text{pred}} \right)_{j,b,k} = \left(N_{Z \to \nu\bar{\nu}}^{\text{pred}} \right)_{j,0,k} \mathcal{F}_{j,b}, \tag{3}$$

where j, b, and k are bin indices (numbered from zero) for the N_{jet}, $N_{\text{b-jet}}$, and kinematic (i.e., H_T and H_T^{miss}) variables, respectively. For example, $j = 1$ corresponds to $N_{\text{jet}} = 3$–4, $b = 3$
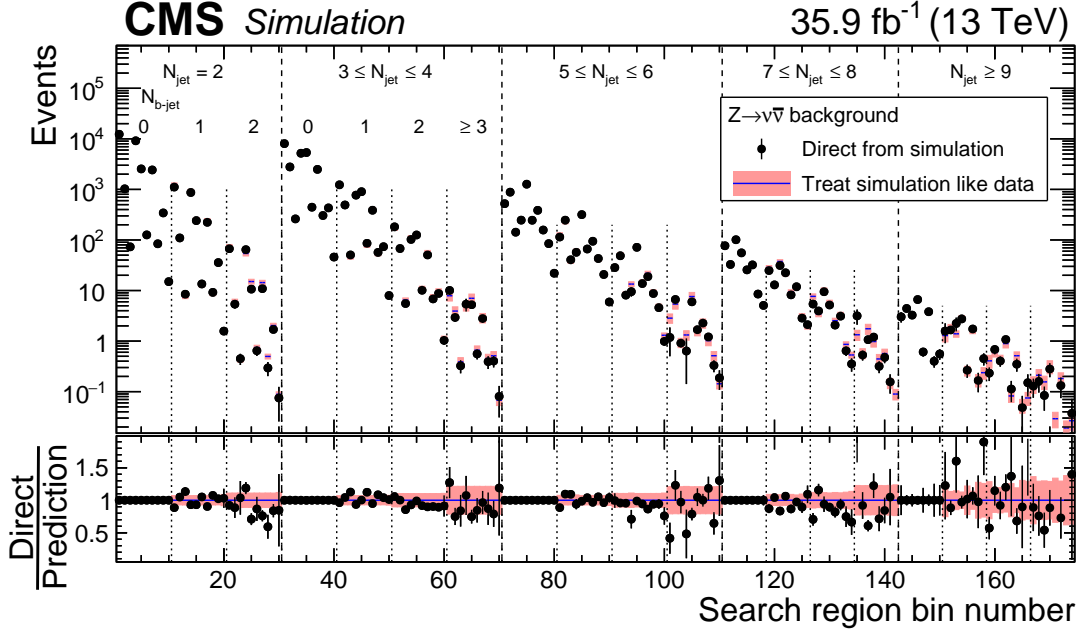
Figure 5: The $Z \to \nu\overline{\nu}$ background in the 174 search regions of the analysis as determined directly from $Z(\to \nu\overline{\nu})$+jets simulation (points, with statistical uncertainties), and as predicted by applying the $Z \to \nu\overline{\nu}$ background determination procedure to statistically independent $Z(\to \ell^+\ell^-)$+jets simulated event samples (histogram, with shaded regions indicating the quadrature sum of the systematic uncertainty associated with the assumption that $\mathcal{F}_{j,b}$ is independent of H_{T} and $H_{\mathrm{T}}^{\mathrm{miss}}$, and the statistical uncertainty). For bins corresponding to $N_{\mathrm{b\text{-}jet}} = 0$, the agreement is exact by construction. The results in the lower panel are obtained through bin-by-bin division of the results in the upper panel, including the uncertainties, by the central values of the "predicted" results. The labeling of the bin numbers is the same as in Fig. 3.

to $N_{\mathrm{b\text{-}jet}} \geq 3$, and $k = 0$ to kinematic interval 1 of Table 1 and Fig. 2. The first term on the right-hand side of Eq. (3) is obtained from Eq. (1).

For all but the $N_{\mathrm{jet}} \geq 9$ bin, corresponding to $j = 4$, the $N_{\mathrm{b\text{-}jet}}$ extrapolation factor $\mathcal{F}_{j,b}$ is obtained from the fitted $Z \to \ell^+\ell^-$ data yields, with data-derived corrections $\beta_{\ell\ell}^{\mathrm{data}}$ to account for the $N_{\mathrm{b\text{-}jet}}$-dependent purity. Other efficiencies cancel in the ratio. Specifically,

$$\mathcal{F}_{j,b} = \left(N_{Z \to \ell^+\ell^-}^{\mathrm{data}} \beta_{\ell\ell}^{\mathrm{data}} \right)_{j,b} \Big/ \left(N_{Z \to \ell^+\ell^-}^{\mathrm{data}} \beta_{\ell\ell}^{\mathrm{data}} \right)_{j,0}; \quad j = 0, 1, 2, 3. \tag{4}$$

For $N_{\mathrm{jet}} \geq 9$, there are very few $Z \to \ell^+\ell^-$ events and we use the measured results for $N_{\mathrm{jet}} = 7 - 8$ (the $j = 3$ bin) multiplied by an $N_{\mathrm{b\text{-}jet}}$ extrapolation factor from simulation:

$$\mathcal{F}_{4,b} = \mathcal{F}_{3,b} \left(\mathcal{F}_{4,b}^{\mathrm{sim}} / \mathcal{F}_{3,b}^{\mathrm{sim}} \right). \tag{5}$$

A systematic uncertainty is assigned to the ratio of simulated yields in Eq. (5) based on a lower bound equal to 1.0 and an upper bound determined using the binomial model of Ref. [17]. The resulting uncertainty ranges from 7 to 40%, depending on $N_{\mathrm{b\text{-}jet}}$.

A closure test of the method is presented in Fig. 5. The shaded bands represent systematic uncertainties of 7, 10, and 20% for $N_{\mathrm{b\text{-}jet}} = 1$, 2, and ≥ 3, respectively, combined with the statistical uncertainties from the simulation. The systematic uncertainties account for the assumption that the $\mathcal{F}_{j,b}$ terms are independent of H_{T} and $H_{\mathrm{T}}^{\mathrm{miss}}$.

The rare process $t\bar{t}Z$ and the even more rare processes ZZ, WWZ, WZZ, and ZZZ can contribute to the background. We add the expectations for these processes, obtained from simulation, to the numerator and denominator of Eq. (5). Note that processes with a Z boson that have a counterpart with the Z boson replaced by a photon are already accounted for in N_γ^{obs} and largely cancel in the $\mathcal{R}_{Z\to\nu\bar{\nu}/\gamma}$ ratio. For search regions with $N_{\text{jet}} \geq 9$ and $N_{\text{b-jet}} \geq 2$, the contribution of $t\bar{t}Z$ events is comparable to that from Z+jets events, with an uncertainty of $\approx$50%, consistent with the rate and uncertainty for $t\bar{t}Z$ events found in Ref. [74].

Besides the uncertainties associated with the $N_{\text{b-jet}}$ extrapolation and the ρ term, discussed above, systematic uncertainties associated with the statistical precision of the simulation, the photon reconstruction efficiency, the photon and dilepton purities, and the $\mathcal{R}_{Z\to\nu\bar{\nu}/\gamma}^{\text{sim}}$ term are evaluated. The principal uncertainty arises from the limited number of events in the CRs.

7.3 Background from QCD events

Background from QCD events is not, in general, expected to be large. Nonetheless, since H_T^{miss} in these events primarily arises from the mismeasurement of jet p_T rather than from genuine missing transverse momentum, it represents a difficult background to model. We employ two methods, complementary to each other, to evaluate the QCD background: the rebalance-and-smear (R&S) method [21, 22] and the low-$\Delta\phi$ extrapolation method [17, 75]. The R&S method is selected as our primary technique because it is more strongly motivated from first principles and is less empirical in nature. Thus the R&S method is used for the interpretation of the data, presented in Section 8. The low-$\Delta\phi$ extrapolation method is used as a cross-check.

7.3.1 The rebalance-and-smear method

The R&S method utilizes a special CR event sample, selected using triggers that require H_T to exceed thresholds ranging from 250 to 800 GeV.

In a first step, called "rebalance," the jet momenta in a CR event are rescaled to effectively undo the effects of detector response. This step is performed using Bayesian inference. The prior probability distribution π is derived from the particle-level QCD simulation, where "particle level" corresponds to the level of an event generator, i.e., without simulation of the detector. It is given by

$$\pi(\vec{H}_T^{\text{miss}}, \vec{p}_{T,j_1}) = \mathcal{P}\left(H_T^{\text{miss}}\right) \mathcal{P}\left(\Delta\phi_{H_T^{\text{miss}},j_{1(b)}}\right), \tag{6}$$

where $\mathcal{P}(H_T^{\text{miss}})$ is the distribution of H_T^{miss}, and $\mathcal{P}(\Delta\phi_{H_T^{\text{miss}},j_{1(b)}})$ the distribution of the azimuthal angle between $\vec{H}_T^{\text{miss}}$ and the highest p_T jet in the event, or between $\vec{H}_T^{\text{miss}}$ and the highest p_T tagged b jet if $N_{\text{b-jet}} \geq 1$. The prior is binned in intervals of H_T and $N_{\text{b-jet}}$. The prior thus incorporates information about both the magnitude and direction of the genuine $\vec{H}_T^{\text{miss}}$ expected in QCD events. This represents a more sophisticated treatment than the one used in Refs. [21, 22], where the prior was merely taken to be a Dirac delta function at $H_T^{\text{miss}} = 0$.

The jets in a CR event are then rescaled, using Bayes' theorem, to represent the event at the particle level. Jets with $p_T > 15$ GeV and $|\eta| < 5.0$ are included in this procedure. The expression of Bayes' theorem is:

$$\mathcal{P}(\vec{J}_{\text{part}}|\vec{J}_{\text{meas}}) \sim \mathcal{P}(\vec{J}_{\text{meas}}|\vec{J}_{\text{part}})\,\pi(\vec{H}_T^{\text{miss}}, \vec{p}_{T,j_1}). \tag{7}$$

The $\mathcal{P}(\vec{J}_{\text{part}}|\vec{J}_{\text{meas}})$ term is the posterior probability density, expressing the probability for a given set of particle-level jet momenta $\vec{J}_{\text{part}}$ given the measured set $\vec{J}_{\text{meas}}$. The $\mathcal{P}(\vec{J}_{\text{meas}}|\vec{J}_{\text{part}})$ term is a likelihood function, defined by the product over the jets in the event of the response

functions for the individual jets. The jet response functions, determined in bins of jet p_T and η, are derived from simulation as the distribution of the ratio of reconstructed jet p_T values to a given generated value, corrected with separate scale factors for the Gaussian cores and non-Gaussian tails to account for jet energy resolution differences with respect to data. The likelihood function is maximized by rescaling the momenta of the measured jets, with the respective jet p_T uncertainties as constraints. The set $\vec{J}_{part}$ corresponding to the resulting most-likely posterior probability defines the rebalanced event.

In a second step, denoted "smear," the magnitudes of the jet momenta are rescaled by p_T- and η-dependent factors obtained from random sampling of the jet response functions. This sampling is performed numerous times for each rebalanced event to increase the statistical precision of the resulting sample. Each event is weighted with a factor inversely proportional to the number of times it is sampled.

Application of the R&S procedure produces an event sample that closely resembles the original sample of CR events, except the contributions of events with genuine H_T^{miss}, viz., top quark, W+jets, Z+jets, and possible signal events, are effectively eliminated [21]. The rebalanced and smeared events are subjected to the standard event selection criteria of Section 4 to obtain the predictions for the QCD background in each search region.

The principal uncertainty in the R&S QCD background prediction is systematic, associated with the uncertainty in the shape of the jet response functions. This uncertainty is evaluated by varying the jet energy resolution scale factors within their uncertainties, resulting in uncertainties in the prediction that range from 20–80% depending on the search region. Smaller uncertainties related to the trigger, the prior, and the statistical uncertainties are also evaluated.
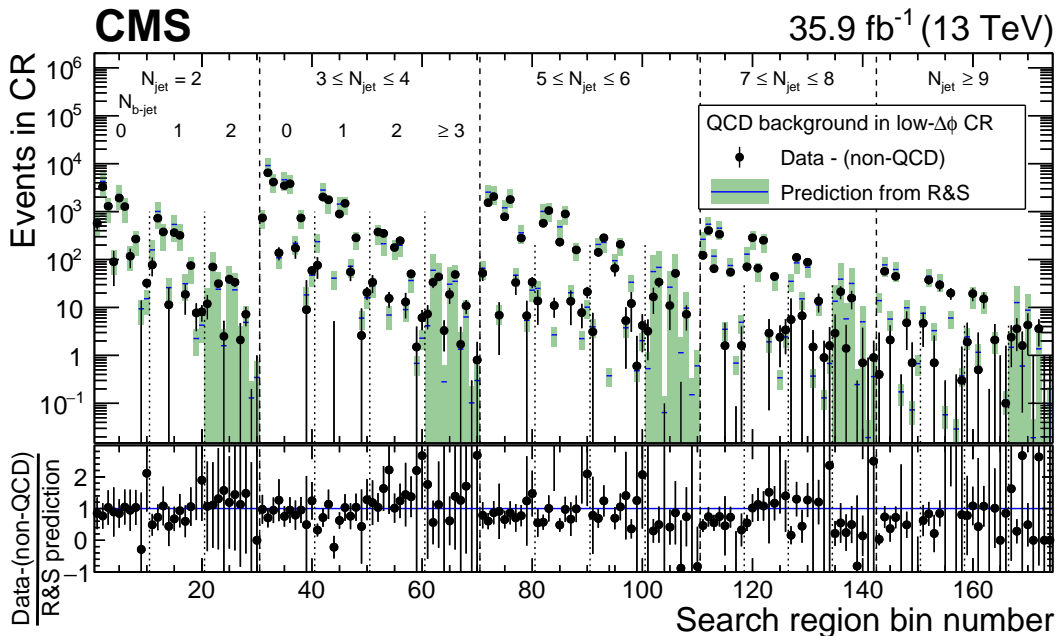

Figure 6: The QCD background in the low-$\Delta\phi$ control region (CR) as predicted by the rebalance-and-smear (R&S) method (histograms, with statistical and systematic uncertainties added in quadrature), compared to the corresponding data from which the expected contributions of top quark, W+jets, and Z+jets events have been subtracted (points, with statistical uncertainties). The lower panel shows the ratio of the measured to the predicted results and its propagated uncertainty. The labeling of the bin numbers is the same as in Fig. 3.

As a test of the method, we determine the R&S prediction for the QCD contribution to a QCD-dominated CR selected with the standard trigger and event selection, except for the $\Delta\phi_{H_T^{miss},j_i}$ requirements of Section 4, which are inverted. Specifically, at least one of the two (for $N_{jet} = 2$), three (for $N_{jet} = 3$), or four (for $N_{jet} \geq 4$) highest p_T jets in an event must fail a $\Delta\phi_{H_T^{miss},j_i}$ selection criterion. The resulting QCD-dominated sample is called the low-$\Delta\phi$ CR. The R&S prediction for the QCD background in the low-$\Delta\phi$ CR is shown in Fig. 6 in comparison to the corresponding measured results, following subtraction from the data of the contributions from top quark, W+jets, and Z+jets events, evaluated as described in the previous sections. Note that because of this subtraction, the resulting difference is sometimes negative. The prediction from the R&S method is seen to agree with the data within the uncertainties.

7.3.2   The low-$\Delta\phi$ extrapolation method

In the low-$\Delta\phi$ extrapolation method, the QCD background in each search region is evaluated by multiplying the observed event yield in the corresponding region of the low-$\Delta\phi$ CR (Section 7.3.1), after accounting for the contributions of non-QCD SM events, by a factor R^{QCD} determined primarily from data. The R^{QCD} terms express the ratio of the expected QCD background in the corresponding signal and low-$\Delta\phi$ regions.

The R^{QCD} term is empirically observed to have a negligible dependence on $N_{b\text{-}jet}$ for a given value of N_{jet}. The functional dependence of R^{QCD} can therefore be expressed in terms of H_T, H_T^{miss}, and N_{jet} alone. The R^{QCD} term is modeled as:

$$R_{i,j,k}^{QCD} = K_{ij}^{data} \, S_{ik}^{sim} \,, \tag{8}$$

with i, j, and k the H_T, N_{jet}, and H_T^{miss} bin indices, respectively. In Ref. [17] we used a model in which the H_T, H_T^{miss}, and N_{jet} dependencies in R^{QCD} factorized. For the $N_{jet} = 2$ search regions, introduced for the present study, this factorization is found to be less well justified and we adopt the parameterization of Eq. (8).

The K_{ij}^{data} factors are determined from a maximum likelihood fit to data in a sideband region defined by $250 < H_T^{miss} < 300\,\text{GeV}$ (regions C1, C2, and C3 in Fig. 2). They are the ratio of the number of QCD events in the high-$\Delta\phi$ region to that in the low-$\Delta\phi$ region, where "high $\Delta\phi$" refers to events selected with the standard (noninverted) $\Delta\phi_{H_T^{miss},j_i}$ requirements. The fit accounts for the contributions of top quark, W+jets, and Z+jets events using the results of the methods described in the preceding sections. Uncertainties in K_{ij}^{data} are determined from the covariance matrix of the fit. The S_{ik}^{sim} terms, taken from the QCD simulation, represent corrections to account for the H_T^{miss} dependence of R^{QCD}. Based on studies of the differing contributions of events in which the jet with the largest p_T mismeasurement is or is not amongst the two (for $N_{jet} = 2$), three (for $N_{jet} = 3$), or four (for $N_{jet} \geq 4$) highest p_T jets, uncertainties between 14 and 100% are assigned to the S_{ik}^{sim} terms to account for potential differences between data and simulation. The total uncertainties in S_{ik}^{sim} are defined by the sum in quadrature of the systematic uncertainties and the statistical uncertainties from the simulation.

Figure 7 presents a closure test for the method. An additional systematic uncertainty is included in R^{QCD} to account for the level of nonclosure. Figure 8 shows a comparison between the predictions of the R&S and $\Delta\phi$ methods, which are seen to be consistent. Residual differences between the results from the two methods are negligible compared to the overall uncertainties.
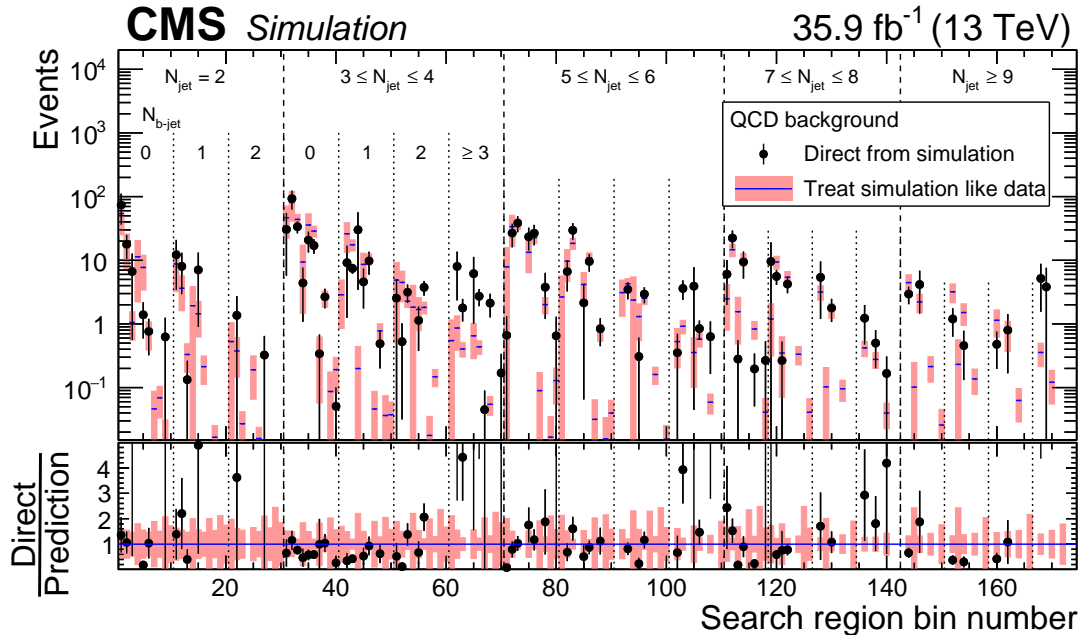
Figure 7: The QCD background in the 174 search regions of the analysis as determined directly from QCD simulation (points, with statistical uncertainties) and as predicted by applying the low-$\Delta\phi$ extrapolation QCD background determination procedure to simulated event samples (histograms, with statistical and systematic uncertainties added in quadrature). Bins without a point have no simulated QCD events in the search region, while bins without a histogram have no simulated QCD events in the corresponding control region. The results in the lower panel are obtained through bin-by-bin division of the results in the upper panel, including the uncertainties, by the central values of the "predicted" results. No result is given in the lower panel if the value of the prediction is zero. The labeling of the bin numbers is the same as in Fig. 3.

8 Results

Figure 9 presents the observed numbers of events in the 174 search regions. The data are shown in comparison with the summed predictions for the SM backgrounds. Numerical values are given in Tables B.1–B.5 of Appendix B. Signal region 126 exhibits a difference of 3.5 standard deviations with respect to the SM expectation. Signal regions 74, 114, and 151 exhibit differences between 2 and 3 standard deviations. The differences for all other signal regions lie below 2 standard deviations. Thus, the evaluated SM background is found to be statistically compatible with the data and we do not obtain evidence for supersymmetry.

In addition to the finely segmented search regions of Fig. 9, we evaluate the background predictions in 12 aggregate regions, determined by summing the results from the nominal search regions while accounting for correlations. The aggregate regions are intended to represent 12 potentially interesting signal topologies. For representative values of the SUSY particle masses, the cross section upper limits from individual aggregate signal regions are found to be around 50–300% larger than those presented below for the full 174 bin fit, with a typical difference of about 100%. Nonetheless, the limits on SUSY particle masses derived using the aggregate regions are generally no more than around 10% lower than those found using the fit based on the 174 regions. While the aggregate regions do not provide as much sensitivity to the presence of new physics as the full set of search regions, they allow our data to be used in a simpler manner for the investigation of signal scenarios not examined in this paper. The aggregate regions, and
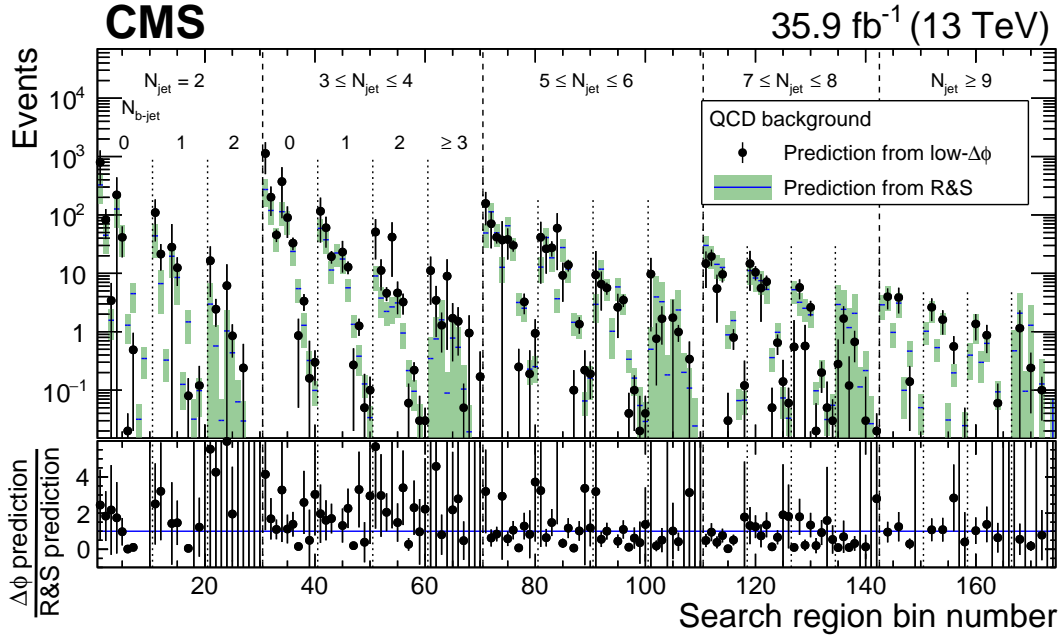
Figure 8: Comparison between the predictions for the number of QCD events in the 174 search regions of the analysis as determined from the rebalance-and-smear (R&S, histograms) and low-$\Delta\phi$ extrapolation (points) methods. For both methods, the error bars indicate the combined statistical and systematic uncertainties. The lower panel shows the ratio of the low-$\Delta\phi$ extrapolation to the R&S results and its propagated uncertainty. The labeling of the bin numbers is the same as in Fig. 3.

the signal topologies they are intended to help probe, are specified in Table 3. The aggregate regions are characterized by their heavy flavor (top or bottom quark) content, parton multiplicity, and the mass difference Δm discussed in Section 6. Aggregate regions 11 and 12 target models with direct top squark production. The results for the aggregate regions are presented in Fig. 10, with numerical values provided in Table B.6 of Appendix B.

In Fig. 11, for purposes of illustration, we present one-dimensional projections of the data and SM predictions in either the H_T^{miss}, N_{jet}, or $N_{\mathrm{b\text{-}jet}}$ variable after imposing criteria, indicated in the legends, to enhance the expected contributions of T1tttt, T1bbbb, T1qqqq, T2tt, T2bb, or T2qq events. In each case, two example signal distributions are shown: one with $\Delta m \gg 0$, and one with $\Delta m \approx 0$, where both example scenarios lie well within the parameter space excluded by the present study.

Limits are evaluated for the production cross sections of the signal scenarios using a likelihood fit, with the SUSY signal strength, the yields of the four classes of background shown in Fig. 9, and various nuisance parameters as fitted parameters, where a nuisance parameter refers to a variable of little physical interest, such as a scale factor in a background determination procedure. The nuisances are constrained in the fit. For the models of gluino (squark) pair production, the limits are derived as a function of $m_{\tilde{g}}$ ($m_{\tilde{q}}$) and $m_{\tilde{\chi}_1^0}$. All 174 search regions are used for each choice of the SUSY particle masses. The likelihood function is given by the product of Poisson probability density functions, one for each search region, and constraints that account for uncertainties in the background predictions and signal yields. These uncertainties are treated as nuisance parameters with log-normal probability density functions. Correlations are taken into account. The signal yield uncertainties associated with the renormalization and factorization scales, ISR, jet energy scale, b jet tagging, pileup, and statistical fluctuations are
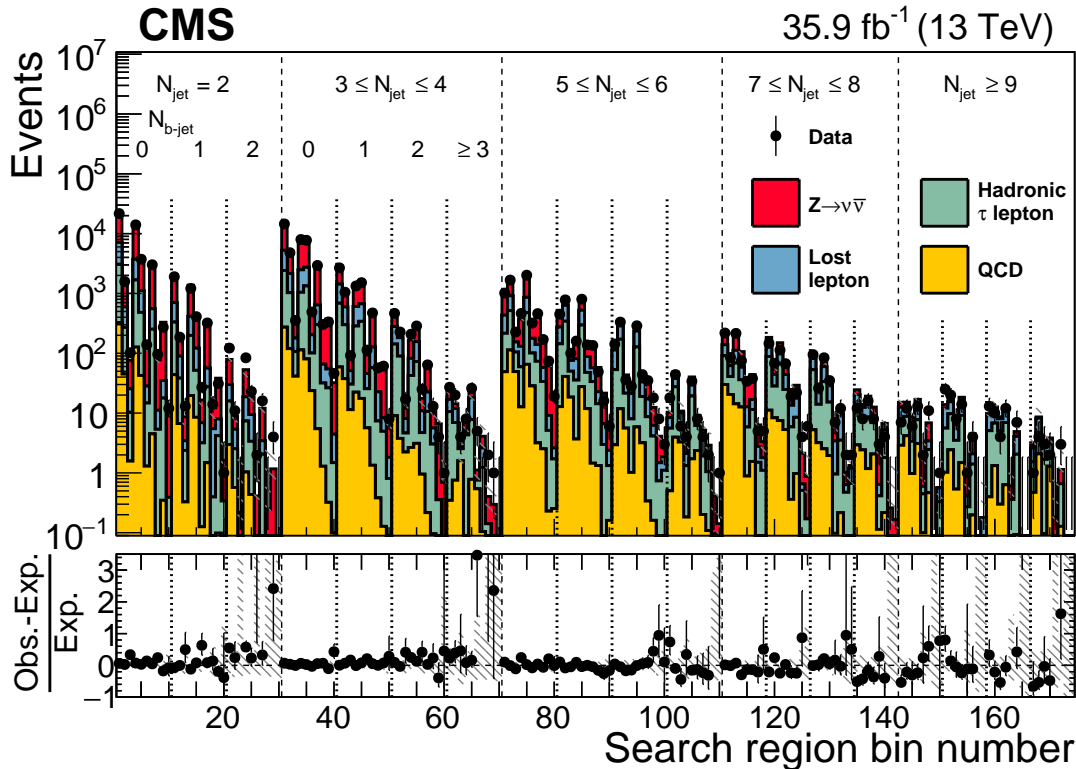
Figure 9: The observed numbers of events and prefit SM background predictions in the 174 search regions of the analysis, where "prefit" means there is no constraint from the likelihood fit. Numerical values are given in Tables B.1–B.5. The hatching indicates the total uncertainty in the background predictions. The lower panel displays the fractional differences between the data and SM predictions. The labeling of the bin numbers is the same as in Fig. 3.

evaluated as a function of $m_{\widetilde{g}}$ and $m_{\widetilde{\chi}_1^0}$, or $m_{\widetilde{q}}$ and $m_{\widetilde{\chi}_1^0}$. The test statistic is $q_\mu = -2 \ln \left(\mathcal{L}_\mu / \mathcal{L}_{\max} \right)$, where $\mathcal{L}_{\max}$ is the maximum likelihood determined by allowing all parameters including the SUSY signal strength μ to vary, and $\mathcal{L}_\mu$ is the maximum likelihood for a fixed signal strength. To set limits, asymptotic results for the test statistic [76] are used, in conjunction with the CL_s criterion described in Refs. [77, 78].

We evaluate 95% confidence level (CL) upper limits on the signal cross sections. The NLO+NLL cross section is used to determine corresponding exclusion curves. When computing the limits, the signal yields are corrected to account for possible signal contamination in the CRs. Beyond the observed exclusion limits, we derive expected exclusion limits by using the expected Poisson fluctuations around the predicted numbers of background events when evaluating the test statistic.

The results for the T1tttt, T1bbbb, T1qqqq, and T5qqqqVV models are shown in the upper and middle rows of Fig. 12. Depending on the value of $m_{\widetilde{\chi}_1^0}$, and using the NLO+NLL cross sections, gluinos with masses as large as 1960, 1950, 1825, and 1800 GeV, respectively, are excluded. These results significantly extend those of our previous study [17], for which the corresponding limits vary between 1440 and 1600 GeV.

The corresponding results for the T1btbt model and for the mixed models of gluino decay to heavy squarks are shown in the lower row of Fig. 12. In this case gluinos with masses as large as 1850 to 1880 GeV are excluded, extending the limits of between 1550 and 1600 GeV presented in Ref. [19]. Note that for the T1btbt model, the acceptance is small for $m_{\widetilde{\chi}_1^0} \lesssim 25$ GeV and we
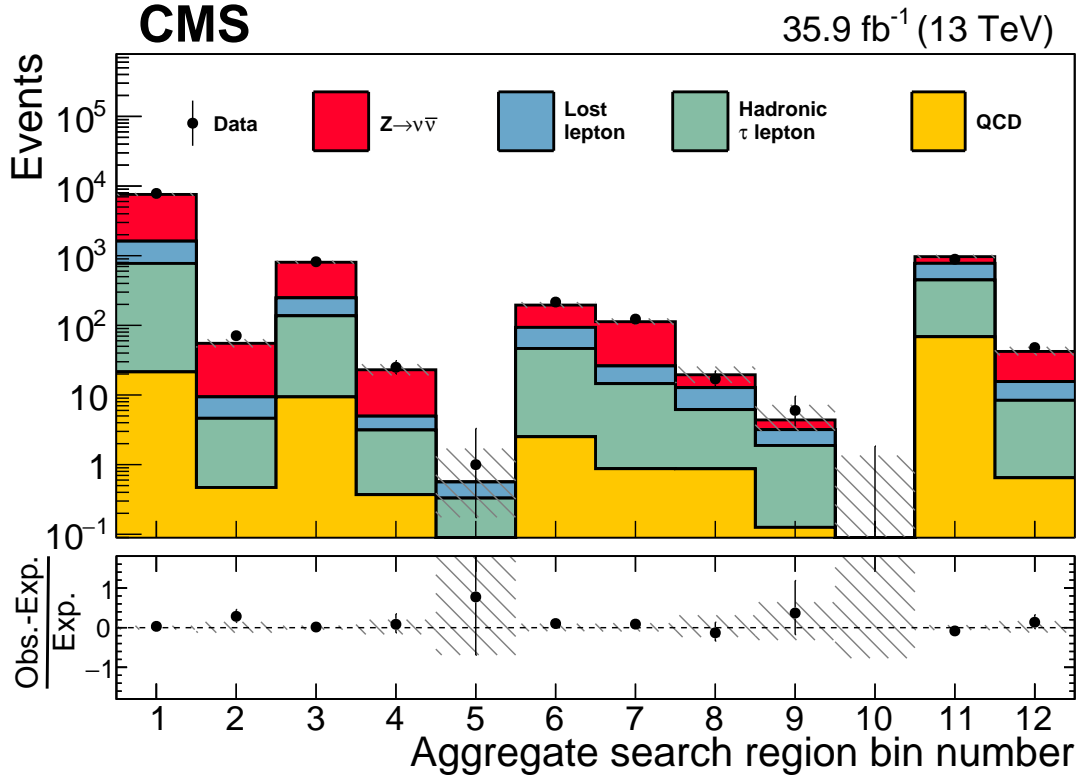
Figure 10: The observed numbers of events and prefit SM background predictions in the 12 aggregate search regions, with fractional differences displayed in the lower panel, where "prefit" means there is no constraint from the likelihood fit. The hatching indicates the total uncertainty in the background predictions. The numerical values are given in Table B.6.

are unable to exclude the scenario. The reason is that as $m_{\tilde{\chi}_1^0}$ approaches zero, the mass of the nearly mass-degenerate $\tilde{\chi}_1^{\pm}$ parent particle also becomes small. The $\tilde{\chi}_1^{\pm}$ becomes highly Lorentz boosted, and more of the momentum from the parent $\tilde{\chi}_1^{\pm}$ is carried by the daughter off-shell W boson [see Fig. 1 (upper right)] and less by the daughter $\tilde{\chi}_1^0$. The net effect is that the H_T^{miss} spectrum becomes softer for hadronic W* decays, leading to reduced signal acceptance, while the charged-lepton or isolated-track p_T spectrum becomes harder for leptonic W* decays, increasing the probability for the event to be vetoed and thus also leading to reduced signal acceptance. Furthermore, jets arising from the W* decay tend to be aligned with the missing transverse momentum from the $\tilde{\chi}_1^0$. When these jets become harder, as $m_{\tilde{\chi}_1^0}$ becomes small, they are more likely to appear amongst the highest p_T jets in the event, causing the event to be rejected by the $\Delta\phi_{H_T^{miss}, j_i}$ requirements. Because of the small signal acceptance for $m_{\tilde{\chi}_1^0} \to 0$, the relative contribution of signal contamination in this region becomes comparable to the true signal content, and a precise determination of the search sensitivity becomes difficult. Therefore, for the T1btbt model, we limit our determination of the cross section upper limit to $m_{\tilde{\chi}_1^0} > 25$ GeV.

Finally, Fig. 13 shows the results for the T2tt, T2bb, and T2qq models. Based on the NLO+NLL cross sections, squarks with masses up to 960, 990, and 1390 GeV, respectively, are excluded. Note that for the T2tt model we do not present cross section upper limits for small values of $m_{\tilde{\chi}_1^0}$ if $m_{\tilde{q}} - m_{\tilde{\chi}_1^0} \approx m_{top}$, corresponding to the unshaded diagonal region at low $m_{\tilde{\chi}_1^0}$ visible in Fig. 13 (upper left). The reason for this is that signal events are essentially indistinguishable from SM $t\bar{t}$ events in this region, rendering the signal event acceptance difficult to model. Note also for
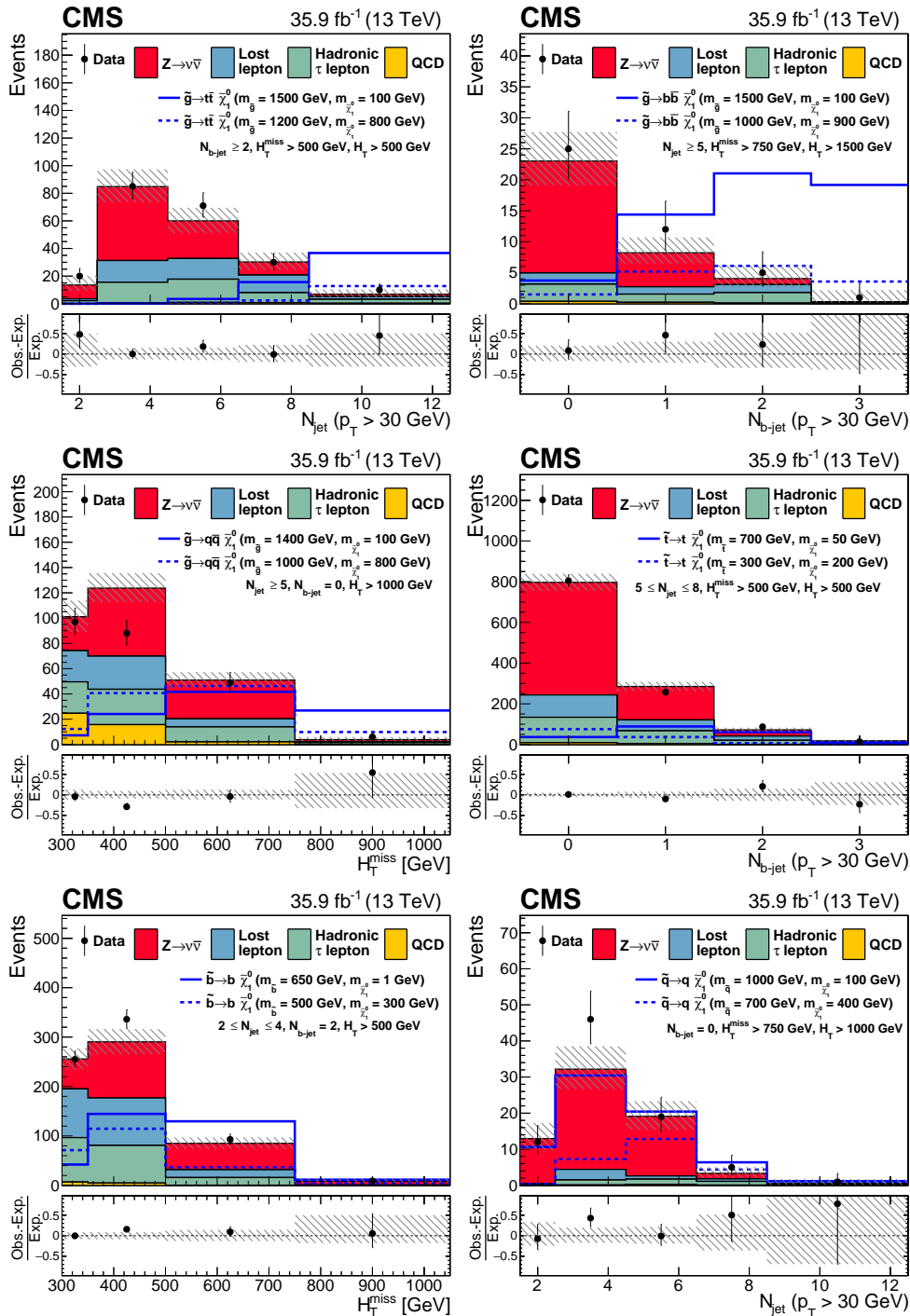
Figure 11: The observed numbers of events and SM background predictions for regions in the search region parameter space particularly sensitive to the production of events in the (upper left) T1tttt, (upper right) T1bbbb, (middle left) T1qqqq, (middle right) T2tt, (lower left) T2bb, and (lower right) T2qq scenarios. The selection requirements are given in the figure legends. The hatched regions indicate the total uncertainties in the background predictions. The (unstacked) results for two example signal scenarios are shown in each instance, one with $\Delta m \gg 0$ and the other with $\Delta m \approx 0$, where Δm is the difference between the gluino or squark mass and the sum of the masses of the particles into which it decays.
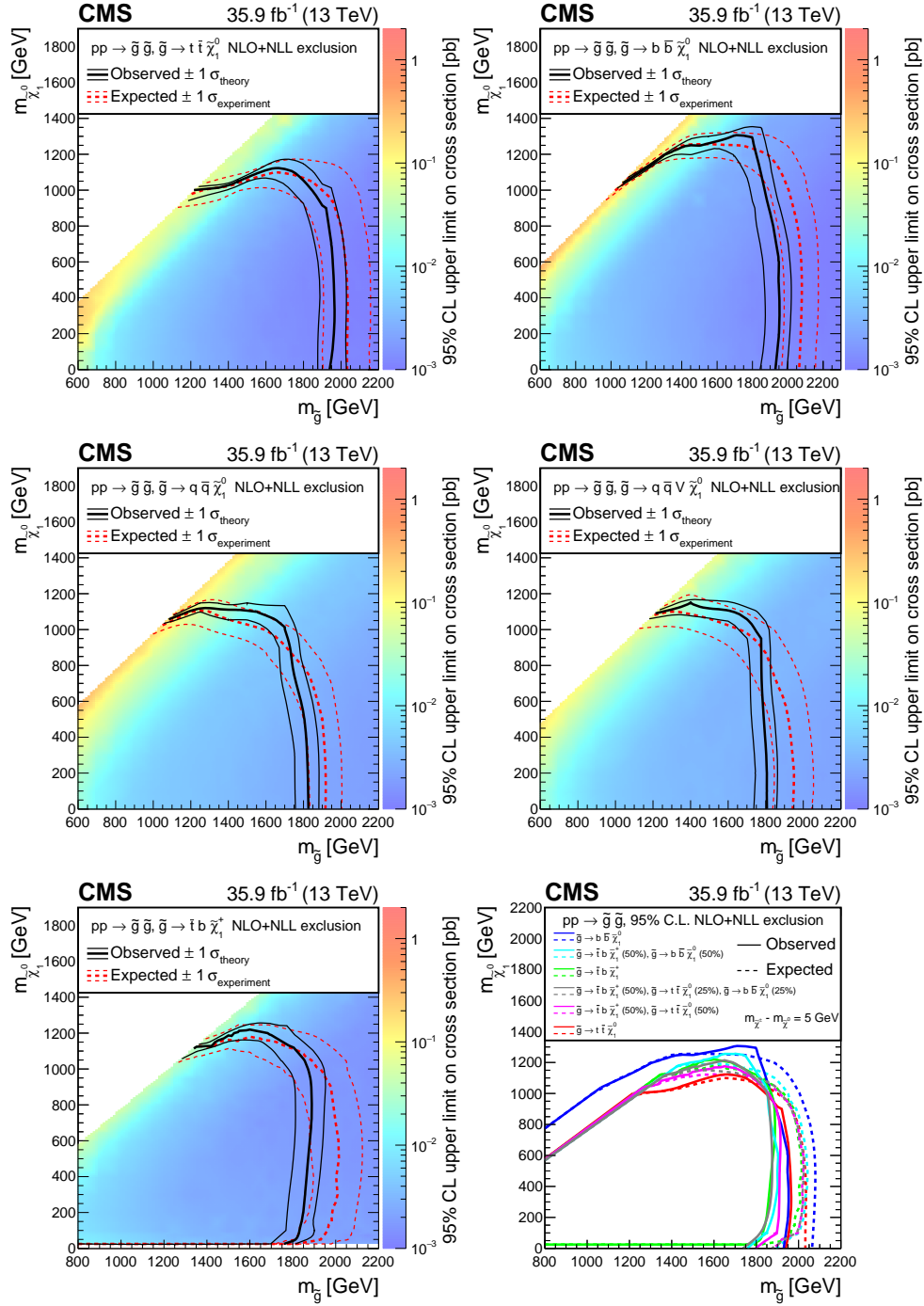
Figure 12: The 95% CL upper limits on the production cross sections for the (upper left) T1tttt, (upper right) T1bbbb, (middle left) T1qqqq, (middle right) T5qqqqVV, and (lower left) T1tbtb simplified models as a function of the gluino and LSP masses $m_{\tilde{g}}$ and $m_{\tilde{\chi}_1^0}$. The thick solid (black) curves show the observed exclusion limits assuming the NLO+NLL cross sections [60–64] and the thin solid (black) curves the change in these limits due to variation of the signal cross sections within their theoretical uncertainties [79]. The thick dashed (red) curves present the expected limits under the background-only hypothesis, while the thin dotted (red) curves indicate the region containing 68% of the distribution of limits expected under this hypothesis. (Lower right) The corresponding 95% NLO+NLL exclusion curves for the mixed models of gluino decays to heavy squarks. For the T1tbtb model, the results are restricted to $m_{\tilde{\chi}_1^0} > 25$ GeV for the reason stated in the text.
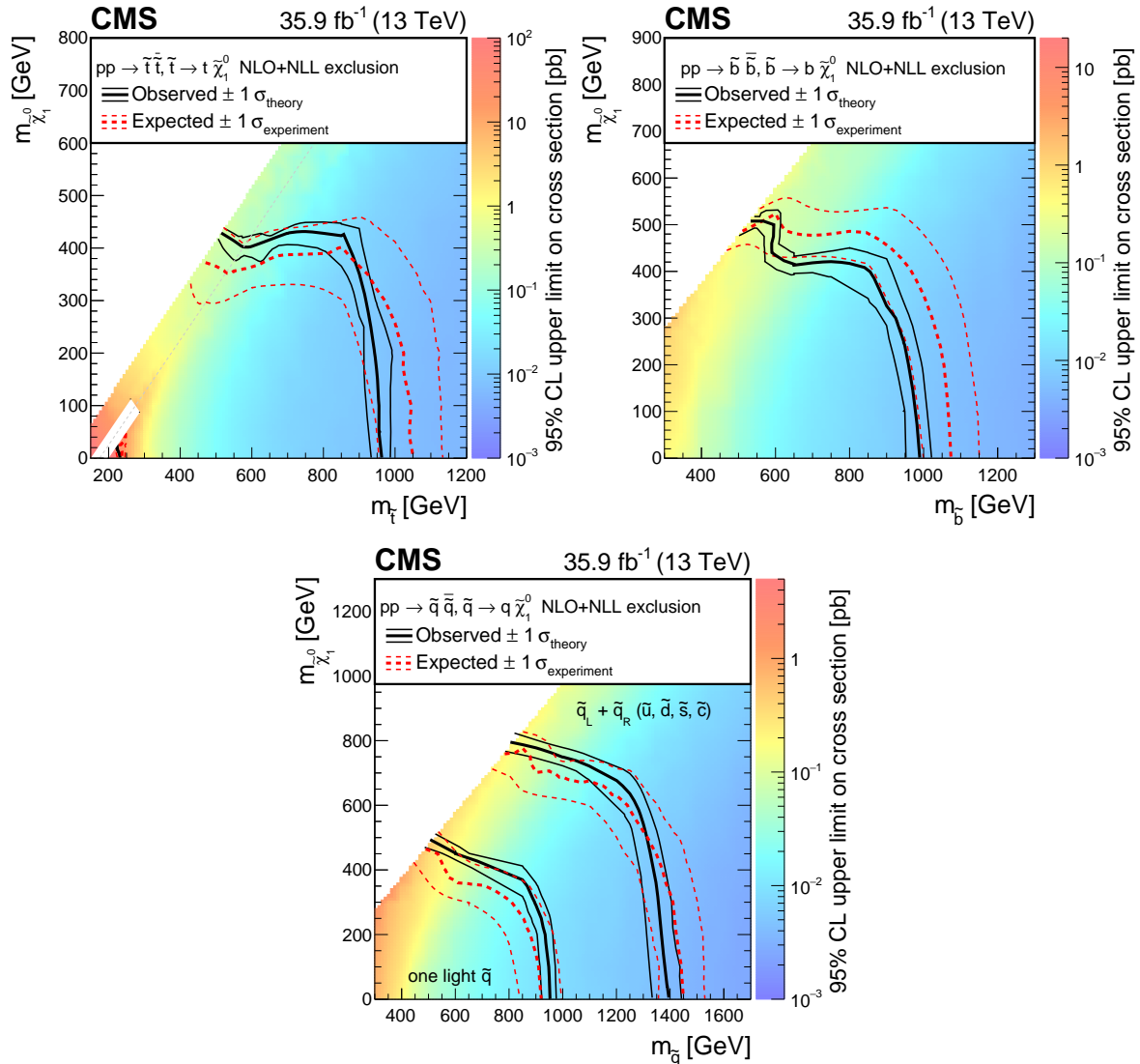
Figure 13: (Left) The 95% CL upper limits on the production cross section for the (upper left) T2tt, (upper right) T2bb, and (lower) T2qq simplified models as a function of the squark and LSP masses $m_{\tilde{q}}$ and $m_{\tilde{\chi}_1^0}$. The diagonal dotted line shown for the T2tt model corresponds to $m_{\tilde{q}} - m_{\tilde{\chi}_1^0} = m_{top}$. Note that for the T2tt model we do not present cross section upper limits in the unshaded diagonal region at low $m_{\tilde{\chi}_1^0}$ for the reasons discussed in the text, and that there is a small region corresponding to $m_{\tilde{t}} \lesssim 230\,\text{GeV}$ and $m_{\tilde{\chi}_1^0} \lesssim 20\,\text{GeV}$ that is not included in the NLO+NLL exclusion region. The results labeled "one light $\tilde{q}$" for the T2qq model are discussed in the text. The meaning of the curves is described in the Fig. 12 caption.

Table 3: Definition of the aggregate search regions. Note that the cross-hatched region in Fig. 2, corresponding to large H_T^{miss} relative to H_T, is excluded from the definition of the aggregate regions.

Region	N_{jet}	$N_{b\text{-}jet}$	H_T [GeV]	H_T^{miss} [GeV]	Parton multiplicity	Heavy flavor ?	Δm
1	≥ 2	0	≥ 500	≥ 500	Low	No	Small
2	≥ 3	0	≥ 1500	≥ 750	Low	No	Large
3	≥ 5	0	≥ 500	≥ 500	Medium	No	Small
4	≥ 5	0	≥ 1500	≥ 750	Medium	No	Large
5	≥ 9	0	≥ 1500	≥ 750	High	No	All
6	≥ 2	≥ 2	≥ 500	≥ 500	Low	Yes	Small
7	≥ 3	≥ 1	≥ 750	≥ 750	Low	Yes	Large
8	≥ 5	≥ 3	≥ 500	≥ 500	Medium	Yes	Small
9	≥ 5	≥ 2	≥ 1500	≥ 750	Medium	Yes	Large
10	≥ 9	≥ 3	≥ 750	≥ 750	High	Yes	All
11	≥ 7	≥ 1	≥ 300	≥ 300	Medium high	Yes	Small
12	≥ 5	≥ 1	≥ 750	≥ 750	Medium	Yes	Large

the T2tt model that there is a small region corresponding to $m_{\tilde{t}} \lesssim 230\,\text{GeV}$ and $m_{\tilde{\chi}_1^0} \lesssim 20\,\text{GeV}$ that is not excluded by the data.

In addition to the main T2qq model, with four mass-degenerate squark flavors (up, down, strange, and charm), each arising from two different quark spin states, Fig. 13 (lower) shows the results should only one of these eight states ("one light $\tilde{q}$") be accessible at the LHC. In this case, the upper limit on the squark mass based on the NLO+NLL cross section is reduced to 950 GeV.

9 Summary

A search for gluino and squark pair production is presented based on a sample of proton-proton collisions collected at a center-of-mass energy of 13 TeV with the CMS detector. The search is performed in the multijet channel, i.e., the visible reconstructed final state consists solely of jets. The data correspond to an integrated luminosity of $35.9\,\text{fb}^{-1}$. Events are required to have at least two jets, $H_T > 300\,\text{GeV}$, and $H_T^{miss} > 300\,\text{GeV}$, where H_T is the scalar sum of jet transverse momenta p_T. The H_T^{miss} variable, used as a measure of missing transverse momentum, is the magnitude of the vector p_T sum of jets. Jets are required to have $p_T > 30\,\text{GeV}$ and to appear in the pseudorapidity range $|\eta| < 2.4$.

The data are examined in 174 exclusive four-dimensional search regions defined by the number of jets, the number of tagged bottom quark jets, H_T, and H_T^{miss}. Background from standard model processes is evaluated using control samples in the data. We also provide results for 12 aggregated search regions, to simplify use of our data by others. The estimates of the standard model background are found to agree with the observed numbers of events for all regions.

The results are interpreted in the context of simplified models. We consider models in which pair-produced gluinos each decay to a $t\bar{t}$ pair and an undetected, stable, lightest-supersymmetric-particle (LSP) neutralino $\tilde{\chi}_1^0$ (T1tttt model); to a $b\bar{b}$ pair and the $\tilde{\chi}_1^0$ (T1bbbb model); to a light-flavored $q\bar{q}$ pair and the $\tilde{\chi}_1^0$ (T1qqqq model); to a light-flavored quark and antiquark and either the second-lightest neutralino $\tilde{\chi}_2^0$ or the lightest chargino $\tilde{\chi}_1^\pm$, followed by decay of the $\tilde{\chi}_2^0$ ($\tilde{\chi}_1^\pm$) to the $\tilde{\chi}_1^0$ and an on- or off-shell Z ($W^\pm$) boson (T5qqqqVV model); or to $\bar{t}b\tilde{\chi}_1^+$ or $t\bar{b}\tilde{\chi}_1^-$, followed by the decay of the $\tilde{\chi}_1^\pm$ to the $\tilde{\chi}_1^0$ and an off-shell W boson (T1tbtb model). To provide more

model independence, we also consider mixed scenarios in which a gluino can decay to $t\bar{t}\widetilde{\chi}_1^0$, $b\bar{b}\widetilde{\chi}_1^0$, $\bar{t}b\widetilde{\chi}_1^+$, or $t\bar{b}\widetilde{\chi}_1^-$ with various probabilities. Beyond the models for gluino production, we examine models for direct squark pair production. We consider scenarios in which each squark decays to a top quark and the $\widetilde{\chi}_1^0$ (T2tt model); to a bottom quark and the $\widetilde{\chi}_1^0$ (T2bb model); or to a light-flavored (u, d, s, c) quark and the $\widetilde{\chi}_1^0$ (T2qq model). We derive upper limits at 95% confidence level on the model cross sections as a function of the gluino and LSP masses, or of the squark and LSP masses.

Using the predicted cross sections with next-to-leading-order plus next-to-leading-logarithm accuracy as a reference, 95% confidence level lower limits on the gluino mass as large as 1800 to 1960 GeV are derived, depending on the scenario. The corresponding limits on the mass of directly produced squarks range from 960 to 1390 GeV. These results extend those from previous searches.

Acknowledgments

References

[1] R. Barbieri and G. F. Giudice, "Upper bounds on supersymmetric particle masses", *Nucl. Phys. B* **306** (1988) 63, `doi:10.1016/0550-3213(88)90171-X`.

[2] ATLAS and CMS Collaborations, "Combined measurement of the Higgs boson mass in pp collisions at $\sqrt{s} = 7$ and 8 TeV with the ATLAS and CMS experiments", *Phys. Rev. Lett.* **114** (2015) 191803, `doi:10.1103/PhysRevLett.114.191803`, `arXiv:1503.07589`.

[3] P. Ramond, "Dual theory for free fermions", *Phys. Rev. D* **3** (1971) 2415, `doi:10.1103/PhysRevD.3.2415`.

[4] Y. A. Golfand and E. P. Likhtman, "Extension of the algebra of Poincaré group generators and violation of P invariance", *JETP Lett.* **13** (1971) 323.

[5] A. Neveu and J. H. Schwarz, "Factorizable dual model of pions", *Nucl. Phys. B* **31** (1971) 86, `doi:10.1016/0550-3213(71)90448-2`.

[6] D. V. Volkov and V. P. Akulov, "Possible universal neutrino interaction", *JETP Lett.* **16** (1972) 438.

[7] J. Wess and B. Zumino, "A Lagrangian model invariant under supergauge transformations", *Phys. Lett. B* **49** (1974) 52, `doi:10.1016/0370-2693(74)90578-4`.

[8] J. Wess and B. Zumino, "Supergauge transformations in four dimensions", *Nucl. Phys. B* **70** (1974) 39, `doi:10.1016/0550-3213(74)90355-1`.

[9] P. Fayet, "Supergauge invariant extension of the Higgs mechanism and a model for the electron and its neutrino", *Nucl. Phys. B* **90** (1975) 104, `doi:10.1016/0550-3213(75)90636-7`.

[10] H. P. Nilles, "Supersymmetry, supergravity and particle physics", *Phys. Rep.* **110** (1984) 1, `doi:10.1016/0370-1573(84)90008-5`.

[11] S. Dimopoulos and G. F. Giudice, "Naturalness constraints in supersymmetric theories with nonuniversal soft terms", *Phys. Lett. B* **357** (1995) 573, `doi:10.1016/0370-2693(95)00961-J`, `arXiv:hep-ph/9507282`.

[12] R. Barbieri and D. Pappadopulo, "S-particles at their naturalness limits", *JHEP* **10** (2009) 061, `doi:10.1088/1126-6708/2009/10/061`, `arXiv:0906.4546`.

[13] M. Papucci, J. T. Ruderman, and A. Weiler, "Natural SUSY endures", *JHEP* **09** (2012) 035, `doi:10.1007/JHEP09(2012)035`, `arXiv:1110.6926`.

[14] G. R. Farrar and P. Fayet, "Phenomenology of the production, decay, and detection of new hadronic states associated with supersymmetry", *Phys. Lett. B* **76** (1978) 575, `doi:10.1016/0370-2693(78)90858-4`.

[15] ATLAS Collaboration, "Search for pair production of gluinos decaying via stop and sbottom in events with b-jets and large missing transverse momentum in pp collisions at $\sqrt{s} = 13$ TeV with the ATLAS detector", *Phys. Rev. D* **94** (2016) 032003, `doi:10.1103/PhysRevD.94.032003`, `arXiv:1605.09318`.

[16] ATLAS Collaboration, "Search for squarks and gluinos in final states with jets and missing transverse momentum at $\sqrt{s} = 13$ TeV with the ATLAS detector", *Eur. Phys. J. C* **76** (2016) 392, `doi:10.1140/epjc/s10052-016-4184-8`, `arXiv:1605.03814`.

[17] CMS Collaboration, "Search for supersymmetry in the multijet and missing transverse momentum final state in pp collisions at 13 TeV", *Phys. Lett. B* **758** (2016) 152, `doi:10.1016/j.physletb.2016.05.002`, `arXiv:1602.06581`.

[18] CMS Collaboration, "Search for new physics with the M_{T2} variable in all-jets final states produced in pp collisions at $\sqrt{s} = 13$ TeV", *JHEP* **10** (2016) 006, `doi:10.1007/JHEP10(2016)006`, `arXiv:1603.04053`.

[19] CMS Collaboration, "Inclusive search for supersymmetry using razor variables in pp collisions at $\sqrt{s} = 13$ TeV", *Phys. Rev. D* **95** (2017) 012003, `doi:10.1103/PhysRevD.95.012003`, `arXiv:1609.07658`.

[20] CMS Collaboration, "A search for new phenomena in pp collisions at $\sqrt{s} = 13$ TeV in final states with missing transverse momentum and at least one jet using the α_T variable", *Eur. Phys. J. C* **77** (2017) 294, `doi:10.1140/epjc/s10052-017-4787-8`, `arXiv:1611.00338`.

[21] CMS Collaboration, "Search for new physics with jets and missing transverse momentum in pp collisions at $\sqrt{s} = 7$ TeV", *JHEP* **08** (2011) 155, `doi:10.1007/JHEP08(2011)155`, `arXiv:1106.4503`.

[22] CMS Collaboration, "Search for new physics in the multijet and missing transverse momentum final state in proton-proton collisions at $\sqrt{s} = 8$ TeV", *JHEP* **06** (2014) 055, `doi:10.1007/JHEP06(2014)055`, `arXiv:1402.4770`.

[23] N. Arkani-Hamed et al., "MARMOSET: The path from LHC data to the new standard model via on-shell effective theories", (2007). `arXiv:hep-ph/0703088`.

[24] J. Alwall, P. C. Schuster, and N. Toro, "Simplified models for a first characterization of new physics at the LHC", *Phys. Rev. D* **79** (2009) 075020, `doi:10.1103/PhysRevD.79.075020`, `arXiv:0810.3921`.

[25] J. Alwall, M.-P. Le, M. Lisanti, and J. G. Wacker, "Model-independent jets plus missing energy searches", *Phys. Rev. D* **79** (2009) 015005, `doi:10.1103/PhysRevD.79.015005`, `arXiv:0809.3264`.

[26] D. Alves et al., "Simplified models for LHC new physics searches", *J. Phys. G* **39** (2012) 105005, `doi:10.1088/0954-3899/39/10/105005`, `arXiv:1105.2838`.

[27] CMS Collaboration, "Interpretation of searches for supersymmetry with simplified models", *Phys. Rev. D* **88** (2013) 052017, `doi:10.1103/PhysRevD.88.052017`, `arXiv:1301.2175`.

[28] CMS Collaboration, "The CMS experiment at the CERN LHC", *JINST* **3** (2008) S08004, `doi:10.1088/1748-0221/3/08/S08004`.

[29] CMS Collaboration, "The CMS trigger system", *JINST* **12** (2017) P01020, `doi:10.1088/1748-0221/12/01/P01020`, `arXiv:1609.02366`.

[30] CMS Collaboration, "Particle-flow reconstruction and global event description with the CMS detector", (2017). `arXiv:1706.04965`. Submitted to *JINST*.

[31] CMS Collaboration, "Performance of electron reconstruction and selection with the CMS detector in proton-proton collisions at $\sqrt{s} = 8$ TeV", *JINST* **10** (2015) P06005, `doi:10.1088/1748-0221/10/06/P06005`, `arXiv:1502.02701`.

[32] CMS Collaboration, "The performance of the CMS muon detector in proton-proton collisions at $\sqrt{s} = 7$ TeV at the LHC", *JINST* **8** (2013) P11002, `doi:10.1088/1748-0221/8/11/P11002`, `arXiv:1306.6905`.

[33] M. Cacciari, G. P. Salam, and G. Soyez, "The anti-k_t jet clustering algorithm", *JHEP* **04** (2008) 063, `doi:10.1088/1126-6708/2008/04/063`, `arXiv:0802.1189`.

[34] M. Cacciari, G. P. Salam, and G. Soyez, "FastJet user manual", *Eur. Phys. J. C* **72** (2012) 1896, `doi:10.1140/epjc/s10052-012-1896-2`, `arXiv:1111.6097`.

[35] M. Cacciari and G. P. Salam, "Pileup subtraction using jet areas", *Phys. Lett. B* **659** (2008) 119, `doi:10.1016/j.physletb.2007.09.077`, `arXiv:0707.1378`.

[36] K. Rehermann and B. Tweedie, "Efficient identification of boosted semileptonic top quarks at the LHC", *JHEP* **03** (2011) 059, `doi:10.1007/JHEP03(2011)059`, `arXiv:1007.2221`.

[37] CMS Collaboration, "Jet performance in pp collisions at $\sqrt{s} = 7$ tev", CMS Physics Analysis Summary CMS-PAS-JME-10-003, CERN, 2010.

[38] CMS Collaboration, "Jet energy scale and resolution in the CMS experiment in pp collisions at 8 TeV", *JINST* **12** (2017) P02014, `doi:10.1088/1748-0221/12/02/P02014`, `arXiv:1607.03663`.

[39] CMS Collaboration, "Identification of b quark jets at the CMS experiment in the lhc run 2", CMS Physics Analysis Summary CMS-PAS-BTV-15-001, CERN, 2016.

[40] UA1 Collaboration, "Experimental observation of isolated large transverse energy electrons with associated missing energy at $\sqrt{s} = 540$ GeV", *Phys. Lett. B* **122** (1983) 103, `doi:10.1016/0370-2693(83)91177-2`.

[41] CMS Collaboration, "Performance of missing energy reconstruction in 13 TeV pp collision data using the CMS detector", CMS Physics Analysis Summary CMS-PAS-JME-16-004, CERN, 2016.

[42] J. Alwall et al., "The automated computation of tree-level and next-to-leading order differential cross sections, and their matching to parton shower simulations", *JHEP* **07** (2014) 079, `doi:10.1007/JHEP07(2014)079`, `arXiv:1405.0301`.

[43] J. Alwall et al., "Comparative study of various algorithms for the merging of parton showers and matrix elements in hadronic collisions", *Eur. Phys. J. C* **53** (2008) 473, `doi:10.1140/epjc/s10052-007-0490-5`, `arXiv:0706.2569`.

[44] R. Frederix and S. Frixione, "Merging meets matching in MC@NLO", *JHEP* **12** (2012) 061, `doi:10.1007/JHEP12(2012)061`, `arXiv:1209.6215`.

[45] P. Nason, "A new method for combining NLO QCD with shower Monte Carlo algorithms", *JHEP* **11** (2004) 040, `doi:10.1088/1126-6708/2004/11/040`, `arXiv:hep-ph/0409146`.

[46] S. Frixione, P. Nason, and C. Oleari, "Matching NLO QCD computations with Parton Shower simulations: the POWHEG method", *JHEP* **11** (2007) 070, `doi:10.1088/1126-6708/2007/11/070`, `arXiv:0709.2092`.

[47] S. Alioli, P. Nason, C. Oleari, and E. Re, "A general framework for implementing NLO calculations in shower Monte Carlo programs: the POWHEG BOX", *JHEP* **06** (2010) 043, `doi:10.1007/JHEP06(2010)043`, `arXiv:1002.2581`.

[48] S. Alioli, P. Nason, C. Oleari, and E. Re, "NLO single-top production matched with shower in POWHEG: *s*- and *t*-channel contributions", *JHEP* **09** (2009) 111, `doi:10.1088/1126-6708/2009/09/111`, `arXiv:0907.4076`. [Erratum: `doi:10.1007/JHEP02(2010)011`].

[49] E. Re, "Single-top *Wt*-channel production matched with parton showers using the POWHEG method", *Eur. Phys. J. C* **71** (2011) 1547, `doi:10.1140/epjc/s10052-011-1547-z`, `arXiv:1009.2450`.

[50] GEANT4 Collaboration, "GEANT4—a simulation toolkit", *Nucl. Instrum. Meth. A* **506** (2003) 250, `doi:10.1016/S0168-9002(03)01368-8`.

[51] T. Melia, P. Nason, R. Rontsch, and G. Zanderighi, "W^+W^-, WZ and ZZ production in the POWHEG BOX", *JHEP* **11** (2011) 078, `doi:10.1007/JHEP11(2011)078`, `arXiv:1107.5051`.

[52] M. Beneke, P. Falgari, S. Klein, and C. Schwinn, "Hadronic top-quark pair production with NNLL threshold resummation", *Nucl. Phys. B* **855** (2012) 695, `doi:10.1016/j.nuclphysb.2011.10.021`, `arXiv:1109.1536`.

[53] M. Cacciari et al., "Top-pair production at hadron colliders with next-to-next-to-leading logarithmic soft-gluon resummation", *Phys. Lett. B* **710** (2012) 612, `doi:10.1016/j.physletb.2012.03.013`, `arXiv:1111.5869`.

[54] P. Bärnreuther, M. Czakon, and A. Mitov, "Percent-level-precision physics at the Tevatron: Next-to-next-to-leading order QCD corrections to $q\bar{q} \to t\bar{t} + X$", *Phys. Rev. Lett.* **109** (2012) 132001, `doi:10.1103/PhysRevLett.109.132001`, `arXiv:1204.5201`.

[55] M. Czakon and A. Mitov, "NNLO corrections to top-pair production at hadron colliders: the all-fermionic scattering channels", *JHEP* **12** (2012) 054, `doi:10.1007/JHEP12(2012)054`, `arXiv:1207.0236`.

[56] M. Czakon and A. Mitov, "NNLO corrections to top pair production at hadron colliders: the quark-gluon reaction", *JHEP* **01** (2013) 080, `doi:10.1007/JHEP01(2013)080`, `arXiv:1210.6832`.

[57] M. Czakon, P. Fiedler, and A. Mitov, "Total top-quark pair-production cross section at hadron colliders through $O(\alpha_S^4)$", *Phys. Rev. Lett.* **110** (2013) 252004, `doi:10.1103/PhysRevLett.110.252004`, `arXiv:1303.6254`.

[58] R. Gavin, Y. Li, F. Petriello, and S. Quackenbush, "W Physics at the LHC with FEWZ 2.1", *Comput. Phys. Commun.* **184** (2013) 208, `doi:10.1016/j.cpc.2012.09.005`, `arXiv:1201.5896`.

[59] R. Gavin, Y. Li, F. Petriello, and S. Quackenbush, "FEWZ 2.0: A code for hadronic Z production at next-to-next-to-leading order", *Comput. Phys. Commun.* **182** (2011) 2388, `doi:10.1016/j.cpc.2011.06.008`, `arXiv:1011.3540`.

[60] W. Beenakker, R. Höpker, M. Spira, and P. M. Zerwas, "Squark and gluino production at hadron colliders", *Nucl. Phys. B* **492** (1997) 51, `doi:10.1016/S0550-3213(97)00084-9`, `arXiv:hep-ph/9610490`.

[61] A. Kulesza and L. Motyka, "Threshold resummation for squark-antisquark and gluino-pair production at the LHC", *Phys. Rev. Lett.* **102** (2009) 111802, `doi:10.1103/PhysRevLett.102.111802`, `arXiv:0807.2405`.

[62] A. Kulesza and L. Motyka, "Soft gluon resummation for the production of gluino-gluino and squark-antisquark pairs at the LHC", *Phys. Rev. D* **80** (2009) 095004, `doi:10.1103/PhysRevD.80.095004`, `arXiv:0905.4749`.

[63] W. Beenakker et al., "Soft-gluon resummation for squark and gluino hadroproduction", *JHEP* **12** (2009) 041, `doi:10.1088/1126-6708/2009/12/041`, `arXiv:0909.4418`.

[64] W. Beenakker et al., "Squark and gluino hadroproduction", *Int. J. Mod. Phys. A* **26** (2011) 2637, `doi:10.1142/S0217751X11053560`, `arXiv:1105.1110`.

[65] T. Sjöstrand et al., "An introduction to PYTHIA 8.2", *Comput. Phys. Commun.* **191** (2015) 159, `doi:10.1016/j.cpc.2015.01.024`, `arXiv:1410.3012`.

[66] CMS Collaboration, "Fast simulation of the CMS detector", *J. Phys. Conf. Ser.* **219** (2010) 032053, `doi:10.1088/1742-6596/219/3/032053`.

[67] CMS Collaboration, "Comparison of the fast simulation of CMS with the first LHC data", CMS Detector Performance Summary CMS-DP-2010-039, CERN, 2010.

[68] NNPDF Collaboration, "Parton distributions for the LHC Run II", *JHEP* **04** (2015) 040, `doi:10.1007/JHEP04(2015)040`, `arXiv:1410.8849`.

[69] S. Catani, D. de Florian, M. Grazzini, and P. Nason, "Soft gluon resummation for Higgs boson production at hadron colliders", *JHEP* **07** (2003) 028, `doi:10.1088/1126-6708/2003/07/028`, `arXiv:hep-ph/0306211`.

[70] M. Cacciari et al., "The $t\bar{t}$ cross-section at 1.8 TeV and 1.96 TeV: a study of the systematics due to parton densities and scale dependence", *JHEP* **04** (2004) 068, `doi:10.1088/1126-6708/2004/04/068`, `arXiv:hep-ph/0303085`.

[71] CMS Collaboration, "CMS luminosity measurements for the 2016 data taking period", CMS Physics Analysis Summary CMS-PAS-LUM-17-001, CERN, 2017.

[72] CMS Collaboration, "Search for new physics in the multijet and missing transverse momentum final state in proton-proton collisions at $\sqrt{s} = 7$ TeV", *Phys. Rev. Lett.* **109** (2012) 171803, `doi:10.1103/PhysRevLett.109.171803`, `arXiv:1207.1898`.

[73] Particle Data Group, C. Patrignani et al., "Review of particle physics", *Chin. Phys. C* **40** (2016) 100001, `doi:10.1088/1674-1137/40/10/100001`.

[74] CMS Collaboration, "Observation of top quark pairs produced in association with a vector boson in pp collisions at $\sqrt{s} = 8$ TeV", *JHEP* **01** (2016) 096, `doi:10.1007/JHEP01(2016)096`, `arXiv:1510.01131`.

[75] CMS Collaboration, "Search for gluino mediated bottom- and top-squark production in multijet final states in pp collisions at 8 TeV", *Phys. Lett. B* **725** (2013) 243, `doi:10.1016/j.physletb.2013.06.058`, `arXiv:1305.2390`.

[76] G. Cowan, K. Cranmer, E. Gross, and O. Vitells, "Asymptotic formulae for likelihood-based tests of new physics", *Eur. Phys. J. C* **71** (2011) 1554, `doi:10.1140/epjc/s10052-011-1554-0`, `arXiv:1007.1727`. [Erratum: `doi:10.1140/epjc/s10052-013-2501-z`].

[77] T. Junk, "Confidence level computation for combining searches with small statistics", *Nucl. Instrum. Meth. A* **434** (1999) 435, `doi:10.1016/S0168-9002(99)00498-2`, `arXiv:hep-ex/9902006`.

[78] A. L. Read, "Presentation of search results: the CL_s technique", *J. Phys. G* **28** (2002) 2693, `doi:10.1088/0954-3899/28/10/313`.

[79] C. Borschensky et al., "Squark and gluino production cross sections in pp collisions at $\sqrt{s}$ = 13, 14, 33 and 100 TeV", *Eur. Phys. J. C* **74** (2014) 3174, `doi:10.1140/epjc/s10052-014-3174-y`, `arXiv:1407.5066`.

A Selection efficiency for representative signal models

Tables A.1 and A.2 present cumulative selection efficiencies for representative simplified models of gluino and squark pair production, respectively.

Table A.1: Absolute cumulative efficiencies in % for each step of the event selection process for representative models of gluino pair production. The uncertainties are statistical. Uncertainties reported as 0.0 correspond to values less than 0.05%.

Selection	$pp \to \widetilde{g}\widetilde{g}, \widetilde{g} \to t\bar{t}\widetilde{\chi}_1^0$ $m_{\widetilde{g}} = 1500\,\text{GeV}$ $m_{\widetilde{\chi}_1^0} = 100\,\text{GeV}$	$pp \to \widetilde{g}\widetilde{g}, \widetilde{g} \to b\bar{b}\widetilde{\chi}_1^0$ $m_{\widetilde{g}} = 1500\,\text{GeV}$ $m_{\widetilde{\chi}_1^0} = 100\,\text{GeV}$	$pp \to \widetilde{g}\widetilde{g}, \widetilde{g} \to q\bar{q}\widetilde{\chi}_1^0$ $m_{\widetilde{g}} = 1400\,\text{GeV}$ $m_{\widetilde{\chi}_1^0} = 100\,\text{GeV}$
$N_{\text{jet}} \geq 2$	100.0 ± 0.0	100.0 ± 0.0	100.0 ± 0.0
$H_{\text{T}} > 300\,\text{GeV}$	100.0 ± 0.0	100.0 ± 0.0	100.0 ± 0.0
$H_{\text{T}}^{\text{miss}} > 300\,\text{GeV}$	76.7 ± 0.3	80.3 ± 0.4	80.0 ± 0.3
$N_{\text{muon}} = 0$	48.6 ± 0.4	79.8 ± 0.4	80.0 ± 0.3
$N_{\text{isolated tracks}}^{(\text{muon})} = 0$	47.8 ± 0.4	79.6 ± 0.4	79.9 ± 0.3
$N_{\text{electron}} = 0$	30.7 ± 0.3	79.2 ± 0.4	79.5 ± 0.3
$N_{\text{isolated tracks}}^{(\text{electron})} = 0$	29.7 ± 0.3	78.7 ± 0.4	79.1 ± 0.3
$N_{\text{isolated tracks}}^{(\text{hadron})} = 0$	28.3 ± 0.3	78.0 ± 0.4	78.3 ± 0.3
$\Delta\phi_{H_{\text{T}}^{\text{miss}},j_1} > 0.5$	27.7 ± 0.3	76.7 ± 0.4	76.9 ± 0.3
$\Delta\phi_{H_{\text{T}}^{\text{miss}},j_2} > 0.5$	25.2 ± 0.3	69.2 ± 0.5	69.8 ± 0.3
$\Delta\phi_{H_{\text{T}}^{\text{miss}},j_3} > 0.3$	23.7 ± 0.3	63.9 ± 0.5	64.4 ± 0.3
$\Delta\phi_{H_{\text{T}}^{\text{miss}},j_4} > 0.3$	22.1 ± 0.3	58.6 ± 0.5	59.4 ± 0.3
Event quality filter	21.8 ± 0.3	57.7 ± 0.5	58.7 ± 0.3
Selection	$pp \to \widetilde{g}\widetilde{g}, \widetilde{g} \to t\bar{t}\widetilde{\chi}_1^0$ $m_{\widetilde{g}} = 1200\,\text{GeV}$ $m_{\widetilde{\chi}_1^0} = 800\,\text{GeV}$	$pp \to \widetilde{g}\widetilde{g}, \widetilde{g} \to b\bar{b}\widetilde{\chi}_1^0$ $m_{\widetilde{g}} = 1000\,\text{GeV}$ $m_{\widetilde{\chi}_1^0} = 900\,\text{GeV}$	$pp \to \widetilde{g}\widetilde{g}, \widetilde{g} \to q\bar{q}\widetilde{\chi}_1^0$ $m_{\widetilde{g}} = 1000\,\text{GeV}$ $m_{\widetilde{\chi}_1^0} = 800\,\text{GeV}$
$N_{\text{jet}} \geq 2$	100.0 ± 0.0	92.5 ± 0.1	99.6 ± 0.0
$H_{\text{T}} > 300\,\text{GeV}$	99.0 ± 0.0	38.6 ± 0.1	81.3 ± 0.1
$H_{\text{T}}^{\text{miss}} > 300\,\text{GeV}$	14.9 ± 0.1	14.1 ± 0.1	19.1 ± 0.1
$N_{\text{muon}} = 0$	9.6 ± 0.1	13.9 ± 0.1	19.1 ± 0.1
$N_{\text{isolated tracks}}^{(\text{muon})} = 0$	9.2 ± 0.1	13.6 ± 0.1	19.1 ± 0.1
$N_{\text{electron}} = 0$	6.2 ± 0.1	13.4 ± 0.1	19.0 ± 0.1
$N_{\text{isolated tracks}}^{(\text{electron})} = 0$	5.8 ± 0.1	13.1 ± 0.1	18.8 ± 0.1
$N_{\text{isolated tracks}}^{(\text{hadron})} = 0$	5.3 ± 0.1	12.8 ± 0.1	18.4 ± 0.1
$\Delta\phi_{H_{\text{T}}^{\text{miss}},j_1} > 0.5$	5.3 ± 0.1	12.8 ± 0.1	18.4 ± 0.1
$\Delta\phi_{H_{\text{T}}^{\text{miss}},j_2} > 0.5$	4.5 ± 0.1	11.4 ± 0.1	16.9 ± 0.1
$\Delta\phi_{H_{\text{T}}^{\text{miss}},j_3} > 0.3$	4.0 ± 0.1	10.4 ± 0.1	15.8 ± 0.1
$\Delta\phi_{H_{\text{T}}^{\text{miss}},j_4} > 0.3$	3.6 ± 0.1	9.6 ± 0.1	14.8 ± 0.1
Event quality filter	3.5 ± 0.1	9.4 ± 0.1	14.6 ± 0.1

B Prefit background predictions

Tables B.1–B.5 present the prefit predictions for the number of standard model background events in each of the 174 search regions of the analysis, along with the observed numbers of events, where "prefit" means there is no constraint from the likelihood fit. The corresponding information for the 12 aggregate search regions is presented in Table B.6.

Table A.2: Absolute cumulative efficiencies in % for each step of the event selection process for representative models of squark pair production. The uncertainties are statistical. Uncertainties reported as 0.0 correspond to values less than 0.05%.

Selection	$pp \to \widetilde{t}\overline{\widetilde{t}}, \widetilde{t} \to t\widetilde{\chi}_1^0$ $m_{\widetilde{t}} = 700\,\text{GeV}$ $m_{\widetilde{\chi}_1^0} = 50\,\text{GeV}$	$pp \to \widetilde{b}\overline{\widetilde{b}}, \widetilde{b} \to b\widetilde{\chi}_1^0$ $m_{\widetilde{b}} = 650\,\text{GeV}$ $m_{\widetilde{\chi}_1^0} = 1\,\text{GeV}$	$pp \to \widetilde{q}\overline{\widetilde{q}}, \widetilde{q} \to q\widetilde{\chi}_1^0$ $m_{\widetilde{q}} = 1000\,\text{GeV}$ $m_{\widetilde{\chi}_1^0} = 100\,\text{GeV}$
$N_\text{jet} \geq 2$	99.8 ± 0.0	98.2 ± 0.1	98.9 ± 0.1
$H_\text{T} > 300\,\text{GeV}$	96.4 ± 0.1	95.4 ± 0.1	98.6 ± 0.1
$H_\text{T}^\text{miss} > 300\,\text{GeV}$	57.8 ± 0.3	59.8 ± 0.2	80.0 ± 0.3
$N_\text{muon} = 0$	46.6 ± 0.3	59.6 ± 0.2	79.9 ± 0.3
$N_\text{isolated tracks}^\text{(muon)} = 0$	46.1 ± 0.3	59.5 ± 0.2	79.8 ± 0.3
$N_\text{electron} = 0$	37.4 ± 0.3	59.2 ± 0.2	79.6 ± 0.3
$N_\text{isolated tracks}^\text{(electron)} = 0$	36.9 ± 0.3	59.0 ± 0.2	79.3 ± 0.3
$N_\text{isolated tracks}^\text{(hadron)} = 0$	35.8 ± 0.3	58.5 ± 0.2	78.7 ± 0.3
$\Delta\phi_{H_\text{T}^\text{miss}, j_1} > 0.5$	35.7 ± 0.3	58.4 ± 0.2	78.6 ± 0.3
$\Delta\phi_{H_\text{T}^\text{miss}, j_2} > 0.5$	34.0 ± 0.3	55.7 ± 0.2	74.5 ± 0.3
$\Delta\phi_{H_\text{T}^\text{miss}, j_3} > 0.3$	33.1 ± 0.3	53.3 ± 0.2	70.6 ± 0.3
$\Delta\phi_{H_\text{T}^\text{miss}, j_4} > 0.3$	31.8 ± 0.3	51.6 ± 0.2	67.9 ± 0.3
Event quality filter	31.4 ± 0.3	50.8 ± 0.3	67.1 ± 0.3

Selection	$pp \to \widetilde{t}\overline{\widetilde{t}}, \widetilde{t} \to t\widetilde{\chi}_1^0$ $m_{\widetilde{t}} = 300\,\text{GeV}$ $m_{\widetilde{\chi}_1^0} = 200\,\text{GeV}$	$pp \to \widetilde{b}\overline{\widetilde{b}}, \widetilde{b} \to b\widetilde{\chi}_1^0$ $m_{\widetilde{b}} = 500\,\text{GeV}$ $m_{\widetilde{\chi}_1^0} = 300\,\text{GeV}$	$pp \to \widetilde{q}\overline{\widetilde{q}}, \widetilde{q} \to q\widetilde{\chi}_1^0$ $m_{\widetilde{q}} = 700\,\text{GeV}$ $m_{\widetilde{\chi}_1^0} = 400\,\text{GeV}$
$N_\text{jet} \geq 2$	86.9 ± 0.0	96.0 ± 0.1	98.0 ± 0.0
$H_\text{T} > 300\,\text{GeV}$	23.3 ± 0.0	68.0 ± 0.1	91.3 ± 0.1
$H_\text{T}^\text{miss} > 300\,\text{GeV}$	2.84 ± 0.0	15.6 ± 0.1	43.8 ± 0.1
$N_\text{muon} = 0$	2.16 ± 0.0	15.6 ± 0.1	43.8 ± 0.1
$N_\text{isolated tracks}^\text{(muon)} = 0$	2.10 ± 0.0	15.5 ± 0.1	43.7 ± 0.1
$N_\text{electron} = 0$	1.60 ± 0.0	15.4 ± 0.1	43.5 ± 0.1
$N_\text{isolated tracks}^\text{(electron)} = 0$	1.52 ± 0.0	15.3 ± 0.1	43.4 ± 0.1
$N_\text{isolated tracks}^\text{(hadron)} = 0$	1.41 ± 0.0	15.2 ± 0.1	43.0 ± 0.1
$\Delta\phi_{H_\text{T}^\text{miss}, j_1} > 0.5$	1.40 ± 0.0	15.1 ± 0.1	42.9 ± 0.1
$\Delta\phi_{H_\text{T}^\text{miss}, j_2} > 0.5$	1.03 ± 0.0	14.1 ± 0.1	41.1 ± 0.1
$\Delta\phi_{H_\text{T}^\text{miss}, j_3} > 0.3$	0.85 ± 0.0	13.5 ± 0.1	39.6 ± 0.1
$\Delta\phi_{H_\text{T}^\text{miss}, j_4} > 0.3$	0.73 ± 0.0	13.1 ± 0.1	38.4 ± 0.1
Event quality filter	0.72 ± 0.0	12.9 ± 0.1	37.9 ± 0.1

Table B.1: Observed numbers of events and prefit background predictions in the $N_{\text{jet}} = 2$ search regions. The first uncertainty is statistical and second systematic.

Bin	H_T^{miss} [GeV]	H_T [GeV]	N_{jet}	$N_{\text{b-jet}}$	Lost-e/μ	$\tau \to$ had	$Z \to \nu\bar{\nu}$	QCD	Total pred.	Obs.
1	300–350	300–500	2	0	$4069^{+67+320}_{-67-320}$	$2744^{+37+510}_{-37-500}$	$13231^{+67+760}_{-66-740}$	$326^{+12+170}_{-12-120}$	$20370^{+120+980}_{-120-960}$	21626
2	300–350	500–1000	2	0	326^{+22+36}_{-22-36}	226^{+11+43}_{-11-42}	944^{+18+55}_{-18-54}	45^{+2+24}_{-2-17}	1541^{+37+82}_{-37-79}	1583
3	300–350	>1000	2	0	$15.2^{+5.8+2.3}_{-5.1-2.3}$	$8.7^{+2.1+2.1}_{-2.0-2.1}$	$50.9^{+4.5+4.4}_{-4.1-3.8}$	$1.57^{+0.16+0.84}_{-0.16-0.61}$	$76.3^{+9.1+5.5}_{-8.2-5.0}$	102
4	350–500	350–500	2	0	$2049^{+46+160}_{-46-160}$	$1553^{+27+290}_{-27-290}$	$9347^{+57+540}_{-57-520}$	126^{+4+67}_{-4-48}	$13076^{+93+630}_{-93-620}$	14019
5	350–500	500–1000	2	0	631^{+25+54}_{-25-54}	439^{+14+84}_{-14-84}	$2502^{+30+150}_{-30-140}$	43^{+7+22}_{-7-16}	$3615^{+49+180}_{-49-170}$	3730
6	350–500	>1000	2	0	$13.5^{+4.9+1.9}_{-4.3-1.9}$	$13.4^{+2.4+2.6}_{-2.3-2.6}$	$94.0^{+6.2+7.9}_{-5.8-6.9}$	$1.30^{+0.06+0.68}_{-0.06-0.49}$	$122.1^{+9.5+8.6}_{-8.8-7.6}$	139
7	500–750	500–1000	2	0	303^{+17+29}_{-17-29}	247^{+10+48}_{-10-47}	$2328^{+30+170}_{-29-160}$	$4.5^{+0.1+2.4}_{-0.1-1.7}$	$2883^{+40+180}_{-40-170}$	3018
8	500–750	>1000	2	0	$5.8^{+2.7+1.5}_{-2.2-1.5}$	$5.3^{+1.4+1.3}_{-1.3-1.3}$	$66.2^{+5.4+5.3}_{-5.0-5.1}$	$0.03^{+0.02+0.02}_{-0.02-0.01}$	$77.3^{+6.8+5.7}_{-6.1-5.4}$	96
9	>750	750–1500	2	0	$17.3^{+4.5+3.0}_{-4.1-3.0}$	$17.4^{+2.5+4.5}_{-2.4-4.5}$	295^{+11+41}_{-11-38}	$0.35^{+0.06+0.18}_{-0.06-0.13}$	330^{+13+42}_{-12-38}	272
10	>750	>1500	2	0	$0.0^{+1.8+0.0}_{-0.0-0.0}$	$0.38^{+0.54+0.09}_{-0.29-0.09}$	$12.6^{+3.0+2.1}_{-2.4-1.9}$	$0.01^{+0.01+0.00}_{-0.01-0.00}$	$13.0^{+3.8+2.1}_{-2.5-1.9}$	12
11	300–350	300–500	2	1	370^{+21+31}_{-21-31}	288^{+11+63}_{-11-63}	1361^{+7+140}_{-7-140}	44^{+6+25}_{-6-17}	$2063^{+33+160}_{-33-160}$	1904
12	300–350	500–1000	2	1	51^{+10+7}_{-10-7}	$31.6^{+4.2+7.2}_{-4.2-7.2}$	97^{+2+10}_{-2-10}	$6.7^{+2.7+3.7}_{-2.7-2.5}$	186^{+15+15}_{-14-14}	186
13	300–350	>1000	2	1	$1.1^{+2.3+0.2}_{-1.1-0.0}$	$2.0^{+1.1+0.5}_{-1.0-0.5}$	$5.23^{+0.46+0.63}_{-0.42-0.59}$	$0.33^{+0.02+0.18}_{-0.02-0.13}$	$8.7^{+3.4+0.9}_{-2.1-0.8}$	13
14	350–500	350–500	2	1	215^{+16+19}_{-16-19}	179^{+9+39}_{-9-39}	962^{+6+99}_{-6-98}	20^{+2+11}_{-2-8}	$1376^{+26+110}_{-26-110}$	1212
15	350–500	500–1000	2	1	$69.8^{+9.3+7.5}_{-9.8-7.5}$	$43.3^{+4.4+9.7}_{-4.4-9.6}$	257^{+3+27}_{-3-26}	$8.5^{+3.0+4.8}_{-3.0-3.2}$	379^{+15+30}_{-15-29}	409
16	350–500	>1000	2	1	$3.7^{+2.5+0.7}_{-1.9-0.7}$	$3.1^{+1.1+0.9}_{-1.0-0.9}$	$9.7^{+0.6+1.2}_{-0.6-1.1}$	$0.13^{+0.04+0.07}_{-0.04-0.05}$	$16.6^{+3.7+1.6}_{-3.0-1.6}$	27
17	500–750	500–1000	2	1	$28.9^{+5.8+3.3}_{-5.6-3.3}$	$26.0^{+2.9+5.8}_{-2.9-5.8}$	240^{+3+27}_{-3-26}	$1.48^{+0.18+0.83}_{-0.18-0.56}$	296^{+9+28}_{-9-27}	321
18	500–750	>1000	2	1	$5.1^{+6.2+1.6}_{-4.1-1.6}$	$0.36^{+0.55+0.12}_{-0.30-0.12}$	$6.81^{+0.56+0.80}_{-0.52-0.78}$	$0.03^{+0.03+0.02}_{-0.03-0.00}$	$12.3^{+6.8+1.8}_{-4.5-1.7}$	14
19	>750	750–1500	2	1	$3.8^{+2.2+0.8}_{-1.7-0.8}$	$4.1^{+1.5+1.1}_{-1.4-1.1}$	$30.4^{+1.1+5.0}_{-1.1-4.7}$	$0.10^{+0.03+0.06}_{-0.03-0.04}$	$38.4^{+3.9+5.1}_{-3.3-4.8}$	31
20	>750	>1500	2	1	$0.0^{+1.4+0.0}_{-0.0-0.0}$	$0.34^{+0.51+0.13}_{-0.22-0.13}$	$1.29^{+0.31+0.24}_{-0.25-0.23}$	$0.00^{+0.01+0.00}_{-0.00-0.00}$	$1.6^{+2.0+0.3}_{-0.3-0.3}$	1
21	300–350	300–500	2	2	$14.1^{+4.5+2.6}_{-4.0-2.6}$	$12.9^{+2.3+2.8}_{-2.2-2.8}$	49^{+0+17}_{-0-17}	$3.0^{+0.8+3.6}_{-0.8-2.1}$	79^{+7+18}_{-6-18}	122
22	300–350	500–1000	2	2	$2.8^{+2.4+0.9}_{-1.7-0.9}$	$2.0^{+1.1+1.0}_{-0.9-1.0}$	$3.5^{+0.1+1.2}_{-0.1-1.2}$	$0.57^{+0.17+0.69}_{-0.17-0.40}$	$8.9^{+3.5+2.0}_{-2.6-1.9}$	11
23	300–350	>1000	2	2	$0.0^{+2.2+0.0}_{-0.0-0.0}$	$0.00^{+0.46+0.00}_{-0.00-0.00}$	$0.19^{+0.02+0.07}_{-0.01-0.07}$	$0.03^{+0.01+0.04}_{-0.01-0.02}$	$0.2^{+2.6+0.1}_{-0.0-0.1}$	0
24	350–500	350–500	2	2	$11.4^{+4.5+2.5}_{-3.9-2.5}$	$6.3^{+1.7+2.1}_{-1.6-2.1}$	35^{+0+12}_{-0-12}	$1.0^{+0.5+1.2}_{-0.5-0.6}$	53^{+6+13}_{-6-13}	84
25	350–500	500–1000	2	2	$6.1^{+2.9+1.5}_{-2.4-1.5}$	$2.9^{+1.2+0.8}_{-1.1-0.8}$	$9.3^{+0.1+3.3}_{-0.1-3.3}$	$0.44^{+0.05+0.52}_{-0.05-0.39}$	$18.7^{+4.1+3.8}_{-3.5-3.7}$	23
26	350–500	>1000	2	2	$0.0^{+1.1+0.0}_{-0.0-0.0}$	$0.00^{+0.00+0.00}_{-0.00-0.00}$	$0.35^{+0.02+0.13}_{-0.02-0.13}$	$0.06^{+0.04+0.08}_{-0.04-0.02}$	$0.4^{+1.5+0.1}_{-0.0-0.1}$	2
27	500–750	500–1000	2	2	$1.4^{+2.9+0.4}_{-1.4-0.0}$	$2.03^{+0.84+0.61}_{-0.70-0.61}$	$8.6^{+0.1+3.1}_{-0.1-3.1}$	$0.03^{+0.01+0.04}_{-0.01-0.03}$	$12.1^{+3.7+3.2}_{-2.1-3.2}$	16
28	500–750	>1000	2	2	$0.0^{+2.2+0.0}_{-0.0-0.0}$	$0.00^{+0.46+0.00}_{-0.00-0.00}$	$0.24^{+0.02+0.09}_{-0.02-0.09}$	$0.00^{+0.01+0.00}_{-0.00-0.00}$	$0.2^{+2.7+0.1}_{-0.0-0.1}$	0
29	>750	750–1500	2	2	$0.0^{+1.6+0.0}_{-0.0-0.0}$	$0.07^{+0.46+0.07}_{-0.04-0.06}$	$1.09^{+0.04+0.41}_{-0.04-0.41}$	$0.01^{+0.01+0.01}_{-0.01-0.00}$	$1.2^{+2.1+0.4}_{-0.1-0.4}$	4
30	>750	>1500	2	2	$0.0^{+2.0+0.0}_{-0.0-0.0}$	$0.00^{+0.46+0.00}_{-0.00-0.00}$	$0.05^{+0.01+0.02}_{-0.01-0.02}$	$0.00^{+0.00+0.00}_{-0.00-0.00}$	$0.0^{+2.5+0.0}_{-0.0-0.0}$	0

Table B.2: Observed numbers of events and prefit background predictions in the $3 \leq N_{\text{jet}} \leq 4$ search regions. The first uncertainty is statistical and second systematic.

Bin	$H_{\text{T}}^{\text{miss}}$ [GeV]	H_{T} [GeV]	N_{jet}	$N_{\text{b-jet}}$	Lost-e/μ	$\tau \to$ had	$Z \to \nu\bar{\nu}$	QCD	Total pred.	Obs.
31	300–350	300–500	3–4	0	$2830^{+45+200}_{-45-200}$	$2152^{+29+160}_{-29-150}$	$8353^{+52+480}_{-52-470}$	$273^{+68+120}_{-68-100}$	$13608^{+110+560}_{-110-540}$	14520
32	300–350	500–1000	3–4	0	$1125^{+25+120}_{-25-120}$	$909^{+18+100}_{-18-100}$	$2487^{+29+140}_{-28-140}$	119^{+8+51}_{-8-45}	$4640^{+52+220}_{-52-210}$	4799
33	300–350	>1000	3–4	0	$72.7^{+7.1+6.1}_{-7.1-6.1}$	$65.3^{+5.2+6.4}_{-5.2-6.3}$	176^{+8+14}_{-8-12}	41^{+2+18}_{-2-16}	356^{+15+24}_{-15-22}	354
34	350–500	350–500	3–4	0	$1439^{+37+110}_{-37-110}$	$930^{+19+120}_{-19-110}$	$5014^{+41+280}_{-41-280}$	114^{+6+48}_{-6-43}	$7496^{+70+330}_{-69-320}$	7973
35	350–500	500–1000	3–4	0	$1402^{+27+140}_{-27-140}$	$1253^{+22+120}_{-22-120}$	$4811^{+40+270}_{-40-260}$	80^{+9+34}_{-9-31}	$7547^{+65+330}_{-64-320}$	7735
36	350–500	>1000	3–4	0	103^{+8+11}_{-8-11}	$77.0^{+5.9+7.6}_{-5.9-7.5}$	303^{+11+24}_{-10-21}	24^{+1+10}_{-1-9}	506^{+18+30}_{-17-26}	490
37	500–750	500–1000	3–4	0	339^{+15+33}_{-15-33}	297^{+10+26}_{-10-26}	$2143^{+28+150}_{-28-140}$	$5.5^{+0.2+2.3}_{-0.2-2.1}$	$2785^{+37+160}_{-37-150}$	2938
38	500–750	>1000	3–4	0	$33.8^{+4.4+3.6}_{-4.3-3.6}$	$30.5^{+3.4+2.9}_{-3.4-2.9}$	219^{+10+16}_{-9-15}	$1.29^{+0.53+0.55}_{-0.53-0.49}$	284^{+12+17}_{-12-16}	303
39	>750	750–1500	3–4	0	$28.2^{+4.4+3.7}_{-4.3-3.7}$	$26.0^{+2.9+3.4}_{-2.9-3.4}$	319^{+11+44}_{-11-40}	$0.32^{+0.03+0.14}_{-0.03-0.12}$	373^{+14+44}_{-13-41}	334
40	>750	>1500	3–4	0	$2.9^{+2.0+0.7}_{-1.5-0.7}$	$1.38^{+0.66+0.17}_{-0.48-0.17}$	$27.8^{+3.9+4.1}_{-3.5-3.8}$	$0.10^{+0.01+0.04}_{-0.01-0.04}$	$32.2^{+4.8+4.2}_{-4.0-3.9}$	46
41	300–350	300–500	3–4	1	746^{+25+55}_{-25-55}	627^{+15+48}_{-15-47}	1235^{+8+130}_{-8-120}	59^{+4+24}_{-4-22}	$2667^{+41+150}_{-41-150}$	2677
42	300–350	500–1000	3–4	1	296^{+15+25}_{-15-25}	262^{+9+27}_{-9-27}	385^{+4+39}_{-4-39}	38^{+4+15}_{-4-14}	981^{+24+56}_{-24-56}	1048
43	300–350	>1000	3–4	1	$20.8^{+4.1+2.1}_{-4.0-2.1}$	$19.0^{+2.6+1.8}_{-2.5-1.8}$	$27.6^{+1.3+3.2}_{-1.2-3.0}$	$11.4^{+0.8+4.7}_{-0.8-4.4}$	$78.8^{+6.9+6.3}_{-6.6-6.0}$	92
44	350–500	350–500	3–4	1	321^{+17+25}_{-17-25}	263^{+10+22}_{-10-21}	738^{+6+74}_{-6-74}	$22.3^{+1.4+9.1}_{-1.4-8.5}$	1343^{+28+82}_{-28-81}	1332
45	350–500	500–1000	3–4	1	329^{+14+26}_{-14-26}	324^{+11+26}_{-11-26}	737^{+6+74}_{-6-74}	$17.6^{+3.4+7.2}_{-3.4-6.7}$	1407^{+26+83}_{-26-83}	1515
46	350–500	>1000	3–4	1	$20.4^{+4.0+2.0}_{-3.8-2.0}$	$19.9^{+2.9+1.8}_{-2.9-1.7}$	$47.5^{+1.7+5.5}_{-1.6-5.1}$	$5.7^{+0.5+2.3}_{-0.5-2.2}$	$93.4^{+7.1+6.5}_{-6.9-6.2}$	113
47	500–750	500–1000	3–4	1	$69.7^{+7.4+6.6}_{-7.3-6.6}$	$56.0^{+4.1+5.0}_{-4.1-4.9}$	322^{+4+35}_{-4-35}	$1.34^{+0.10+0.55}_{-0.10-0.51}$	449^{+12+36}_{-12-36}	472
48	500–750	>1000	3–4	1	$15.3^{+3.4+1.9}_{-3.3-1.9}$	$7.0^{+1.4+0.7}_{-1.4-0.7}$	$34.4^{+1.5+3.8}_{-1.4-3.8}$	$0.38^{+0.14+0.16}_{-0.14-0.15}$	$57.0^{+5.1+4.4}_{-4.9-4.3}$	57
49	>750	750–1500	3–4	1	$3.3^{+1.5+0.5}_{-1.3-0.5}$	$4.8^{+1.3+0.8}_{-1.2-0.8}$	$48.5^{+1.7+7.9}_{-1.7-7.3}$	$0.13^{+0.01+0.05}_{-0.01-0.05}$	$56.8^{+3.3+7.9}_{-3.0-7.4}$	61
50	>750	>1500	3–4	1	$1.0^{+1.2+0.3}_{-0.7-0.3}$	$0.77^{+0.75+0.16}_{-0.59-0.16}$	$4.40^{+0.62+0.75}_{-0.55-0.71}$	$0.03^{+0.01+0.01}_{-0.01-0.01}$	$6.2^{+2.0+0.8}_{-1.4-0.8}$	8
51	300–350	300–500	3–4	2	137^{+11+11}_{-11-11}	133^{+7+11}_{-7-11}	145^{+1+26}_{-1-26}	$9.0^{+1.1+3.9}_{-1.1-3.4}$	424^{+18+31}_{-17-31}	464
52	300–350	500–1000	3–4	2	$92.3^{+9.1+9.5}_{-9.0-9.5}$	$85.6^{+5.7+7.5}_{-5.7-7.4}$	$53.0^{+0.6+9.6}_{-0.6-9.4}$	$3.8^{+1.2+1.6}_{-1.2-1.4}$	235^{+15+16}_{-15-15}	227
53	300–350	>1000	3–4	2	$3.4^{+2.2+0.8}_{-1.7-0.8}$	$2.41^{+0.91+0.50}_{-0.78-0.50}$	$3.95^{+0.18+0.75}_{-0.17-0.73}$	$2.23^{+0.18+0.96}_{-0.18-0.86}$	$12.0^{+3.1+1.6}_{-2.5-1.5}$	17
54	350–500	350–500	3–4	2	$39.6^{+6.1+3.8}_{-5.9-3.8}$	$39.8^{+3.9+3.8}_{-3.8-3.8}$	84^{+1+15}_{-1-15}	$2.7^{+0.6+1.1}_{-0.6-1.0}$	166^{+10+16}_{-10-16}	208
55	350–500	500–1000	3–4	2	$83.9^{+8.2+7.8}_{-8.1-7.8}$	$69.4^{+4.9+5.9}_{-4.9-5.8}$	97^{+1+18}_{-1-17}	$3.1^{+0.2+1.3}_{-0.2-1.2}$	254^{+13+20}_{-13-20}	286
56	350–500	>1000	3–4	2	$6.2^{+4.0+1.0}_{-3.6-1.0}$	$3.8^{+1.1+0.6}_{-1.0-0.6}$	$6.8^{+0.2+1.3}_{-0.2-1.3}$	$0.95^{+0.16+0.41}_{-0.16-0.36}$	$17.7^{+5.2+1.8}_{-4.6-1.8}$	25
57	500–750	500–1000	3–4	2	$11.8^{+3.3+2.0}_{-3.1-2.0}$	$10.5^{+1.8+1.6}_{-1.7-1.6}$	$39.7^{+0.5+7.4}_{-0.5-7.3}$	$0.22^{+0.04+0.09}_{-0.04-0.08}$	$62.1^{+5.1+7.8}_{-4.8-7.7}$	64
58	500–750	>1000	3–4	2	$2.6^{+2.3+0.6}_{-1.6-0.6}$	$2.9^{+1.5+0.6}_{-1.5-0.6}$	$4.90^{+0.21+0.92}_{-0.21-0.91}$	$0.10^{+0.03+0.04}_{-0.03-0.04}$	$10.5^{+3.8+1.2}_{-3.1-1.2}$	13
59	>750	750–1500	3–4	2	$0.0^{+1.1+0.0}_{-0.0-0.0}$	$0.32^{+0.48+0.09}_{-0.13-0.09}$	$6.3^{+0.2+1.4}_{-0.2-1.3}$	$0.03^{+0.02+0.01}_{-0.02-0.01}$	$6.6^{+1.6+1.4}_{-0.3-1.3}$	4
60	>750	>1500	3–4	2	$0.0^{+1.1+0.0}_{-0.0-0.0}$	$0.03^{+0.46+0.01}_{-0.02-0.01}$	$0.65^{+0.09+0.15}_{-0.08-0.14}$	$0.01^{+0.01+0.01}_{-0.01-0.00}$	$0.7^{+1.6+0.1}_{-0.1-0.1}$	1
61	300–350	300–500	3–4	≥3	$6.4^{+2.8+0.7}_{-2.3-0.7}$	$10.3^{+1.9+2.7}_{-1.9-2.7}$	$5.0^{+0.0+2.8}_{-0.0-2.8}$	$0.35^{+0.18+0.42}_{-0.18-0.16}$	$22.0^{+4.7+3.9}_{-4.2-3.9}$	27
62	300–350	500–1000	3–4	≥3	$4.9^{+2.7+0.6}_{-2.2-0.6}$	$6.2^{+1.4+1.7}_{-1.3-1.7}$	$2.5^{+0.0+1.4}_{-0.0-1.4}$	$0.75^{+0.52+0.90}_{-0.52-0.24}$	$14.4^{+4.2+2.4}_{-3.6-2.2}$	20
63	300–350	>1000	3–4	≥3	$0.0^{+1.1+0.0}_{-0.0-0.0}$	$0.94^{+0.87+0.44}_{-0.74-0.44}$	$0.21^{+0.01+0.12}_{-0.01-0.12}$	$1.6^{+0.2+1.9}_{-0.2-1.4}$	$2.7^{+2.0+2.0}_{-0.8-1.5}$	4
64	350–500	350–500	3–4	≥3	$0.6^{+1.2+0.1}_{-0.6-0.0}$	$4.2^{+1.5+1.3}_{-1.4-1.3}$	$2.5^{+0.0+1.4}_{-0.0-1.4}$	$0.09^{+0.04+0.11}_{-0.04-0.05}$	$7.4^{+2.6+1.9}_{-1.9-1.9}$	8
65	350–500	500–1000	3–4	≥3	$10.2^{+6.3+2.1}_{-5.7-2.1}$	$7.0^{+1.5+1.9}_{-1.5-1.9}$	$4.3^{+0.0+2.4}_{-0.0-2.4}$	$0.78^{+0.18+0.94}_{-0.18-0.60}$	$22.3^{+7.9+3.8}_{-7.2-3.7}$	26
66	350–500	>1000	3–4	≥3	$0.0^{+1.1+0.0}_{-0.0-0.0}$	$0.21^{+0.49+0.13}_{-0.16-0.13}$	$0.36^{+0.01+0.20}_{-0.01-0.20}$	$0.54^{+0.15+0.65}_{-0.15-0.39}$	$1.1^{+1.6+0.7}_{-0.2-0.5}$	5
67	500–750	500–1000	3–4	≥3	$1.4^{+2.9+0.4}_{-1.4-0.0}$	$1.13^{+0.74+0.45}_{-0.58-0.45}$	$1.50^{+0.02+0.83}_{-0.02-0.83}$	$0.10^{+0.08+0.13}_{-0.10-0.00}$	$4.1^{+3.6+1.0}_{-2.0-0.9}$	0
68	500–750	>1000	3–4	≥3	$0.00^{+0.95+0.00}_{-0.00-0.00}$	$0.12^{+0.46+0.09}_{-0.06-0.09}$	$0.26^{+0.01+0.15}_{-0.01-0.15}$	$0.02^{+0.03+0.02}_{-0.02-0.00}$	$0.4^{+1.4+0.2}_{-0.1-0.2}$	2
69	>750	750–1500	3–4	≥3	$0.00^{+0.97+0.00}_{-0.00-0.00}$	$0.00^{+0.46+0.00}_{-0.00-0.00}$	$0.29^{+0.01+0.16}_{-0.01-0.16}$	$0.01^{+0.02+0.01}_{-0.01-0.00}$	$0.3^{+1.4+0.2}_{-0.0-0.2}$	1
70	>750	>1500	3–4	≥3	$0.0^{+1.4+0.0}_{-0.0-0.0}$	$0.00^{+0.46+0.00}_{-0.00-0.00}$	$0.04^{+0.01+0.02}_{-0.00-0.02}$	$0.01^{+0.03+0.02}_{-0.01-0.00}$	$0.0^{+1.8+0.0}_{-0.0-0.0}$	0

Table B.3: Observed numbers of events and prefit background predictions in the $5 \leq N_{\text{jet}} \leq 6$ search regions. The first uncertainty is statistical and second systematic.

Bin	H_T^{miss} [GeV]	H_T [GeV]	N_{jet}	$N_{\text{b-jet}}$	Lost-e/μ	$\tau \to$ had	$Z \to \nu\bar{\nu}$	QCD	Total pred.	Obs.
71	300–350	300–500	5–6	0	217^{+11+22}_{-11-22}	166^{+6+27}_{-6-27}	489^{+12+42}_{-12-39}	49^{+5+21}_{-5-19}	922^{+21+58}_{-21-56}	1015
72	300–350	500–1000	5–6	0	397^{+13+37}_{-13-37}	403^{+9+36}_{-9-36}	772^{+16+61}_{-15-57}	113^{+4+47}_{-4-43}	1686^{+27+93}_{-27-88}	1673
73	300–350	>1000	5–6	0	$49.6^{+4.5+5.4}_{-4.5-5.4}$	$55.1^{+3.8+8.3}_{-3.8-8.3}$	$100.0^{+6.4+8.2}_{-6.0-7.1}$	49^{+1+21}_{-1-19}	254^{+11+24}_{-10-22}	226
74	350–500	350–500	5–6	0	71^{+7+11}_{-6-11}	47^{+3+16}_{-3-16}	242^{+9+20}_{-9-19}	$12.7^{+2.3+5.3}_{-2.3-4.8}$	372^{+13+29}_{-13-28}	464
75	350–500	500–1000	5–6	0	384^{+12+33}_{-12-33}	412^{+11+32}_{-11-32}	1110^{+19+84}_{-19-78}	65^{+2+27}_{-2-25}	1971^{+30+99}_{-29-93}	2018
76	350–500	>1000	5–6	0	$76.9^{+6.4+8.9}_{-6.4-8.9}$	$72.4^{+4.8+9.3}_{-4.8-9.3}$	170^{+8+14}_{-8-12}	28^{+1+12}_{-1-11}	347^{+14+22}_{-14-21}	320
77	500–750	500–1000	5–6	0	$66.7^{+5.1+7.3}_{-5.0-7.3}$	$70.1^{+4.3+6.1}_{-4.2-6.0}$	302^{+10+23}_{-10-22}	$3.2^{+0.1+1.3}_{-0.1-1.2}$	442^{+14+25}_{-14-24}	460
78	500–750	>1000	5–6	0	$23.9^{+2.9+4.5}_{-2.9-4.5}$	$31.2^{+3.1+4.0}_{-3.1-4.0}$	$123.5^{+7.3+9.4}_{-6.9-8.9}$	$2.5^{+0.1+1.1}_{-0.1-1.0}$	181^{+10+11}_{-9-11}	170
79	>750	750–1500	5–6	0	$4.0^{+1.2+0.7}_{-1.1-0.7}$	$4.90^{+0.89+0.52}_{-0.76-0.52}$	$52.2^{+6.4+7.5}_{-4.2-6.8}$	$0.23^{+0.04+0.10}_{-0.04-0.09}$	$61.3^{+5.0+7.5}_{-4.6-6.9}$	74
80	>750	>1500	5–6	0	$0.90^{+0.61+0.19}_{-0.45-0.19}$	$1.46^{+0.67+0.16}_{-0.49-0.16}$	$16.5^{+2.9+2.7}_{-2.5-2.5}$	$0.25^{+0.06+0.11}_{-0.06-0.10}$	$19.1^{+3.2+2.7}_{-2.7-2.5}$	19
81	300–350	300–500	5–6	1	130^{+8+11}_{-8-11}	131^{+6+17}_{-6-17}	133^{+3+19}_{-3-19}	$12.8^{+2.8+5.2}_{-2.8-4.9}$	407^{+15+29}_{-15-28}	450
82	300–350	500–1000	5–6	1	290^{+11+25}_{-11-25}	302^{+8+25}_{-8-25}	218^{+4+31}_{-4-30}	41^{+4+17}_{-4-16}	851^{+20+50}_{-20-49}	781
83	300–350	>1000	5–6	1	$25.8^{+3.4+2.5}_{-3.4-2.5}$	$31.6^{+2.9+5.9}_{-2.9-5.9}$	$29.0^{+1.8+4.1}_{-1.7-4.0}$	$18.4^{+0.8+7.5}_{-0.8-7.1}$	105^{+7+11}_{-6-10}	100
84	350–500	350–500	5–6	1	$45.4^{+5.5+5.4}_{-5.4-5.4}$	32^{+3+11}_{-3-11}	$65.1^{+2.4+9.3}_{-2.3-9.1}$	$3.7^{+0.5+1.5}_{-0.5-1.4}$	146^{+9+16}_{-8-16}	160
85	350–500	500–1000	5–6	1	228^{+10+20}_{-10-20}	269^{+8+21}_{-8-21}	310^{+5+43}_{-5-42}	28^{+3+11}_{-3-11}	834^{+19+53}_{-19-52}	801
86	350–500	>1000	5–6	1	$40.5^{+5.5+4.2}_{-5.4-4.2}$	$36.0^{+3.3+4.3}_{-3.3-4.2}$	$49.4^{+2.3+7.0}_{-2.2-6.7}$	$11.9^{+0.7+4.8}_{-0.7-4.5}$	138^{+9+10}_{-9-10}	138
87	500–750	500–1000	5–6	1	$23.4^{+3.5+2.6}_{-3.4-2.6}$	$32.1^{+2.8+3.3}_{-2.8-3.3}$	84^{+3+12}_{-3-12}	$1.45^{+0.11+0.59}_{-0.11-0.55}$	141^{+7+13}_{-7-12}	135
88	500–750	>1000	5–6	1	$8.5^{+1.8+1.1}_{-1.7-1.1}$	$13.0^{+1.8+1.5}_{-1.7-1.5}$	$35.3^{+2.1+4.9}_{-2.0-4.8}$	$1.33^{+0.17+0.54}_{-0.17-0.51}$	$58.0^{+4.1+5.3}_{-3.9-5.2}$	49
89	>750	750–1500	5–6	1	$3.7^{+1.4+0.7}_{-1.2-0.7}$	$2.9^{+1.0+0.4}_{-0.9-0.4}$	$14.9^{+1.3+2.8}_{-1.2-2.6}$	$0.07^{+0.01+0.03}_{-0.01-0.03}$	$21.6^{+2.8+2.9}_{-2.5-2.7}$	16
90	>750	>1500	5–6	1	$1.06^{+0.74+0.26}_{-0.56-0.26}$	$1.16^{+0.73+0.18}_{-0.57-0.18}$	$4.79^{+0.85+0.96}_{-0.73-0.92}$	$0.16^{+0.07+0.07}_{-0.07-0.06}$	$7.2^{+1.7+1.0}_{-1.3-1.0}$	6
91	300–350	300–500	5–6	2	$60.1^{+7.1+6.0}_{-7.0-6.0}$	$50.2^{+3.3+4.9}_{-3.3-4.9}$	$23.8^{+0.6+7.1}_{-0.6-7.1}$	$2.9^{+0.9+1.1}_{-0.9-1.1}$	137^{+10+11}_{-10-11}	143
92	300–350	500–1000	5–6	2	137^{+9+13}_{-9-13}	160^{+6+14}_{-6-14}	39^{+1+12}_{-1-11}	$11.8^{+1.8+4.6}_{-1.8-4.5}$	347^{+15+22}_{-15-22}	332
93	300–350	>1000	5–6	2	$16.9^{+3.8+2.0}_{-3.7-2.0}$	$15.9^{+2.1+2.1}_{-2.1-2.1}$	$5.1^{+0.3+1.5}_{-0.3-1.5}$	$5.6^{+0.4+2.2}_{-0.4-2.2}$	$43.5^{+5.9+3.9}_{-5.8-3.9}$	36
94	350–500	350–500	5–6	2	$13.3^{+3.1+1.9}_{-2.9-1.9}$	$7.0^{+1.1+2.3}_{-1.0-2.3}$	$11.7^{+0.4+3.5}_{-0.4-3.5}$	$1.02^{+0.54+0.40}_{-0.54-0.39}$	$32.9^{+4.3+4.6}_{-4.0-4.6}$	28
95	350–500	500–1000	5–6	2	$107.5^{+7.6+9.6}_{-7.6-9.6}$	$121.2^{+5.8+9.9}_{-5.8-9.8}$	55^{+1+16}_{-1-16}	$5.9^{+1.0+2.3}_{-1.0-2.2}$	290^{+14+22}_{-13-21}	288
96	350–500	>1000	5–6	2	$14.2^{+2.8+1.8}_{-2.7-1.8}$	$15.7^{+2.2+2.0}_{-2.1-2.0}$	$8.7^{+0.4+2.6}_{-0.4-2.6}$	$3.2^{+0.1+1.2}_{-0.1-1.2}$	$41.8^{+5.0+4.0}_{-4.8-3.9}$	44
97	500–750	500–1000	5–6	2	$8.4^{+2.3+1.1}_{-2.2-1.1}$	$8.3^{+1.3+1.0}_{-1.2-1.0}$	$15.0^{+0.5+4.4}_{-0.5-4.4}$	$0.34^{+0.05+0.13}_{-0.05-0.13}$	$32.1^{+3.7+4.7}_{-3.4-4.7}$	35
98	500–750	>1000	5–6	2	$2.1^{+1.3+0.3}_{-1.0-0.3}$	$4.0^{+1.1+0.6}_{-1.0-0.6}$	$6.2^{+0.4+1.9}_{-0.3-1.8}$	$0.16^{+0.05+0.06}_{-0.05-0.06}$	$12.5^{+2.4+2.0}_{-2.0-2.0}$	18
99	>750	750–1500	5–6	2	$0.74^{+0.87+0.22}_{-0.53-0.22}$	$0.68^{+0.64+0.16}_{-0.45-0.16}$	$2.64^{+0.23+0.85}_{-0.21-0.83}$	$0.05^{+0.05+0.02}_{-0.05-0.00}$	$4.1^{+1.5+0.9}_{-1.0-0.9}$	8
100	>750	>1500	5–6	2	$0.77^{+0.65+0.24}_{-0.45-0.24}$	$1.07^{+0.72+0.33}_{-0.56-0.33}$	$0.84^{+0.15+0.28}_{-0.13-0.27}$	$0.03^{+0.03+0.01}_{-0.03-0.00}$	$2.7^{+1.4+0.5}_{-1.0-0.5}$	3
101	300–350	300–500	5–6	≥3	$2.8^{+1.5+0.3}_{-1.2-0.3}$	$5.1^{+1.0+0.8}_{-0.9-0.8}$	$2.0^{+0.0+1.1}_{-0.0-1.1}$	$0.50^{+0.37+0.57}_{-0.37-0.13}$	$10.4^{+2.5+1.5}_{-2.1-1.4}$	18
102	300–350	500–1000	5–6	≥3	$17.0^{+3.2+1.6}_{-3.1-1.6}$	$23.5^{+2.4+3.2}_{-2.3-3.2}$	$4.2^{+0.1+2.3}_{-0.1-2.3}$	$3.9^{+2.3+4.5}_{-2.3-1.6}$	$48.7^{+6.0+6.2}_{-5.9-4.5}$	44
103	300–350	>1000	5–6	≥3	$4.4^{+2.1+0.6}_{-1.8-0.6}$	$2.50^{+0.86+0.47}_{-0.73-0.47}$	$0.65^{+0.04+0.35}_{-0.04-0.35}$	$3.3^{+0.4+3.7}_{-0.4-2.8}$	$10.8^{+3.0+3.8}_{-2.6-3.0}$	6
104	350–500	350–500	5–6	≥3	$0.8^{+1.7+0.2}_{-0.8-0.0}$	$1.14^{+0.75+0.33}_{-0.59-0.33}$	$0.87^{+0.03+0.47}_{-0.03-0.47}$	$0.18^{+0.24+0.21}_{-0.08-0.10}$	$3.0^{+2.4+0.6}_{-1.4-0.6}$	4
105	350–500	500–1000	5–6	≥3	$15.2^{+2.6+1.5}_{-2.6-1.5}$	$17.6^{+2.2+2.7}_{-2.1-2.7}$	$5.7^{+0.1+3.1}_{-0.1-3.1}$	$1.7^{+0.1+1.9}_{-0.1-1.6}$	$40.2^{+4.8+4.8}_{-4.7-4.6}$	34
106	350–500	>1000	5–6	≥3	$1.9^{+1.1+0.3}_{-0.8-0.3}$	$3.8^{+1.1+0.7}_{-1.0-0.7}$	$1.14^{+0.05+0.62}_{-0.05-0.62}$	$2.4^{+0.3+2.7}_{-0.3-2.1}$	$9.2^{+2.2+2.8}_{-1.9-2.3}$	8
107	500–750	500–1000	5–6	≥3	$1.8^{+1.1+0.3}_{-0.8-0.3}$	$1.71^{+0.77+0.67}_{-0.61-0.67}$	$1.48^{+0.05+0.81}_{-0.05-0.80}$	$0.20^{+0.04+0.23}_{-0.04-0.17}$	$5.2^{+1.8+1.1}_{-1.5-1.1}$	4
108	500–750	>1000	5–6	≥3	$1.13^{+0.96+0.25}_{-0.66-0.25}$	$0.94^{+0.67+0.27}_{-0.49-0.27}$	$0.73^{+0.04+0.40}_{-0.04-0.40}$	$0.11^{+0.03+0.12}_{-0.03-0.08}$	$2.9^{+1.6+0.6}_{-1.1-0.6}$	2
109	>750	750–1500	5–6	≥3	$0.00^{+0.72+0.00}_{-0.00-0.00}$	$0.07^{+0.46+0.04}_{-0.06-0.04}$	$0.31^{+0.03+0.17}_{-0.03-0.17}$	$0.02^{+0.04+0.03}_{-0.02-0.00}$	$0.4^{+1.2+0.2}_{-0.1-0.2}$	0
110	>750	>1500	5–6	≥3	$0.00^{+0.63+0.00}_{-0.00-0.00}$	$0.03^{+0.46+0.01}_{-0.02-0.01}$	$0.11^{+0.02+0.06}_{-0.02-0.06}$	$0.00^{+0.02+0.01}_{-0.00-0.00}$	$0.1^{+1.1+0.1}_{-0.0-0.1}$	1

Table B.4: Observed numbers of events and prefit background predictions in the $7 \leq N_{jet} \leq 8$ search regions. The first uncertainty is statistical and second systematic.

Bin	H_T^{miss} [GeV]	H_T [GeV]	N_{jet}	$N_{b\text{-}jet}$	Lost-e/μ	$\tau \to$ had	$Z \to \nu\bar{\nu}$	QCD	Total pred.	Obs.
111	300–350	500–1000	7–8	0	$48.0^{+3.9+5.4}_{-3.8-5.4}$	$60.8^{+3.4+6.0}_{-3.4-6.0}$	76^{+5+11}_{-5-10}	30^{+2+12}_{-2-11}	215^{+9+18}_{-9-17}	218
112	300–350	>1000	7–8	0	$21.2^{+2.9+2.3}_{-2.9-2.3}$	$20.3^{+2.2+2.8}_{-2.1-2.8}$	$23.9^{+3.3+2.8}_{-2.9-2.5}$	$20.5^{+0.5+8.5}_{-0.5-7.8}$	$85.9^{+6.1+9.6}_{-5.8-9.0}$	85
113	350–500	500–1000	7–8	0	$43.2^{+3.9+4.9}_{-3.9-4.9}$	$54.2^{+3.6+5.7}_{-3.5-5.7}$	89^{+6+11}_{-5-10}	$14.3^{+1.9+5.9}_{-1.9-5.4}$	201^{+10+14}_{-9-14}	215
114	350–500	>1000	7–8	0	$22.5^{+2.8+2.7}_{-2.7-2.7}$	$23.3^{+2.5+2.3}_{-2.4-2.3}$	$48.3^{+4.7+5.4}_{-4.3-4.8}$	$12.6^{+0.7+5.2}_{-0.7-4.8}$	$106.7^{+7.1+8.3}_{-6.7-7.7}$	75
115	500–750	500–1000	7–8	0	$6.9^{+1.8+1.4}_{-1.7-1.4}$	$4.96^{+0.95+0.77}_{-0.84-0.77}$	$26.5^{+3.6+3.3}_{-3.2-3.0}$	$0.88^{+0.10+0.36}_{-0.10-0.34}$	$39.2^{+4.5+3.7}_{-4.1-3.5}$	34
116	500–750	>1000	7–8	0	$5.4^{+1.1+0.9}_{-1.0-0.9}$	$9.9^{+1.6+1.7}_{-1.5-1.7}$	$27.2^{+3.7+3.1}_{-3.2-2.8}$	$1.56^{+0.12+0.64}_{-0.12-0.59}$	$44.1^{+4.5+3.7}_{-4.1-3.5}$	38
117	>750	750–1500	7–8	0	$1.26^{+0.70+0.50}_{-0.58-0.50}$	$1.44^{+0.74+0.24}_{-0.57-0.24}$	$3.6^{+1.4+0.7}_{-1.0-0.6}$	$0.07^{+0.02+0.03}_{-0.02-0.03}$	$6.4^{+2.0+0.9}_{-1.5-0.8}$	5
118	>750	>1500	7–8	0	$0.69^{+0.47+0.16}_{-0.35-0.16}$	$1.03^{+0.69+0.15}_{-0.51-0.15}$	$1.5^{+1.2+0.3}_{-0.7-0.3}$	$0.07^{+0.01+0.03}_{-0.01-0.03}$	$3.3^{+1.7+0.4}_{-1.1-0.4}$	5
119	300–350	500–1000	7–8	1	$64.7^{+5.1+6.4}_{-5.1-6.4}$	$77.0^{+3.9+7.5}_{-3.8-7.4}$	$31.7^{+2.1+8.6}_{-1.9-8.4}$	$11.2^{+0.5+4.7}_{-0.5-4.3}$	184^{+9+14}_{-9-14}	146
120	300–350	>1000	7–8	1	$16.3^{+2.4+1.7}_{-2.4-1.7}$	$19.9^{+2.2+2.1}_{-2.1-2.1}$	$10.3^{+1.4+2.7}_{-1.2-2.6}$	$8.3^{+0.2+3.5}_{-0.2-3.2}$	$54.8^{+4.8+5.2}_{-4.7-5.0}$	68
121	350–500	500–1000	7–8	1	$46.9^{+4.4+5.0}_{-4.4-5.0}$	$58.6^{+3.7+5.7}_{-3.7-5.7}$	$37.0^{+2.4+9.7}_{-2.2-9.5}$	$7.5^{+0.4+3.2}_{-0.5-2.9}$	150^{+8+13}_{-8-12}	113
122	350–500	>1000	7–8	1	$19.5^{+2.5+2.1}_{-2.4-2.1}$	$19.5^{+2.3+2.0}_{-2.3-2.0}$	$21.0^{+2.0+5.4}_{-1.9-5.3}$	$5.3^{+0.5+2.2}_{-0.5-2.0}$	$65.3^{+5.2+6.5}_{-5.1-6.4}$	67
123	500–750	500–1000	7–8	1	$7.6^{+2.0+1.4}_{-1.9-1.4}$	$5.5^{+1.1+0.8}_{-1.1-0.8}$	$11.5^{+1.6+3.0}_{-1.4-3.0}$	$0.36^{+0.04+0.15}_{-0.04-0.14}$	$24.9^{+3.5+3.4}_{-3.3-3.4}$	19
124	500–750	>1000	7–8	1	$9.3^{+2.1+1.3}_{-2.0-1.3}$	$7.5^{+1.5+0.8}_{-1.4-0.8}$	$11.4^{+1.5+3.0}_{-1.4-2.9}$	$0.98^{+0.12+0.41}_{-0.12-0.37}$	$29.2^{+3.9+3.3}_{-3.7-3.3}$	22
125	>750	750–1500	7–8	1	$0.14^{+0.30+0.05}_{-0.14-0.00}$	$0.44^{+0.51+0.10}_{-0.22-0.10}$	$1.48^{+0.56+0.44}_{-0.42-0.43}$	$0.07^{+0.03+0.03}_{-0.03-0.03}$	$2.14^{+0.99+0.46}_{-0.56-0.45}$	4
126	>750	>1500	7–8	1	$0.00^{+0.47+0.01}_{-0.00-0.00}$	$0.14^{+0.47+0.02}_{-0.08-0.02}$	$0.70^{+0.55+0.22}_{-0.34-0.21}$	$0.03^{+0.01+0.01}_{-0.01-0.01}$	$0.9^{+1.1+0.2}_{-0.3-0.2}$	6
127	300–350	500–1000	7–8	2	$34.7^{+3.5+3.6}_{-3.5-3.6}$	$47.7^{+3.0+4.4}_{-3.0-4.4}$	$8.1^{+0.5+3.6}_{-0.5-3.5}$	$5.3^{+0.5+2.1}_{-0.5-2.1}$	$95.8^{+6.6+7.1}_{-6.5-7.0}$	95
128	300–350	>1000	7–8	2	$9.0^{+2.1+1.2}_{-2.1-1.2}$	$10.8^{+1.4+1.3}_{-1.4-1.3}$	$2.4^{+0.3+1.0}_{-0.3-1.0}$	$3.2^{+0.1+1.3}_{-0.1-1.3}$	$25.4^{+3.6+2.4}_{-3.4-2.4}$	26
129	350–500	500–1000	7–8	2	$26.2^{+3.0+2.9}_{-3.0-2.9}$	$31.0^{+2.5+3.3}_{-2.5-3.2}$	$9.6^{+0.6+4.1}_{-0.6-4.1}$	$2.5^{+0.2+1.0}_{-0.2-1.0}$	$69.3^{+5.6+6.1}_{-5.5-6.1}$	84
130	350–500	>1000	7–8	2	$13.3^{+2.5+1.5}_{-2.4-1.5}$	$13.3^{+1.8+1.3}_{-1.7-1.3}$	$4.7^{+0.5+2.0}_{-0.4-2.0}$	$1.95^{+0.13+0.78}_{-0.13-0.75}$	$33.3^{+4.3+3.0}_{-4.2-2.9}$	35
131	500–750	500–1000	7–8	2	$2.5^{+1.4+0.5}_{-1.2-0.5}$	$0.86^{+0.50+0.21}_{-0.18-0.21}$	$2.6^{+0.3+1.1}_{-0.3-1.1}$	$0.10^{+0.01+0.04}_{-0.01-0.04}$	$6.0^{+1.9+1.3}_{-1.4-1.3}$	7
132	500–750	>1000	7–8	2	$6.0^{+2.3+1.0}_{-2.2-1.0}$	$3.3^{+1.0+0.6}_{-0.9-0.6}$	$2.9^{+0.4+1.2}_{-0.3-1.2}$	$0.22^{+0.06+0.09}_{-0.06-0.08}$	$12.4^{+3.4+1.7}_{-3.1-1.7}$	12
133	>750	750–1500	7–8	2	$0.16^{+0.34+0.08}_{-0.16-0.00}$	$0.44^{+0.56+0.15}_{-0.32-0.15}$	$0.39^{+0.15+0.18}_{-0.13-0.18}$	$0.03^{+0.01+0.01}_{-0.01-0.01}$	$1.03^{+0.91+0.25}_{-0.49-0.23}$	2
134	>750	>1500	7–8	2	$0.53^{+0.62+0.20}_{-0.38-0.20}$	$0.61^{+0.57+0.22}_{-0.33-0.22}$	$0.13^{+0.10+0.06}_{-0.06-0.06}$	$0.06^{+0.02+0.02}_{-0.02-0.02}$	$1.3^{+1.2+0.3}_{-0.7-0.3}$	2
135	300–350	500–1000	7–8	≥3	$8.1^{+1.8+1.0}_{-1.7-1.0}$	$9.4^{+1.4+1.3}_{-1.3-1.3}$	$4.1^{+0.3+2.3}_{-0.2-2.3}$	$2.9^{+0.6+3.3}_{-0.6-2.3}$	$24.6^{+3.2+4.3}_{-3.1-3.7}$	12
136	300–350	>1000	7–8	≥3	$4.7^{+2.0+0.7}_{-1.8-0.7}$	$5.4^{+1.2+0.8}_{-1.1-0.8}$	$1.51^{+0.21+0.85}_{-0.18-0.84}$	$2.4^{+0.3+2.7}_{-0.3-2.1}$	$13.9^{+3.2+3.0}_{-2.9-2.5}$	8
137	350–500	500–1000	7–8	≥3	$5.9^{+1.9+0.8}_{-1.7-0.8}$	$7.4^{+1.4+1.2}_{-1.3-1.2}$	$4.7^{+0.3+2.7}_{-0.3-2.7}$	$1.2^{+0.1+1.3}_{-0.1-1.1}$	$19.2^{+3.2+3.3}_{-3.1-3.2}$	16
138	350–500	>1000	7–8	≥3	$2.6^{+1.1+0.3}_{-1.0-0.3}$	$4.8^{+1.3+0.7}_{-1.2-0.7}$	$3.1^{+0.3+1.8}_{-0.3-1.8}$	$2.1^{+0.3+2.3}_{-0.2-2.6}$	$12.6^{+2.5+3.0}_{-2.2-2.6}$	8
139	500–750	500–1000	7–8	≥3	$0.23^{+0.48+0.08}_{-0.23-0.00}$	$0.30^{+0.48+0.10}_{-0.13-0.10}$	$1.70^{+0.23+0.96}_{-0.20-0.96}$	$0.11^{+0.04+0.12}_{-0.04-0.08}$	$2.34^{+0.99+0.98}_{-0.41-0.96}$	3
140	500–750	>1000	7–8	≥3	$3.4^{+2.4+0.7}_{-2.1-0.7}$	$1.59^{+0.83+0.49}_{-0.69-0.49}$	$1.51^{+0.20+0.85}_{-0.18-0.85}$	$0.22^{+0.08+0.24}_{-0.08-0.14}$	$6.7^{+3.2+1.2}_{-2.7-1.2}$	4
141	>750	750–1500	7–8	≥3	$0.00^{+0.56+0.00}_{-0.00-0.00}$	$0.05^{+0.46+0.02}_{-0.03-0.02}$	$0.19^{+0.07+0.11}_{-0.05-0.11}$	$0.03^{+0.04+0.03}_{-0.03-0.00}$	$0.3^{+1.0+0.1}_{-0.1-0.1}$	0
142	>750	>1500	7–8	≥3	$0.00^{+0.72+0.00}_{-0.00-0.00}$	$0.04^{+0.46+0.02}_{-0.02-0.02}$	$0.12^{+0.10+0.07}_{-0.06-0.07}$	$0.01^{+0.03+0.01}_{-0.01-0.00}$	$0.2^{+1.2+0.1}_{-0.1-0.1}$	0

Table B.5: Observed numbers of events and prefit background predictions in the $N_{\text{jet}} \geq 9$ search regions. The first uncertainty is statistical and second systematic.

Bin	H_T^{miss} [GeV]	H_T [GeV]	N_{jet}	$N_{\text{b-jet}}$	Lost-e/μ	$\tau \to$ had	$Z \to \nu\bar{\nu}$	QCD	Total pred.	Obs.
143	300–350	500–1000	≥ 9	0	$6.2^{+2.7+1.7}_{-2.6-1.7}$	$3.46^{+0.89+0.59}_{-0.77-0.59}$	$2.6^{+1.2+0.7}_{-0.9-0.7}$	$2.9^{+0.3+1.3}_{-0.3-1.1}$	$15.1^{+3.8+2.3}_{-3.5-2.2}$	7
144	300–350	>1000	≥ 9	0	$3.5^{+1.2+0.6}_{-1.1-0.6}$	$4.6^{+1.0+0.6}_{-0.9-0.6}$	$3.0^{+1.4+0.6}_{-1.0-0.6}$	$4.2^{+0.3+1.9}_{-0.3-1.6}$	$15.2^{+2.7+2.1}_{-2.3-1.9}$	12
145	350–500	500–1000	≥ 9	0	$2.39^{+0.99+0.69}_{-0.89-0.69}$	$2.39^{+0.86+0.48}_{-0.73-0.48}$	$2.9^{+1.3+0.7}_{-0.9-0.6}$	$0.97^{+0.08+0.43}_{-0.08-0.37}$	$8.6^{+2.3+1.2}_{-1.9-1.1}$	6
146	350–500	>1000	≥ 9	0	$3.7^{+1.1+0.6}_{-1.1-0.6}$	$4.6^{+1.0+0.6}_{-0.9-0.6}$	$5.5^{+1.9+1.0}_{-1.5-0.9}$	$3.1^{+0.2+1.4}_{-0.2-1.2}$	$17.0^{+2.9+1.9}_{-2.5-1.7}$	13
147	500–750	500–1000	≥ 9	0	$0.15^{+0.32+0.10}_{-0.15-0.04}$	$0.35^{+0.55+0.12}_{-0.30-0.12}$	$1.0^{+1.3+0.4}_{-0.7-0.4}$	$0.10^{+0.05+0.04}_{-0.05-0.04}$	$1.6^{+1.6+0.5}_{-0.8-0.4}$	2
148	500–750	>1000	≥ 9	0	$0.98^{+0.50+0.26}_{-0.41-0.26}$	$1.98^{+0.74+0.30}_{-0.58-0.30}$	$3.5^{+1.6+0.7}_{-1.1-0.7}$	$0.47^{+0.05+0.21}_{-0.05-0.18}$	$6.9^{+2.0+0.8}_{-1.5-0.8}$	11
149	>750	750–1500	≥ 9	0	$0.00^{+0.44+0.00}_{-0.00-0.00}$	$0.00^{+0.46+0.00}_{-0.00-0.00}$	$0.00^{+0.64+0.00}_{-0.00-0.00}$	$0.01^{+0.02+0.00}_{-0.01-0.00}$	$0.0^{+1.1+0.0}_{-0.0-0.0}$	0
150	>750	>1500	≥ 9	0	$0.23^{+0.27+0.16}_{-0.17-0.16}$	$0.28^{+0.50+0.08}_{-0.21-0.08}$	$0.00^{+0.82+0.00}_{-0.00-0.00}$	$0.05^{+0.03+0.02}_{-0.03-0.02}$	$0.6^{+1.1+0.2}_{-0.4-0.2}$	1
151	300–350	500–1000	≥ 9	1	$6.5^{+1.8+1.1}_{-1.7-1.1}$	$4.57^{+0.93+0.77}_{-0.81-0.77}$	$1.83^{+0.84+0.68}_{-0.60-0.74}$	$1.02^{+0.06+0.42}_{-0.06-0.40}$	$13.9^{+2.8+1.5}_{-2.6-1.6}$	25
152	300–350	>1000	≥ 9	1	$5.7^{+1.6+0.7}_{-1.5-0.7}$	$7.3^{+1.3+1.1}_{-1.2-1.1}$	$2.08^{+0.95+0.69}_{-0.68-0.77}$	$2.43^{+0.06+0.99}_{-0.06-0.94}$	$17.5^{+3.0+1.8}_{-2.8-1.8}$	20
153	350–500	500–1000	≥ 9	1	$2.92^{+0.94+0.57}_{-0.84-0.57}$	$2.96^{+0.77+0.60}_{-0.61-0.60}$	$2.00^{+0.91+0.71}_{-0.65-0.78}$	$0.53^{+0.05+0.22}_{-0.05-0.21}$	$8.4^{+1.9+1.1}_{-1.6-1.2}$	8
154	350–500	>1000	≥ 9	1	$5.4^{+1.4+0.7}_{-1.3-0.7}$	$7.7^{+1.4+1.1}_{-1.3-1.1}$	$3.9^{+1.3+1.3}_{-1.0-1.4}$	$1.48^{+0.05+0.60}_{-0.05-0.57}$	$18.4^{+3.1+1.9}_{-2.8-2.0}$	14
155	500–750	500–1000	≥ 9	1	$0.14^{+0.30+0.08}_{-0.14-0.00}$	$0.24^{+0.49+0.21}_{-0.18-0.16}$	$0.71^{+0.94+0.35}_{-0.46-0.36}$	$0.03^{+0.03+0.01}_{-0.03-0.00}$	$1.1^{+1.2+0.4}_{-0.6-0.4}$	1
156	500–750	>1000	≥ 9	1	$0.68^{+0.58+0.12}_{-0.41-0.12}$	$1.20^{+0.64+0.21}_{-0.44-0.21}$	$2.4^{+1.1+0.8}_{-0.8-0.9}$	$0.20^{+0.02+0.08}_{-0.02-0.07}$	$4.5^{+1.6+0.8}_{-1.2-0.9}$	4
157	>750	750–1500	≥ 9	1	$0.00^{+0.73+0.00}_{-0.00-0.00}$	$0.04^{+0.46+0.02}_{-0.04-0.00}$	$0.00^{+0.45+0.00}_{-0.00-0.00}$	$0.01^{+0.01+0.00}_{-0.01-0.00}$	$0.1^{+1.3+0.0}_{-0.0-0.0}$	0
158	>750	>1500	≥ 9	1	$0.13^{+0.27+0.06}_{-0.13-0.00}$	$0.03^{+0.46+0.01}_{-0.02-0.01}$	$0.00^{+0.57+0.00}_{-0.00-0.00}$	$0.02^{+0.01+0.01}_{-0.01-0.01}$	$0.18^{+0.93+0.06}_{-0.15-0.01}$	0
159	300–350	500–1000	≥ 9	2	$4.1^{+1.3+0.7}_{-1.2-0.7}$	$4.68^{+0.92+0.85}_{-0.80-0.85}$	$0.64^{+0.29+0.34}_{-0.21-0.36}$	$0.40^{+0.06+0.24}_{-0.05-0.21}$	$9.8^{+2.2+1.2}_{-2.0-1.2}$	13
160	300–350	>1000	≥ 9	2	$5.2^{+1.6+0.7}_{-1.5-0.7}$	$5.5^{+1.2+1.0}_{-1.1-1.0}$	$0.73^{+0.33+0.37}_{-0.24-0.39}$	$1.32^{+0.15+0.68}_{-0.15-0.58}$	$12.7^{+2.8+1.4}_{-2.6-1.4}$	10
161	350–500	500–1000	≥ 9	2	$3.01^{+0.91+0.63}_{-0.82-0.63}$	$4.7^{+1.1+0.9}_{-1.0-0.9}$	$0.70^{+0.32+0.36}_{-0.23-0.39}$	$0.30^{+0.08+0.14}_{-0.08-0.12}$	$8.7^{+2.0+1.1}_{-1.8-1.1}$	4
162	350–500	>1000	≥ 9	2	$4.4^{+1.1+0.6}_{-1.1-0.6}$	$6.3^{+1.4+0.8}_{-1.3-0.8}$	$1.35^{+0.47+0.67}_{-0.36-0.72}$	$0.63^{+0.03+0.32}_{-0.03-0.27}$	$12.7^{+2.6+1.3}_{-2.4-1.3}$	12
163	500–750	500–1000	≥ 9	2	$0.00^{+0.39+0.00}_{-0.00-0.00}$	$0.35^{+0.49+0.17}_{-0.18-0.17}$	$0.25^{+0.33+0.15}_{-0.16-0.16}$	$0.01^{+0.01+0.01}_{-0.01-0.00}$	$0.61^{+0.95+0.23}_{-0.24-0.23}$	0
164	500–750	>1000	≥ 9	2	$2.0^{+1.1+0.4}_{-0.9-0.4}$	$1.95^{+0.87+0.45}_{-0.73-0.45}$	$0.84^{+0.39+0.43}_{-0.28-0.46}$	$0.09^{+0.02+0.04}_{-0.02-0.04}$	$4.9^{+2.0+0.7}_{-1.7-0.7}$	7
165	>750	750–1500	≥ 9	2	$0.00^{+0.60+0.00}_{-0.00-0.00}$	$0.01^{+0.46+0.01}_{-0.00-0.00}$	$0.00^{+0.16+0.00}_{-0.00-0.00}$	$0.00^{+0.01+0.00}_{-0.00-0.00}$	$0.0^{+1.1+0.0}_{-0.0-0.0}$	0
166	>750	>1500	≥ 9	2	$0.00^{+0.38+0.00}_{-0.00-0.00}$	$0.00^{+0.46+0.00}_{-0.00-0.00}$	$0.00^{+0.20+0.00}_{-0.00-0.00}$	$0.01^{+0.02+0.00}_{-0.01-0.00}$	$0.01^{+0.87+0.00}_{-0.01-0.00}$	0
167	300–350	500–1000	≥ 9	≥ 3	$1.06^{+0.63+0.27}_{-0.50-0.27}$	$1.06^{+0.57+0.29}_{-0.34-0.29}$	$0.37^{+0.17+0.26}_{-0.12-0.28}$	$0.47^{+0.13+0.56}_{-0.13-0.34}$	$3.0^{+1.2+0.7}_{-0.9-0.6}$	1
168	300–350	>1000	≥ 9	≥ 3	$3.5^{+1.7+0.5}_{-1.5-0.5}$	$2.6^{+1.0+0.7}_{-0.9-0.7}$	$0.42^{+0.19+0.29}_{-0.14-0.31}$	$2.1^{+0.3+2.4}_{-0.3-1.8}$	$8.6^{+2.7+2.6}_{-2.4-2.0}$	4
169	350–500	500–1000	≥ 9	≥ 3	$1.03^{+0.60+0.30}_{-0.47-0.30}$	$1.58^{+0.71+0.43}_{-0.55-0.43}$	$0.40^{+0.18+0.28}_{-0.13-0.31}$	$0.10^{+0.03+0.11}_{-0.03-0.07}$	$3.1^{+1.3+0.6}_{-1.0-0.6}$	3
170	350–500	>1000	≥ 9	≥ 3	$0.81^{+0.56+0.14}_{-0.41-0.14}$	$0.96^{+0.54+0.16}_{-0.27-0.16}$	$0.77^{+0.27+0.53}_{-0.20-0.58}$	$1.3^{+0.2+1.5}_{-0.2-1.1}$	$3.8^{+1.1+1.6}_{-0.7-1.3}$	2
171	500–750	500–1000	≥ 9	≥ 3	$0.00^{+0.43+0.00}_{-0.00-0.00}$	$0.03^{+0.46+0.03}_{-0.02-0.03}$	$0.14^{+0.19+0.11}_{-0.09-0.11}$	$0.01^{+0.02+0.01}_{-0.01-0.00}$	$0.18^{+0.91+0.11}_{-0.09-0.11}$	0
172	500–750	>1000	≥ 9	≥ 3	$0.00^{+0.48+0.00}_{-0.00-0.00}$	$0.53^{+0.56+0.13}_{-0.31-0.13}$	$0.48^{+0.22+0.33}_{-0.16-0.37}$	$0.13^{+0.14+0.15}_{-0.13-0.00}$	$1.1^{+1.1+0.4}_{-0.4-0.4}$	3
173	>750	750–1500	≥ 9	≥ 3	$0.00^{+0.50+0.00}_{-0.00-0.00}$	$0.00^{+0.46+0.00}_{-0.00-0.00}$	$0.00^{+0.09+0.00}_{-0.00-0.00}$	$0.01^{+0.05+0.02}_{-0.01-0.00}$	$0.01^{+0.97+0.02}_{-0.01-0.00}$	0
174	>750	>1500	≥ 9	≥ 3	$0.00^{+0.42+0.00}_{-0.00-0.00}$	$0.00^{+0.46+0.00}_{-0.00-0.00}$	$0.00^{+0.11+0.00}_{-0.00-0.00}$	$0.02^{+0.05+0.02}_{-0.02-0.00}$	$0.02^{+0.89+0.02}_{-0.02-0.00}$	0

Table B.6: Observed numbers of events and prefit background predictions in the aggregate search regions. The first uncertainty is statistical and second systematic.

Bin	H_T^{miss} [GeV]	H_T [GeV]	N_{jet}	$N_{b\text{-jet}}$	Lost-e/μ	$\tau \to$ had	$Z \to \nu\bar{\nu}$	QCD	Total pred.	Obs.
1	>500	>500	≥2	0	842^{+25+48}_{-25-46}	753^{+16+65}_{-16-65}	$5968^{+48+360}_{-47-350}$	$21.4^{+0.6+8.5}_{-0.6-7.1}$	$7584^{+63+370}_{-62-360}$	7838
2	>750	>1500	≥3	0	$4.8^{+2.2+0.6}_{-1.6-0.6}$	$4.2^{+1.3+0.3}_{-0.9-0.3}$	$45.8^{+5.1+5.2}_{-4.3-4.9}$	$0.47^{+0.06+0.18}_{-0.06-0.16}$	$55.2^{+6.2+5.3}_{-5.0-4.9}$	71
3	>500	>500	≥5	0	$111.0^{+6.4+8.3}_{-6.3-7.9}$	$127.6^{+5.9+8.5}_{-5.7-8.6}$	558^{+15+36}_{-14-34}	$9.4^{+0.2+3.5}_{-0.2-3.1}$	806^{+19+38}_{-18-37}	819
4	>750	>1500	≥5	0	$1.82^{+0.82+0.26}_{-0.59-0.21}$	$2.8^{+1.1+0.2}_{-0.7-0.2}$	$18.1^{+3.3+2.7}_{-2.6-2.6}$	$0.37^{+0.06+0.15}_{-0.06-0.13}$	$23.0^{+3.8+2.7}_{-2.9-2.6}$	25
5	>750	>1500	≥9	0	$0.23^{+0.27+0.14}_{-0.17-0.07}$	$0.28^{+0.50+0.08}_{-0.21-0.07}$	$0.00^{+0.82+0.00}_{-0.00-0.00}$	$0.05^{+0.03+0.02}_{-0.03-0.02}$	$0.6^{+1.1+0.2}_{-0.4-0.1}$	1
6	>500	>500	≥2	≥2	$46.9^{+8.9+3.1}_{-5.9-3.0}$	$44.0^{+4.4+3.2}_{-3.4-3.2}$	102^{+2+14}_{-1-14}	$2.5^{+0.3+1.5}_{-0.2-1.3}$	196^{+13+15}_{-9-15}	216
7	>750	>750	≥3	≥1	$11.5^{+4.1+1.0}_{-2.2-0.9}$	$13.7^{+3.0+1.2}_{-2.0-1.2}$	87^{+3+10}_{-3-10}	$0.87^{+0.15+0.34}_{-0.11-0.31}$	113^{+8+10}_{-5-10}	123
8	>500	>500	≥5	≥3	$6.6^{+3.3+0.6}_{-2.3-0.6}$	$5.3^{+1.9+0.9}_{-1.1-0.9}$	$6.8^{+0.5+2.8}_{-0.3-2.8}$	$0.87^{+0.20+0.96}_{-0.17-0.70}$	$19.5^{+5.2+3.2}_{-3.4-3.1}$	17
9	>750	>1500	≥5	≥2	$1.3^{+1.4+0.2}_{-0.6-0.2}$	$1.8^{+1.3+0.4}_{-0.7-0.4}$	$1.20^{+0.41+0.33}_{-0.19-0.33}$	$0.13^{+0.07+0.06}_{-0.04-0.05}$	$4.4^{+2.8+0.6}_{-1.3-0.6}$	6
10	>750	>750	≥9	≥3	$0.00^{+0.66+0.00}_{-0.00-0.00}$	$0.00^{+0.65+0.00}_{-0.00-0.00}$	$0.00^{+0.15+0.00}_{-0.00-0.00}$	$0.03^{+0.07+0.04}_{-0.02-0.01}$	$0.0^{+1.3+0.0}_{-0.0-0.0}$	0
11	>300	>300	≥7	≥1	328^{+12+21}_{-12-20}	380^{+10+22}_{-9-22}	193^{+8+38}_{-6-38}	69^{+1+29}_{-1-26}	969^{+23+57}_{-22-55}	890
12	>750	>750	≥5	≥1	$7.2^{+2.8+0.8}_{-1.6-0.7}$	$7.7^{+2.4+0.8}_{-1.4-0.8}$	$26.6^{+2.4+3.9}_{-1.8-3.7}$	$0.65^{+0.14+0.26}_{-0.11-0.23}$	$42.2^{+5.7+4.0}_{-3.5-3.9}$	48

C The CMS Collaboration

Yerevan Physics Institute, Yerevan, Armenia
A.M. Sirunyan, A. Tumasyan

Institut für Hochenergiephysik, Wien, Austria
W. Adam, F. Ambrogi, E. Asilar, T. Bergauer, J. Brandstetter, E. Brondolin, M. Dragicevic, J. Erö, M. Flechl, M. Friedl, R. Frühwirth[1], V.M. Ghete, J. Grossmann, J. Hrubec, M. Jeitler[1], A. König, N. Krammer, I. Krätschmer, D. Liko, T. Madlener, I. Mikulec, E. Pree, D. Rabady, N. Rad, H. Rohringer, J. Schieck[1], R. Schöfbeck, M. Spanring, D. Spitzbart, J. Strauss, W. Waltenberger, J. Wittmann, C.-E. Wulz[1], M. Zarucki

Institute for Nuclear Problems, Minsk, Belarus
V. Chekhovsky, V. Mossolov, J. Suarez Gonzalez

Universiteit Antwerpen, Antwerpen, Belgium
E.A. De Wolf, D. Di Croce, X. Janssen, J. Lauwers, M. Van De Klundert, H. Van Haevermaet, P. Van Mechelen, N. Van Remortel, A. Van Spilbeeck

Vrije Universiteit Brussel, Brussel, Belgium
S. Abu Zeid, F. Blekman, J. D'Hondt, I. De Bruyn, J. De Clercq, K. Deroover, G. Flouris, D. Lontkovskyi, S. Lowette, S. Moortgat, L. Moreels, A. Olbrechts, Q. Python, K. Skovpen, S. Tavernier, W. Van Doninck, P. Van Mulders, I. Van Parijs

Université Libre de Bruxelles, Bruxelles, Belgium
H. Brun, B. Clerbaux, G. De Lentdecker, H. Delannoy, G. Fasanella, L. Favart, R. Goldouzian, A. Grebenyuk, G. Karapostoli, T. Lenzi, J. Luetic, T. Maerschalk, A. Marinov, A. Randle-conde, T. Seva, C. Vander Velde, P. Vanlaer, D. Vannerom, R. Yonamine, F. Zenoni, F. Zhang[2]

Ghent University, Ghent, Belgium
A. Cimmino, T. Cornelis, D. Dobur, A. Fagot, M. Gul, I. Khvastunov, D. Poyraz, C. Roskas, S. Salva, M. Tytgat, W. Verbeke, N. Zaganidis

Université Catholique de Louvain, Louvain-la-Neuve, Belgium
H. Bakhshiansohi, O. Bondu, S. Brochet, G. Bruno, A. Caudron, S. De Visscher, C. Delaere, M. Delcourt, B. Francois, A. Giammanco, A. Jafari, M. Komm, G. Krintiras, V. Lemaitre, A. Magitteri, A. Mertens, M. Musich, K. Piotrzkowski, L. Quertenmont, M. Vidal Marono, S. Wertz

Université de Mons, Mons, Belgium
N. Beliy

Centro Brasileiro de Pesquisas Fisicas, Rio de Janeiro, Brazil
W.L. Aldá Júnior, F.L. Alves, G.A. Alves, L. Brito, M. Correa Martins Junior, C. Hensel, A. Moraes, M.E. Pol, P. Rebello Teles

Universidade do Estado do Rio de Janeiro, Rio de Janeiro, Brazil
E. Belchior Batista Das Chagas, W. Carvalho, J. Chinellato[3], A. Custódio, E.M. Da Costa, G.G. Da Silveira[4], D. De Jesus Damiao, S. Fonseca De Souza, L.M. Huertas Guativa, H. Malbouisson, M. Melo De Almeida, C. Mora Herrera, L. Mundim, H. Nogima, A. Santoro, A. Sznajder, E.J. Tonelli Manganote[3], F. Torres Da Silva De Araujo, A. Vilela Pereira

Universidade Estadual Paulista [a], Universidade Federal do ABC [b], São Paulo, Brazil
S. Ahuja[a], C.A. Bernardes[a], T.R. Fernandez Perez Tomei[a], E.M. Gregores[b], P.G. Mercadante[b], C.S. Moon[a], S.F. Novaes[a], Sandra S. Padula[a], D. Romero Abad[b], J.C. Ruiz Vargas[a]

Institute for Nuclear Research and Nuclear Energy of Bulgaria Academy of Sciences
A. Aleksandrov, R. Hadjiiska, P. Iaydjiev, M. Misheva, M. Rodozov, M. Shopova, S. Stoykova, G. Sultanov

University of Sofia, Sofia, Bulgaria
A. Dimitrov, I. Glushkov, L. Litov, B. Pavlov, P. Petkov

Beihang University, Beijing, China
W. Fang[5], X. Gao[5]

Institute of High Energy Physics, Beijing, China
M. Ahmad, J.G. Bian, G.M. Chen, H.S. Chen, M. Chen, Y. Chen, C.H. Jiang, D. Leggat, Z. Liu, F. Romeo, S.M. Shaheen, A. Spiezia, J. Tao, C. Wang, Z. Wang, E. Yazgan, H. Zhang, J. Zhao

State Key Laboratory of Nuclear Physics and Technology, Peking University, Beijing, China
Y. Ban, G. Chen, Q. Li, S. Liu, Y. Mao, S.J. Qian, D. Wang, Z. Xu

Universidad de Los Andes, Bogota, Colombia
C. Avila, A. Cabrera, L.F. Chaparro Sierra, C. Florez, C.F. González Hernández, J.D. Ruiz Alvarez

University of Split, Faculty of Electrical Engineering, Mechanical Engineering and Naval Architecture, Split, Croatia
B. Courbon, N. Godinovic, D. Lelas, I. Puljak, P.M. Ribeiro Cipriano, T. Sculac

University of Split, Faculty of Science, Split, Croatia
Z. Antunovic, M. Kovac

Institute Rudjer Boskovic, Zagreb, Croatia
V. Brigljevic, D. Ferencek, K. Kadija, B. Mesic, T. Susa

University of Cyprus, Nicosia, Cyprus
M.W. Ather, A. Attikis, G. Mavromanolakis, J. Mousa, C. Nicolaou, F. Ptochos, P.A. Razis, H. Rykaczewski

Charles University, Prague, Czech Republic
M. Finger[6], M. Finger Jr.[6]

Universidad San Francisco de Quito, Quito, Ecuador
E. Carrera Jarrin

Academy of Scientific Research and Technology of the Arab Republic of Egypt, Egyptian Network of High Energy Physics, Cairo, Egypt
Y. Assran[7,8], S. Elgammal[8], A. Mahrous[9]

National Institute of Chemical Physics and Biophysics, Tallinn, Estonia
R.K. Dewanjee, M. Kadastik, L. Perrini, M. Raidal, A. Tiko, C. Veelken

Department of Physics, University of Helsinki, Helsinki, Finland
P. Eerola, J. Pekkanen, M. Voutilainen

Helsinki Institute of Physics, Helsinki, Finland
J. Härkönen, T. Järvinen, V. Karimäki, R. Kinnunen, T. Lampén, K. Lassila-Perini, S. Lehti, T. Lindén, P. Luukka, E. Tuominen, J. Tuominiemi, E. Tuovinen

Lappeenranta University of Technology, Lappeenranta, Finland
J. Talvitie, T. Tuuva

IRFU, CEA, Université Paris-Saclay, Gif-sur-Yvette, France
M. Besancon, F. Couderc, M. Dejardin, D. Denegri, J.L. Faure, F. Ferri, S. Ganjour, S. Ghosh, A. Givernaud, P. Gras, G. Hamel de Monchenault, P. Jarry, I. Kucher, E. Locci, M. Machet, J. Malcles, G. Negro, J. Rander, A. Rosowsky, M.Ö. Sahin, M. Titov

Laboratoire Leprince-Ringuet, Ecole polytechnique, CNRS/IN2P3, Université Paris-Saclay, Palaiseau, France
A. Abdulsalam, I. Antropov, S. Baffioni, F. Beaudette, P. Busson, L. Cadamuro, C. Charlot, O. Davignon, R. Granier de Cassagnac, M. Jo, S. Lisniak, A. Lobanov, J. Martin Blanco, M. Nguyen, C. Ochando, G. Ortona, P. Paganini, P. Pigard, S. Regnard, R. Salerno, J.B. Sauvan, Y. Sirois, A.G. Stahl Leiton, T. Strebler, Y. Yilmaz, A. Zabi

Université de Strasbourg, CNRS, IPHC UMR 7178, F-67000 Strasbourg, France
J.-L. Agram[10], J. Andrea, D. Bloch, J.-M. Brom, M. Buttignol, E.C. Chabert, N. Chanon, C. Collard, E. Conte[10], X. Coubez, J.-C. Fontaine[10], D. Gelé, U. Goerlach, M. Jansová, A.-C. Le Bihan, N. Tonon, P. Van Hove

Centre de Calcul de l'Institut National de Physique Nucleaire et de Physique des Particules, CNRS/IN2P3, Villeurbanne, France
S. Gadrat

Université de Lyon, Université Claude Bernard Lyon 1, CNRS-IN2P3, Institut de Physique Nucléaire de Lyon, Villeurbanne, France
S. Beauceron, C. Bernet, G. Boudoul, R. Chierici, D. Contardo, P. Depasse, H. El Mamouni, J. Fay, L. Finco, S. Gascon, M. Gouzevitch, G. Grenier, B. Ille, F. Lagarde, I.B. Laktineh, M. Lethuillier, L. Mirabito, A.L. Pequegnot, S. Perries, A. Popov[11], V. Sordini, M. Vander Donckt, S. Viret

Georgian Technical University, Tbilisi, Georgia
A. Khvedelidze[6]

Tbilisi State University, Tbilisi, Georgia
D. Lomidze

RWTH Aachen University, I. Physikalisches Institut, Aachen, Germany
C. Autermann, S. Beranek, L. Feld, M.K. Kiesel, K. Klein, M. Lipinski, M. Preuten, C. Schomakers, J. Schulz, T. Verlage

RWTH Aachen University, III. Physikalisches Institut A, Aachen, Germany
A. Albert, M. Brodski, E. Dietz-Laursonn, D. Duchardt, M. Endres, M. Erdmann, S. Erdweg, T. Esch, R. Fischer, A. Güth, M. Hamer, T. Hebbeker, C. Heidemann, K. Hoepfner, S. Knutzen, M. Merschmeyer, A. Meyer, P. Millet, S. Mukherjee, M. Olschewski, K. Padeken, T. Pook, M. Radziej, H. Reithler, M. Rieger, F. Scheuch, D. Teyssier, S. Thüer

RWTH Aachen University, III. Physikalisches Institut B, Aachen, Germany
G. Flügge, B. Kargoll, T. Kress, A. Künsken, J. Lingemann, T. Müller, A. Nehrkorn, A. Nowack, C. Pistone, O. Pooth, A. Stahl[12]

Deutsches Elektronen-Synchrotron, Hamburg, Germany
M. Aldaya Martin, T. Arndt, C. Asawatangtrakuldee, K. Beernaert, O. Behnke, U. Behrens, A.A. Bin Anuar, K. Borras[13], V. Botta, A. Campbell, P. Connor, C. Contreras-Campana, F. Costanza, C. Diez Pardos, G. Eckerlin, D. Eckstein, T. Eichhorn, E. Eren, E. Gallo[14], J. Garay Garcia, A. Geiser, A. Gizhko, J.M. Grados Luyando, A. Grohsjean, P. Gunnellini, A. Harb, J. Hauk, M. Hempel[15], H. Jung, A. Kalogeropoulos, M. Kasemann, J. Keaveney, C. Kleinwort,

I. Korol, D. Krücker, W. Lange, A. Lelek, T. Lenz, J. Leonard, K. Lipka, W. Lohmann[15], R. Mankel, I.-A. Melzer-Pellmann, A.B. Meyer, G. Mittag, J. Mnich, A. Mussgiller, E. Ntomari, D. Pitzl, R. Placakyte, A. Raspereza, B. Roland, M. Savitskyi, P. Saxena, R. Shevchenko, S. Spannagel, N. Stefaniuk, G.P. Van Onsem, R. Walsh, Y. Wen, K. Wichmann, C. Wissing, O. Zenaiev

University of Hamburg, Hamburg, Germany
S. Bein, V. Blobel, M. Centis Vignali, A.R. Draeger, T. Dreyer, E. Garutti, D. Gonzalez, J. Haller, M. Hoffmann, A. Junkes, A. Karavdina, R. Klanner, R. Kogler, N. Kovalchuk, S. Kurz, T. Lapsien, I. Marchesini, D. Marconi, M. Meyer, M. Niedziela, D. Nowatschin, F. Pantaleo[12], T. Peiffer, A. Perieanu, C. Scharf, P. Schleper, A. Schmidt, S. Schumann, J. Schwandt, J. Sonneveld, H. Stadie, G. Steinbrück, F.M. Stober, M. Stöver, H. Tholen, D. Troendle, E. Usai, L. Vanelderen, A. Vanhoefer, B. Vormwald

Institut für Experimentelle Kernphysik, Karlsruhe, Germany
M. Akbiyik, C. Barth, S. Baur, E. Butz, R. Caspart, T. Chwalek, F. Colombo, W. De Boer, A. Dierlamm, B. Freund, R. Friese, M. Giffels, A. Gilbert, D. Haitz, F. Hartmann[12], S.M. Heindl, U. Husemann, F. Kassel[12], S. Kudella, H. Mildner, M.U. Mozer, Th. Müller, M. Plagge, G. Quast, K. Rabbertz, M. Schröder, I. Shvetsov, G. Sieber, H.J. Simonis, R. Ulrich, S. Wayand, M. Weber, T. Weiler, S. Williamson, C. Wöhrmann, R. Wolf

Institute of Nuclear and Particle Physics (INPP), NCSR Demokritos, Aghia Paraskevi, Greece
G. Anagnostou, G. Daskalakis, T. Geralis, V.A. Giakoumopoulou, A. Kyriakis, D. Loukas, I. Topsis-Giotis

National and Kapodistrian University of Athens, Athens, Greece
S. Kesisoglou, A. Panagiotou, N. Saoulidou

University of Ioánnina, Ioánnina, Greece
I. Evangelou, C. Foudas, P. Kokkas, N. Manthos, I. Papadopoulos, E. Paradas, J. Strologas, F.A. Triantis

MTA-ELTE Lendület CMS Particle and Nuclear Physics Group, Eötvös Loránd University, Budapest, Hungary
M. Csanad, N. Filipovic, G. Pasztor

Wigner Research Centre for Physics, Budapest, Hungary
G. Bencze, C. Hajdu, D. Horvath[16], Á. Hunyadi, F. Sikler, V. Veszpremi, G. Vesztergombi[17], A.J. Zsigmond

Institute of Nuclear Research ATOMKI, Debrecen, Hungary
N. Beni, S. Czellar, J. Karancsi[18], A. Makovec, J. Molnar, Z. Szillasi

Institute of Physics, University of Debrecen, Debrecen, Hungary
M. Bartók[17], P. Raics, Z.L. Trocsanyi, B. Ujvari

Indian Institute of Science (IISc), Bangalore, India
S. Choudhury, J.R. Komaragiri

National Institute of Science Education and Research, Bhubaneswar, India
S. Bahinipati[19], S. Bhowmik, P. Mal, K. Mandal, A. Nayak[20], D.K. Sahoo[19], N. Sahoo, S.K. Swain

Panjab University, Chandigarh, India
S. Bansal, S.B. Beri, V. Bhatnagar, U. Bhawandeep, R. Chawla, N. Dhingra, A.K. Kalsi, A. Kaur, M. Kaur, R. Kumar, P. Kumari, A. Mehta, J.B. Singh, G. Walia

University of Delhi, Delhi, India
Ashok Kumar, Aashaq Shah, A. Bhardwaj, S. Chauhan, B.C. Choudhary, R.B. Garg, S. Keshri, A. Kumar, S. Malhotra, M. Naimuddin, K. Ranjan, R. Sharma, V. Sharma

Saha Institute of Nuclear Physics, HBNI, Kolkata, India
R. Bhardwaj, R. Bhattacharya, S. Bhattacharya, S. Dey, S. Dutt, S. Dutta, S. Ghosh, N. Majumdar, A. Modak, K. Mondal, S. Mukhopadhyay, S. Nandan, A. Purohit, A. Roy, D. Roy, S. Roy Chowdhury, S. Sarkar, M. Sharan, S. Thakur

Indian Institute of Technology Madras, Madras, India
P.K. Behera

Bhabha Atomic Research Centre, Mumbai, India
R. Chudasama, D. Dutta, V. Jha, V. Kumar, A.K. Mohanty[12], P.K. Netrakanti, L.M. Pant, P. Shukla, A. Topkar

Tata Institute of Fundamental Research-A, Mumbai, India
T. Aziz, S. Dugad, B. Mahakud, S. Mitra, G.B. Mohanty, B. Parida, N. Sur, B. Sutar

Tata Institute of Fundamental Research-B, Mumbai, India
S. Banerjee, S. Bhattacharya, S. Chatterjee, P. Das, M. Guchait, Sa. Jain, S. Kumar, M. Maity[21], G. Majumder, K. Mazumdar, T. Sarkar[21], N. Wickramage[22]

Indian Institute of Science Education and Research (IISER), Pune, India
S. Chauhan, S. Dube, V. Hegde, A. Kapoor, K. Kothekar, S. Pandey, A. Rane, S. Sharma

Institute for Research in Fundamental Sciences (IPM), Tehran, Iran
S. Chenarani[23], E. Eskandari Tadavani, S.M. Etesami[23], M. Khakzad, M. Mohammadi Najafabadi, M. Naseri, S. Paktinat Mehdiabadi[24], F. Rezaei Hosseinabadi, B. Safarzadeh[25], M. Zeinali

University College Dublin, Dublin, Ireland
M. Felcini, M. Grunewald

INFN Sezione di Bari [a], Università di Bari [b], Politecnico di Bari [c], Bari, Italy
M. Abbrescia[a,b], C. Calabria[a,b], C. Caputo[a,b], A. Colaleo[a], D. Creanza[a,c], L. Cristella[a,b], N. De Filippis[a,c], M. De Palma[a,b], F. Errico[a,b], L. Fiore[a], G. Iaselli[a,c], G. Maggi[a,c], M. Maggi[a], G. Miniello[a,b], S. My[a,b], S. Nuzzo[a,b], A. Pompili[a,b], G. Pugliese[a,c], R. Radogna[a,b], A. Ranieri[a], G. Selvaggi[a,b], A. Sharma[a], L. Silvestris[a,12], R. Venditti[a], P. Verwilligen[a]

INFN Sezione di Bologna [a], Università di Bologna [b], Bologna, Italy
G. Abbiendi[a], C. Battilana, D. Bonacorsi[a,b], S. Braibant-Giacomelli[a,b], L. Brigliadori[a,b], R. Campanini[a,b], P. Capiluppi[a,b], A. Castro[a,b], F.R. Cavallo[a], S.S. Chhibra[a,b], G. Codispoti[a,b], M. Cuffiani[a,b], G.M. Dallavalle[a], F. Fabbri[a], A. Fanfani[a,b], D. Fasanella[a,b], P. Giacomelli[a], L. Guiducci[a,b], S. Marcellini[a], G. Masetti[a], F.L. Navarria[a,b], A. Perrotta[a], A.M. Rossi[a,b], T. Rovelli[a,b], G.P. Siroli[a,b], N. Tosi[a,b,12]

INFN Sezione di Catania [a], Università di Catania [b], Catania, Italy
S. Albergo[a,b], S. Costa[a,b], A. Di Mattia[a], F. Giordano[a,b], R. Potenza[a,b], A. Tricomi[a,b], C. Tuve[a,b]

INFN Sezione di Firenze [a]**, Università di Firenze** [b]**, Firenze, Italy**
G. Barbagli[a], K. Chatterjee[a,b], V. Ciulli[a,b], C. Civinini[a], R. D'Alessandro[a,b], E. Focardi[a,b],
P. Lenzi[a,b], M. Meschini[a], S. Paoletti[a], L. Russo[a,26], G. Sguazzoni[a], D. Strom[a], L. Viliani[a,b,12]

INFN Laboratori Nazionali di Frascati, Frascati, Italy
L. Benussi, S. Bianco, F. Fabbri, D. Piccolo, F. Primavera[12]

INFN Sezione di Genova [a]**, Università di Genova** [b]**, Genova, Italy**
V. Calvelli[a,b], F. Ferro[a], E. Robutti[a], S. Tosi[a,b]

INFN Sezione di Milano-Bicocca [a]**, Università di Milano-Bicocca** [b]**, Milano, Italy**
L. Brianza[a,b], F. Brivio[a,b], V. Ciriolo[a,b], M.E. Dinardo[a,b], S. Fiorendi[a,b], S. Gennai[a], A. Ghezzi[a,b],
P. Govoni[a,b], M. Malberti[a,b], S. Malvezzi[a], R.A. Manzoni[a,b], D. Menasce[a], L. Moroni[a],
M. Paganoni[a,b], K. Pauwels[a,b], D. Pedrini[a], S. Pigazzini[a,b,27], S. Ragazzi[a,b], T. Tabarelli de
Fatis[a,b]

INFN Sezione di Napoli [a]**, Università di Napoli 'Federico II'** [b]**, Napoli, Italy, Università della
Basilicata** [c]**, Potenza, Italy, Università G. Marconi** [d]**, Roma, Italy**
S. Buontempo[a], N. Cavallo[a,c], S. Di Guida[a,d,12], M. Esposito[a,b], F. Fabozzi[a,c], F. Fienga[a,b],
A.O.M. Iorio[a,b], W.A. Khan[a], G. Lanza[a], L. Lista[a], S. Meola[a,d,12], P. Paolucci[a,12], C. Sciacca[a,b],
F. Thyssen[a]

INFN Sezione di Padova [a]**, Università di Padova** [b]**, Padova, Italy, Università di Trento** [c]**,
Trento, Italy**
P. Azzi[a,12], N. Bacchetta[a], S. Badoer[a], M. Bellato[a], L. Benato[a,b], M. Benettoni[a], D. Bisello[a,b],
A. Boletti[a,b], R. Carlin[a,b], A. Carvalho Antunes De Oliveira[a,b], P. De Castro Manzano[a],
T. Dorigo[a], F. Gasparini[a,b], U. Gasparini[a,b], S. Lacaprara[a], M. Margoni[a,b], A.T. Meneguzzo[a,b],
N. Pozzobon[a,b], P. Ronchese[a,b], R. Rossin[a,b], F. Simonetto[a,b], E. Torassa[a], M. Zanetti[a,b],
P. Zotto[a,b], G. Zumerle[a,b]

INFN Sezione di Pavia [a]**, Università di Pavia** [b]**, Pavia, Italy**
A. Braghieri[a], F. Fallavollita[a,b], A. Magnani[a,b], P. Montagna[a,b], S.P. Ratti[a,b], V. Re[a], M. Ressegotti,
C. Riccardi[a,b], P. Salvini[a], I. Vai[a,b], P. Vitulo[a,b]

INFN Sezione di Perugia [a]**, Università di Perugia** [b]**, Perugia, Italy**
L. Alunni Solestizi[a,b], G.M. Bilei[a], D. Ciangottini[a,b], L. Fanò[a,b], P. Lariccia[a,b], R. Leonardi[a,b],
G. Mantovani[a,b], V. Mariani[a,b], M. Menichelli[a], A. Saha[a], A. Santocchia[a,b], D. Spiga

INFN Sezione di Pisa [a]**, Università di Pisa** [b]**, Scuola Normale Superiore di Pisa** [c]**, Pisa, Italy**
K. Androsov[a], P. Azzurri[a,12], G. Bagliesi[a], J. Bernardini[a], T. Boccali[a], L. Borrello, R. Castaldi[a],
M.A. Ciocci[a,b], R. Dell'Orso[a], G. Fedi[a], L. Giannini[a,c], A. Giassi[a], M.T. Grippo[a,26], F. Ligabue[a,c],
T. Lomtadze[a], E. Manca[a,c], G. Mandorli[a,c], L. Martini[a,b], A. Messineo[a,b], F. Palla[a], A. Rizzi[a,b],
A. Savoy-Navarro[a,28], P. Spagnolo[a], R. Tenchini[a], G. Tonelli[a,b], A. Venturi[a], P.G. Verdini[a]

INFN Sezione di Roma [a]**, Sapienza Università di Roma** [b]**, Rome, Italy**
L. Barone[a,b], F. Cavallari[a], M. Cipriani[a,b], D. Del Re[a,b,12], M. Diemoz[a], S. Gelli[a,b], E. Longo[a,b],
F. Margaroli[a,b], B. Marzocchi[a,b], P. Meridiani[a], G. Organtini[a,b], R. Paramatti[a,b], F. Preiato[a,b],
S. Rahatlou[a,b], C. Rovelli[a], F. Santanastasio[a,b]

INFN Sezione di Torino [a]**, Università di Torino** [b]**, Torino, Italy, Università del Piemonte
Orientale** [c]**, Novara, Italy**
N. Amapane[a,b], R. Arcidiacono[a,c,12], S. Argiro[a,b], M. Arneodo[a,c], N. Bartosik[a], R. Bellan[a,b],
C. Biino[a], N. Cartiglia[a], F. Cenna[a,b], M. Costa[a,b], R. Covarelli[a,b], A. Degano[a,b], N. Demaria[a],
B. Kiani[a,b], C. Mariotti[a], S. Maselli[a], E. Migliore[a,b], V. Monaco[a,b], E. Monteil[a,b], M. Monteno[a],

M.M. Obertino[a,b], L. Pacher[a,b], N. Pastrone[a], M. Pelliccioni[a], G.L. Pinna Angioni[a,b], F. Ravera[a,b], A. Romero[a,b], M. Ruspa[a,c], R. Sacchi[a,b], K. Shchelina[a,b], V. Sola[a], A. Solano[a,b], A. Staiano[a], P. Traczyk[a,b]

INFN Sezione di Trieste [a], Università di Trieste [b], Trieste, Italy
S. Belforte[a], M. Casarsa[a], F. Cossutti[a], G. Della Ricca[a,b], A. Zanetti[a]

Kyungpook National University, Daegu, Korea
D.H. Kim, G.N. Kim, M.S. Kim, J. Lee, S. Lee, S.W. Lee, Y.D. Oh, S. Sekmen, D.C. Son, Y.C. Yang

Chonbuk National University, Jeonju, Korea
A. Lee

Chonnam National University, Institute for Universe and Elementary Particles, Kwangju, Korea
H. Kim, D.H. Moon, G. Oh

Hanyang University, Seoul, Korea
J.A. Brochero Cifuentes, J. Goh, T.J. Kim

Korea University, Seoul, Korea
S. Cho, S. Choi, Y. Go, D. Gyun, S. Ha, B. Hong, Y. Jo, Y. Kim, K. Lee, K.S. Lee, S. Lee, J. Lim, S.K. Park, Y. Roh

Seoul National University, Seoul, Korea
J. Almond, J. Kim, J.S. Kim, H. Lee, K. Lee, K. Nam, S.B. Oh, B.C. Radburn-Smith, S.h. Seo, U.K. Yang, H.D. Yoo, G.B. Yu

University of Seoul, Seoul, Korea
M. Choi, H. Kim, J.H. Kim, J.S.H. Lee, I.C. Park, G. Ryu

Sungkyunkwan University, Suwon, Korea
Y. Choi, C. Hwang, J. Lee, I. Yu

Vilnius University, Vilnius, Lithuania
V. Dudenas, A. Juodagalvis, J. Vaitkus

National Centre for Particle Physics, Universiti Malaya, Kuala Lumpur, Malaysia
I. Ahmed, Z.A. Ibrahim, M.A.B. Md Ali[29], F. Mohamad Idris[30], W.A.T. Wan Abdullah, M.N. Yusli, Z. Zolkapli

Centro de Investigacion y de Estudios Avanzados del IPN, Mexico City, Mexico
H. Castilla-Valdez, E. De La Cruz-Burelo, I. Heredia-De La Cruz[31], R. Lopez-Fernandez, J. Mejia Guisao, A. Sanchez-Hernandez

Universidad Iberoamericana, Mexico City, Mexico
S. Carrillo Moreno, C. Oropeza Barrera, F. Vazquez Valencia

Benemerita Universidad Autonoma de Puebla, Puebla, Mexico
I. Pedraza, H.A. Salazar Ibarguen, C. Uribe Estrada

Universidad Autónoma de San Luis Potosí, San Luis Potosí, Mexico
A. Morelos Pineda

University of Auckland, Auckland, New Zealand
D. Krofcheck

University of Canterbury, Christchurch, New Zealand
P.H. Butler

National Centre for Physics, Quaid-I-Azam University, Islamabad, Pakistan
A. Ahmad, M. Ahmad, Q. Hassan, H.R. Hoorani, A. Saddique, M.A. Shah, M. Shoaib, M. Waqas

National Centre for Nuclear Research, Swierk, Poland
H. Bialkowska, M. Bluj, B. Boimska, T. Frueboes, M. Górski, M. Kazana, K. Nawrocki, K. Romanowska-Rybinska, M. Szleper, P. Zalewski

Institute of Experimental Physics, Faculty of Physics, University of Warsaw, Warsaw, Poland
K. Bunkowski, A. Byszuk[32], K. Doroba, A. Kalinowski, M. Konecki, J. Krolikowski, M. Misiura, M. Olszewski, A. Pyskir, M. Walczak

Laboratório de Instrumentação e Física Experimental de Partículas, Lisboa, Portugal
P. Bargassa, C. Beirão Da Cruz E Silva, B. Calpas, A. Di Francesco, P. Faccioli, M. Gallinaro, J. Hollar, N. Leonardo, L. Lloret Iglesias, M.V. Nemallapudi, J. Seixas, O. Toldaiev, D. Vadruccio, J. Varela

Joint Institute for Nuclear Research, Dubna, Russia
S. Afanasiev, P. Bunin, M. Gavrilenko, I. Golutvin, I. Gorbunov, A. Kamenev, V. Karjavin, A. Lanev, A. Malakhov, V. Matveev[33,34], V. Palichik, V. Perelygin, S. Shmatov, S. Shulha, N. Skatchkov, V. Smirnov, N. Voytishin, A. Zarubin

Petersburg Nuclear Physics Institute, Gatchina (St. Petersburg), Russia
Y. Ivanov, V. Kim[35], E. Kuznetsova[36], P. Levchenko, V. Murzin, V. Oreshkin, I. Smirnov, V. Sulimov, L. Uvarov, S. Vavilov, A. Vorobyev

Institute for Nuclear Research, Moscow, Russia
Yu. Andreev, A. Dermenev, S. Gninenko, N. Golubev, A. Karneyeu, M. Kirsanov, N. Krasnikov, A. Pashenkov, D. Tlisov, A. Toropin

Institute for Theoretical and Experimental Physics, Moscow, Russia
V. Epshteyn, V. Gavrilov, N. Lychkovskaya, V. Popov, I. Pozdnyakov, G. Safronov, A. Spiridonov, A. Stepennov, M. Toms, E. Vlasov, A. Zhokin

Moscow Institute of Physics and Technology, Moscow, Russia
T. Aushev, A. Bylinkin[34]

National Research Nuclear University 'Moscow Engineering Physics Institute' (MEPhI), Moscow, Russia
M. Chadeeva[37], P. Parygin, D. Philippov, S. Polikarpov, E. Popova, V. Rusinov

P.N. Lebedev Physical Institute, Moscow, Russia
V. Andreev, M. Azarkin[34], I. Dremin[34], M. Kirakosyan[34], A. Terkulov

Skobeltsyn Institute of Nuclear Physics, Lomonosov Moscow State University, Moscow, Russia
A. Baskakov, A. Belyaev, E. Boos, M. Dubinin[38], L. Dudko, A. Ershov, A. Gribushin, V. Klyukhin, O. Kodolova, I. Lokhtin, I. Miagkov, S. Obraztsov, S. Petrushanko, V. Savrin, A. Snigirev

Novosibirsk State University (NSU), Novosibirsk, Russia
V. Blinov[39], Y.Skovpen[39], D. Shtol[39]

State Research Center of Russian Federation, Institute for High Energy Physics, Protvino, Russia

I. Azhgirey, I. Bayshev, S. Bitioukov, D. Elumakhov, V. Kachanov, A. Kalinin, D. Konstantinov, V. Krychkine, V. Petrov, R. Ryutin, A. Sobol, S. Troshin, N. Tyurin, A. Uzunian, A. Volkov

University of Belgrade, Faculty of Physics and Vinca Institute of Nuclear Sciences, Belgrade, Serbia

P. Adzic[40], P. Cirkovic, D. Devetak, M. Dordevic, J. Milosevic, V. Rekovic

Centro de Investigaciones Energéticas Medioambientales y Tecnológicas (CIEMAT), Madrid, Spain

J. Alcaraz Maestre, M. Barrio Luna, M. Cerrada, N. Colino, B. De La Cruz, A. Delgado Peris, A. Escalante Del Valle, C. Fernandez Bedoya, J.P. Fernández Ramos, J. Flix, M.C. Fouz, P. Garcia-Abia, O. Gonzalez Lopez, S. Goy Lopez, J.M. Hernandez, M.I. Josa, A. Pérez-Calero Yzquierdo, J. Puerta Pelayo, A. Quintario Olmeda, I. Redondo, L. Romero, M.S. Soares, A. Álvarez Fernández

Universidad Autónoma de Madrid, Madrid, Spain

J.F. de Trocóniz, M. Missiroli, D. Moran

Universidad de Oviedo, Oviedo, Spain

J. Cuevas, C. Erice, J. Fernandez Menendez, I. Gonzalez Caballero, J.R. González Fernández, E. Palencia Cortezon, S. Sanchez Cruz, I. Suárez Andrés, P. Vischia, J.M. Vizan Garcia

Instituto de Física de Cantabria (IFCA), CSIC-Universidad de Cantabria, Santander, Spain

I.J. Cabrillo, A. Calderon, B. Chazin Quero, E. Curras, M. Fernandez, J. Garcia-Ferrero, G. Gomez, A. Lopez Virto, J. Marco, C. Martinez Rivero, P. Martinez Ruiz del Arbol, F. Matorras, J. Piedra Gomez, T. Rodrigo, A. Ruiz-Jimeno, L. Scodellaro, N. Trevisani, I. Vila, R. Vilar Cortabitarte

CERN, European Organization for Nuclear Research, Geneva, Switzerland

D. Abbaneo, E. Auffray, P. Baillon, A.H. Ball, D. Barney, M. Bianco, P. Bloch, A. Bocci, C. Botta, T. Camporesi, R. Castello, M. Cepeda, G. Cerminara, E. Chapon, Y. Chen, D. d'Enterria, A. Dabrowski, V. Daponte, A. David, M. De Gruttola, A. De Roeck, E. Di Marco[41], M. Dobson, B. Dorney, T. du Pree, M. Dünser, N. Dupont, A. Elliott-Peisert, P. Everaerts, G. Franzoni, J. Fulcher, W. Funk, D. Gigi, K. Gill, F. Glege, D. Gulhan, S. Gundacker, M. Guthoff, P. Harris, J. Hegeman, V. Innocente, P. Janot, O. Karacheban[15], J. Kieseler, H. Kirschenmann, V. Knünz, A. Kornmayer[12], M.J. Kortelainen, C. Lange, P. Lecoq, C. Lourenço, M.T. Lucchini, L. Malgeri, M. Mannelli, A. Martelli, F. Meijers, J.A. Merlin, S. Mersi, E. Meschi, P. Milenovic[42], F. Moortgat, M. Mulders, H. Neugebauer, S. Orfanelli, L. Orsini, L. Pape, E. Perez, M. Peruzzi, A. Petrilli, G. Petrucciani, A. Pfeiffer, M. Pierini, A. Racz, T. Reis, G. Rolandi[43], M. Rovere, H. Sakulin, C. Schäfer, C. Schwick, M. Seidel, M. Selvaggi, A. Sharma, P. Silva, P. Sphicas[44], J. Steggemann, M. Stoye, M. Tosi, D. Treille, A. Triossi, A. Tsirou, V. Veckalns[45], G.I. Veres[17], M. Verweij, N. Wardle, W.D. Zeuner

Paul Scherrer Institut, Villigen, Switzerland

W. Bertl[†], K. Deiters, W. Erdmann, R. Horisberger, Q. Ingram, H.C. Kaestli, D. Kotlinski, U. Langenegger, T. Rohe, S.A. Wiederkehr

Institute for Particle Physics, ETH Zurich, Zurich, Switzerland

F. Bachmair, L. Bäni, P. Berger, L. Bianchini, B. Casal, G. Dissertori, M. Dittmar, M. Donegà, C. Grab, C. Heidegger, D. Hits, J. Hoss, G. Kasieczka, T. Klijnsma, W. Lustermann, B. Mangano, M. Marionneau, M.T. Meinhard, D. Meister, F. Micheli, P. Musella, F. Nessi-Tedaldi, F. Pandolfi,

J. Pata, F. Pauss, G. Perrin, L. Perrozzi, M. Quittnat, M. Rossini, M. Schönenberger, L. Shchutska, A. Starodumov[46], V.R. Tavolaro, K. Theofilatos, M.L. Vesterbacka Olsson, R. Wallny, A. Zagozdzinska[32], D.H. Zhu

Universität Zürich, Zurich, Switzerland
T.K. Aarrestad, C. Amsler[47], L. Caminada, M.F. Canelli, A. De Cosa, S. Donato, C. Galloni, A. Hinzmann, T. Hreus, B. Kilminster, J. Ngadiuba, D. Pinna, G. Rauco, P. Robmann, D. Salerno, C. Seitz, A. Zucchetta

National Central University, Chung-Li, Taiwan
V. Candelise, T.H. Doan, Sh. Jain, R. Khurana, M. Konyushikhin, C.M. Kuo, W. Lin, A. Pozdnyakov, S.S. Yu

National Taiwan University (NTU), Taipei, Taiwan
Arun Kumar, P. Chang, Y. Chao, K.F. Chen, P.H. Chen, F. Fiori, W.-S. Hou, Y. Hsiung, Y.F. Liu, R.-S. Lu, M. Miñano Moya, E. Paganis, A. Psallidas, J.f. Tsai

Chulalongkorn University, Faculty of Science, Department of Physics, Bangkok, Thailand
B. Asavapibhop, K. Kovitanggoon, G. Singh, N. Srimanobhas

ukurova University, Physics Department, Science and Art Faculty, Adana, Turkey
A. Adiguzel[48], M.N. Bakirci[49], F. Boran, S. Damarseckin, Z.S. Demiroglu, C. Dozen, E. Eskut, S. Girgis, G. Gokbulut, Y. Guler, I. Hos[50], E.E. Kangal[51], O. Kara, U. Kiminsu, M. Oglakci, G. Onengut[52], K. Ozdemir[53], S. Ozturk[49], A. Polatoz, D. Sunar Cerci[54], S. Turkcapar, I.S. Zorbakir, C. Zorbilmez

Middle East Technical University, Physics Department, Ankara, Turkey
B. Bilin, G. Karapinar[55], K. Ocalan[56], M. Yalvac, M. Zeyrek

Bogazici University, Istanbul, Turkey
E. Gülmez, M. Kaya[57], O. Kaya[58], S. Tekten, E.A. Yetkin[59]

Istanbul Technical University, Istanbul, Turkey
M.N. Agaras, S. Atay, A. Cakir, K. Cankocak

Institute for Scintillation Materials of National Academy of Science of Ukraine, Kharkov, Ukraine
B. Grynyov

National Scientific Center, Kharkov Institute of Physics and Technology, Kharkov, Ukraine
L. Levchuk, P. Sorokin

University of Bristol, Bristol, United Kingdom
R. Aggleton, F. Ball, L. Beck, J.J. Brooke, D. Burns, E. Clement, D. Cussans, H. Flacher, J. Goldstein, M. Grimes, G.P. Heath, H.F. Heath, J. Jacob, L. Kreczko, C. Lucas, D.M. Newbold[60], S. Paramesvaran, A. Poll, T. Sakuma, S. Seif El Nasr-storey, D. Smith, V.J. Smith

Rutherford Appleton Laboratory, Didcot, United Kingdom
K.W. Bell, A. Belyaev[61], C. Brew, R.M. Brown, L. Calligaris, D. Cieri, D.J.A. Cockerill, J.A. Coughlan, K. Harder, S. Harper, E. Olaiya, D. Petyt, C.H. Shepherd-Themistocleous, A. Thea, I.R. Tomalin, T. Williams

Imperial College, London, United Kingdom
M. Baber, R. Bainbridge, S. Breeze, O. Buchmuller, A. Bundock, S. Casasso, M. Citron, D. Colling, L. Corpe, P. Dauncey, G. Davies, A. De Wit, M. Della Negra, R. Di Maria, P. Dunne, A. Elwood, D. Futyan, Y. Haddad, G. Hall, G. Iles, T. James, R. Lane, C. Laner, L. Lyons,

A.-M. Magnan, S. Malik, L. Mastrolorenzo, T. Matsushita, J. Nash, A. Nikitenko[46], J. Pela, M. Pesaresi, D.M. Raymond, A. Richards, A. Rose, E. Scott, C. Seez, A. Shtipliyski, S. Summers, A. Tapper, K. Uchida, M. Vazquez Acosta[62], T. Virdee[12], D. Winterbottom, J. Wright, S.C. Zenz

Brunel University, Uxbridge, United Kingdom
J.E. Cole, P.R. Hobson, A. Khan, P. Kyberd, I.D. Reid, P. Symonds, L. Teodorescu, M. Turner

Baylor University, Waco, USA
A. Borzou, K. Call, J. Dittmann, K. Hatakeyama, H. Liu, N. Pastika

Catholic University of America, Washington DC, USA
R. Bartek, A. Dominguez

The University of Alabama, Tuscaloosa, USA
A. Buccilli, S.I. Cooper, C. Henderson, P. Rumerio, C. West

Boston University, Boston, USA
D. Arcaro, A. Avetisyan, T. Bose, D. Gastler, D. Rankin, C. Richardson, J. Rohlf, L. Sulak, D. Zou

Brown University, Providence, USA
G. Benelli, D. Cutts, A. Garabedian, J. Hakala, U. Heintz, J.M. Hogan, K.H.M. Kwok, E. Laird, G. Landsberg, Z. Mao, M. Narain, S. Piperov, S. Sagir, R. Syarif, D. Yu

University of California, Davis, Davis, USA
R. Band, C. Brainerd, D. Burns, M. Calderon De La Barca Sanchez, M. Chertok, J. Conway, R. Conway, P.T. Cox, R. Erbacher, C. Flores, G. Funk, M. Gardner, W. Ko, R. Lander, C. Mclean, M. Mulhearn, D. Pellett, J. Pilot, S. Shalhout, M. Shi, J. Smith, M. Squires, D. Stolp, K. Tos, M. Tripathi, Z. Wang

University of California, Los Angeles, USA
M. Bachtis, C. Bravo, R. Cousins, A. Dasgupta, A. Florent, J. Hauser, M. Ignatenko, N. Mccoll, D. Saltzberg, C. Schnaible, V. Valuev

University of California, Riverside, Riverside, USA
E. Bouvier, K. Burt, R. Clare, J. Ellison, J.W. Gary, S.M.A. Ghiasi Shirazi, G. Hanson, J. Heilman, P. Jandir, E. Kennedy, F. Lacroix, O.R. Long, M. Olmedo Negrete, M.I. Paneva, A. Shrinivas, W. Si, H. Wei, S. Wimpenny, B. R. Yates

University of California, San Diego, La Jolla, USA
J.G. Branson, S. Cittolin, M. Derdzinski, B. Hashemi, A. Holzner, D. Klein, G. Kole, V. Krutelyov, J. Letts, I. Macneill, M. Masciovecchio, D. Olivito, S. Padhi, M. Pieri, M. Sani, V. Sharma, S. Simon, M. Tadel, A. Vartak, S. Wasserbaech[63], J. Wood, F. Würthwein, A. Yagil, G. Zevi Della Porta

University of California, Santa Barbara - Department of Physics, Santa Barbara, USA
N. Amin, R. Bhandari, J. Bradmiller-Feld, C. Campagnari, A. Dishaw, V. Dutta, M. Franco Sevilla, C. George, F. Golf, L. Gouskos, J. Gran, R. Heller, J. Incandela, S.D. Mullin, A. Ovcharova, H. Qu, J. Richman, D. Stuart, I. Suarez, J. Yoo

California Institute of Technology, Pasadena, USA
D. Anderson, J. Bendavid, A. Bornheim, J.M. Lawhorn, H.B. Newman, T. Nguyen, C. Pena, M. Spiropulu, J.R. Vlimant, S. Xie, Z. Zhang, R.Y. Zhu

Carnegie Mellon University, Pittsburgh, USA
M.B. Andrews, T. Ferguson, T. Mudholkar, M. Paulini, J. Russ, M. Sun, H. Vogel, I. Vorobiev, M. Weinberg

University of Colorado Boulder, Boulder, USA
J.P. Cumalat, W.T. Ford, F. Jensen, A. Johnson, M. Krohn, S. Leontsinis, T. Mulholland, K. Stenson, S.R. Wagner

Cornell University, Ithaca, USA
J. Alexander, J. Chaves, J. Chu, S. Dittmer, K. Mcdermott, N. Mirman, J.R. Patterson, A. Rinkevicius, A. Ryd, L. Skinnari, L. Soffi, S.M. Tan, Z. Tao, J. Thom, J. Tucker, P. Wittich, M. Zientek

Fermi National Accelerator Laboratory, Batavia, USA
S. Abdullin, M. Albrow, G. Apollinari, A. Apresyan, A. Apyan, S. Banerjee, L.A.T. Bauerdick, A. Beretvas, J. Berryhill, P.C. Bhat, G. Bolla, K. Burkett, J.N. Butler, A. Canepa, G.B. Cerati, H.W.K. Cheung, F. Chlebana, M. Cremonesi, J. Duarte, V.D. Elvira, J. Freeman, Z. Gecse, E. Gottschalk, L. Gray, D. Green, S. Grünendahl, O. Gutsche, R.M. Harris, S. Hasegawa, J. Hirschauer, Z. Hu, B. Jayatilaka, S. Jindariani, M. Johnson, U. Joshi, B. Klima, B. Kreis, S. Lammel, D. Lincoln, R. Lipton, M. Liu, T. Liu, R. Lopes De Sá, J. Lykken, K. Maeshima, N. Magini, J.M. Marraffino, S. Maruyama, D. Mason, P. McBride, P. Merkel, S. Mrenna, S. Nahn, V. O'Dell, K. Pedro, O. Prokofyev, G. Rakness, L. Ristori, B. Schneider, E. Sexton-Kennedy, A. Soha, W.J. Spalding, L. Spiegel, S. Stoynev, J. Strait, N. Strobbe, L. Taylor, S. Tkaczyk, N.V. Tran, L. Uplegger, E.W. Vaandering, C. Vernieri, M. Verzocchi, R. Vidal, M. Wang, H.A. Weber, A. Whitbeck

University of Florida, Gainesville, USA
D. Acosta, P. Avery, P. Bortignon, A. Brinkerhoff, A. Carnes, M. Carver, D. Curry, S. Das, R.D. Field, I.K. Furic, J. Konigsberg, A. Korytov, K. Kotov, P. Ma, K. Matchev, H. Mei, G. Mitselmakher, D. Rank, D. Sperka, N. Terentyev, L. Thomas, J. Wang, S. Wang, J. Yelton

Florida International University, Miami, USA
Y.R. Joshi, S. Linn, P. Markowitz, G. Martinez, J.L. Rodriguez

Florida State University, Tallahassee, USA
A. Ackert, T. Adams, A. Askew, S. Hagopian, V. Hagopian, K.F. Johnson, T. Kolberg, T. Perry, H. Prosper, A. Santra, R. Yohay

Florida Institute of Technology, Melbourne, USA
M.M. Baarmand, V. Bhopatkar, S. Colafranceschi, M. Hohlmann, D. Noonan, T. Roy, F. Yumiceva

University of Illinois at Chicago (UIC), Chicago, USA
M.R. Adams, L. Apanasevich, D. Berry, R.R. Betts, R. Cavanaugh, X. Chen, O. Evdokimov, C.E. Gerber, D.A. Hangal, D.J. Hofman, K. Jung, J. Kamin, I.D. Sandoval Gonzalez, M.B. Tonjes, H. Trauger, N. Varelas, H. Wang, Z. Wu, J. Zhang

The University of Iowa, Iowa City, USA
B. Bilki[64], W. Clarida, K. Dilsiz[65], S. Durgut, R.P. Gandrajula, M. Haytmyradov, V. Khristenko, J.-P. Merlo, H. Mermerkaya[66], A. Mestvirishvili, A. Moeller, J. Nachtman, H. Ogul[67], Y. Onel, F. Ozok[68], A. Penzo, C. Snyder, E. Tiras, J. Wetzel, K. Yi

Johns Hopkins University, Baltimore, USA
B. Blumenfeld, A. Cocoros, N. Eminizer, D. Fehling, L. Feng, A.V. Gritsan, P. Maksimovic, J. Roskes, U. Sarica, M. Swartz, M. Xiao, C. You

The University of Kansas, Lawrence, USA
A. Al-bataineh, P. Baringer, A. Bean, S. Boren, J. Bowen, J. Castle, S. Khalil, A. Kropivnitskaya,

D. Majumder, W. Mcbrayer, M. Murray, C. Royon, S. Sanders, E. Schmitz, R. Stringer, J.D. Tapia Takaki, Q. Wang

Kansas State University, Manhattan, USA
A. Ivanov, K. Kaadze, Y. Maravin, A. Mohammadi, L.K. Saini, N. Skhirtladze, S. Toda

Lawrence Livermore National Laboratory, Livermore, USA
F. Rebassoo, D. Wright

University of Maryland, College Park, USA
C. Anelli, A. Baden, O. Baron, A. Belloni, B. Calvert, S.C. Eno, C. Ferraioli, N.J. Hadley, S. Jabeen, G.Y. Jeng, R.G. Kellogg, J. Kunkle, A.C. Mignerey, F. Ricci-Tam, Y.H. Shin, A. Skuja, S.C. Tonwar

Massachusetts Institute of Technology, Cambridge, USA
D. Abercrombie, B. Allen, V. Azzolini, R. Barbieri, A. Baty, R. Bi, S. Brandt, W. Busza, I.A. Cali, M. D'Alfonso, Z. Demiragli, G. Gomez Ceballos, M. Goncharov, D. Hsu, Y. Iiyama, G.M. Innocenti, M. Klute, D. Kovalskyi, Y.S. Lai, Y.-J. Lee, A. Levin, P.D. Luckey, B. Maier, A.C. Marini, C. Mcginn, C. Mironov, S. Narayanan, X. Niu, C. Paus, C. Roland, G. Roland, J. Salfeld-Nebgen, G.S.F. Stephans, K. Tatar, D. Velicanu, J. Wang, T.W. Wang, B. Wyslouch

University of Minnesota, Minneapolis, USA
A.C. Benvenuti, R.M. Chatterjee, A. Evans, P. Hansen, S. Kalafut, Y. Kubota, Z. Lesko, J. Mans, S. Nourbakhsh, N. Ruckstuhl, R. Rusack, J. Turkewitz

University of Mississippi, Oxford, USA
J.G. Acosta, S. Oliveros

University of Nebraska-Lincoln, Lincoln, USA
E. Avdeeva, K. Bloom, D.R. Claes, C. Fangmeier, R. Gonzalez Suarez, R. Kamalieddin, I. Kravchenko, J. Monroy, J.E. Siado, G.R. Snow, B. Stieger

State University of New York at Buffalo, Buffalo, USA
M. Alyari, J. Dolen, A. Godshalk, C. Harrington, I. Iashvili, D. Nguyen, A. Parker, S. Rappoccio, B. Roozbahani

Northeastern University, Boston, USA
G. Alverson, E. Barberis, A. Hortiangtham, A. Massironi, D.M. Morse, D. Nash, T. Orimoto, R. Teixeira De Lima, D. Trocino, R.-J. Wang, D. Wood

Northwestern University, Evanston, USA
S. Bhattacharya, O. Charaf, K.A. Hahn, N. Mucia, N. Odell, B. Pollack, M.H. Schmitt, K. Sung, M. Trovato, M. Velasco

University of Notre Dame, Notre Dame, USA
N. Dev, M. Hildreth, K. Hurtado Anampa, C. Jessop, D.J. Karmgard, N. Kellams, K. Lannon, N. Loukas, N. Marinelli, F. Meng, C. Mueller, Y. Musienko[33], M. Planer, A. Reinsvold, R. Ruchti, G. Smith, S. Taroni, M. Wayne, M. Wolf, A. Woodard

The Ohio State University, Columbus, USA
J. Alimena, L. Antonelli, B. Bylsma, L.S. Durkin, S. Flowers, B. Francis, A. Hart, C. Hill, W. Ji, B. Liu, W. Luo, D. Puigh, B.L. Winer, H.W. Wulsin

Princeton University, Princeton, USA
A. Benaglia, S. Cooperstein, O. Driga, P. Elmer, J. Hardenbrook, P. Hebda, D. Lange, J. Luo,

D. Marlow, K. Mei, I. Ojalvo, J. Olsen, C. Palmer, P. Piroué, D. Stickland, A. Svyatkovskiy, C. Tully

University of Puerto Rico, Mayaguez, USA
S. Malik, S. Norberg

Purdue University, West Lafayette, USA
A. Barker, V.E. Barnes, S. Folgueras, L. Gutay, M.K. Jha, M. Jones, A.W. Jung, A. Khatiwada, D.H. Miller, N. Neumeister, J.F. Schulte, J. Sun, F. Wang, W. Xie

Purdue University Northwest, Hammond, USA
T. Cheng, N. Parashar, J. Stupak

Rice University, Houston, USA
A. Adair, B. Akgun, Z. Chen, K.M. Ecklund, F.J.M. Geurts, M. Guilbaud, W. Li, B. Michlin, M. Northup, B.P. Padley, J. Roberts, J. Rorie, Z. Tu, J. Zabel

University of Rochester, Rochester, USA
A. Bodek, P. de Barbaro, R. Demina, Y.t. Duh, T. Ferbel, M. Galanti, A. Garcia-Bellido, J. Han, O. Hindrichs, A. Khukhunaishvili, K.H. Lo, P. Tan, M. Verzetti

The Rockefeller University, New York, USA
R. Ciesielski, K. Goulianos, C. Mesropian

Rutgers, The State University of New Jersey, Piscataway, USA
A. Agapitos, J.P. Chou, Y. Gershtein, T.A. Gómez Espinosa, E. Halkiadakis, M. Heindl, E. Hughes, S. Kaplan, R. Kunnawalkam Elayavalli, S. Kyriacou, A. Lath, R. Montalvo, K. Nash, M. Osherson, H. Saka, S. Salur, S. Schnetzer, D. Sheffield, S. Somalwar, R. Stone, S. Thomas, P. Thomassen, M. Walker

University of Tennessee, Knoxville, USA
M. Foerster, J. Heideman, G. Riley, K. Rose, S. Spanier, K. Thapa

Texas A&M University, College Station, USA
O. Bouhali[69], A. Castaneda Hernandez[69], A. Celik, M. Dalchenko, M. De Mattia, A. Delgado, S. Dildick, R. Eusebi, J. Gilmore, T. Huang, T. Kamon[70], R. Mueller, Y. Pakhotin, R. Patel, A. Perloff, L. Perniè, D. Rathjens, A. Safonov, A. Tatarinov, K.A. Ulmer

Texas Tech University, Lubbock, USA
N. Akchurin, J. Damgov, F. De Guio, P.R. Dudero, J. Faulkner, E. Gurpinar, S. Kunori, K. Lamichhane, S.W. Lee, T. Libeiro, T. Peltola, S. Undleeb, I. Volobouev, Z. Wang

Vanderbilt University, Nashville, USA
S. Greene, A. Gurrola, R. Janjam, W. Johns, C. Maguire, A. Melo, H. Ni, P. Sheldon, S. Tuo, J. Velkovska, Q. Xu

University of Virginia, Charlottesville, USA
M.W. Arenton, P. Barria, B. Cox, R. Hirosky, A. Ledovskoy, H. Li, C. Neu, T. Sinthuprasith, X. Sun, Y. Wang, E. Wolfe, F. Xia

Wayne State University, Detroit, USA
C. Clarke, R. Harr, P.E. Karchin, J. Sturdy, S. Zaleski

University of Wisconsin - Madison, Madison, WI, USA
J. Buchanan, C. Caillol, S. Dasu, L. Dodd, S. Duric, B. Gomber, M. Grothe, M. Herndon,

A. Hervé, U. Hussain, P. Klabbers, A. Lanaro, A. Levine, K. Long, R. Loveless, G.A. Pierro, G. Polese, T. Ruggles, A. Savin, N. Smith, W.H. Smith, D. Taylor, N. Woods

†: Deceased
1: Also at Vienna University of Technology, Vienna, Austria
2: Also at State Key Laboratory of Nuclear Physics and Technology, Peking University, Beijing, China
3: Also at Universidade Estadual de Campinas, Campinas, Brazil
4: Also at Universidade Federal de Pelotas, Pelotas, Brazil
5: Also at Université Libre de Bruxelles, Bruxelles, Belgium
6: Also at Joint Institute for Nuclear Research, Dubna, Russia
7: Also at Suez University, Suez, Egypt
8: Now at British University in Egypt, Cairo, Egypt
9: Now at Helwan University, Cairo, Egypt
10: Also at Université de Haute Alsace, Mulhouse, France
11: Also at Skobeltsyn Institute of Nuclear Physics, Lomonosov Moscow State University, Moscow, Russia
12: Also at CERN, European Organization for Nuclear Research, Geneva, Switzerland
13: Also at RWTH Aachen University, III. Physikalisches Institut A, Aachen, Germany
14: Also at University of Hamburg, Hamburg, Germany
15: Also at Brandenburg University of Technology, Cottbus, Germany
16: Also at Institute of Nuclear Research ATOMKI, Debrecen, Hungary
17: Also at MTA-ELTE Lendület CMS Particle and Nuclear Physics Group, Eötvös Loránd University, Budapest, Hungary
18: Also at Institute of Physics, University of Debrecen, Debrecen, Hungary
19: Also at Indian Institute of Technology Bhubaneswar, Bhubaneswar, India
20: Also at Institute of Physics, Bhubaneswar, India
21: Also at University of Visva-Bharati, Santiniketan, India
22: Also at University of Ruhuna, Matara, Sri Lanka
23: Also at Isfahan University of Technology, Isfahan, Iran
24: Also at Yazd University, Yazd, Iran
25: Also at Plasma Physics Research Center, Science and Research Branch, Islamic Azad University, Tehran, Iran
26: Also at Università degli Studi di Siena, Siena, Italy
27: Also at INFN Sezione di Milano-Bicocca; Università di Milano-Bicocca, Milano, Italy
28: Also at Purdue University, West Lafayette, USA
29: Also at International Islamic University of Malaysia, Kuala Lumpur, Malaysia
30: Also at Malaysian Nuclear Agency, MOSTI, Kajang, Malaysia
31: Also at Consejo Nacional de Ciencia y Tecnología, Mexico city, Mexico
32: Also at Warsaw University of Technology, Institute of Electronic Systems, Warsaw, Poland
33: Also at Institute for Nuclear Research, Moscow, Russia
34: Now at National Research Nuclear University 'Moscow Engineering Physics Institute' (MEPhI), Moscow, Russia
35: Also at St. Petersburg State Polytechnical University, St. Petersburg, Russia
36: Also at University of Florida, Gainesville, USA
37: Also at P.N. Lebedev Physical Institute, Moscow, Russia
38: Also at California Institute of Technology, Pasadena, USA
39: Also at Budker Institute of Nuclear Physics, Novosibirsk, Russia
40: Also at Faculty of Physics, University of Belgrade, Belgrade, Serbia
41: Also at INFN Sezione di Roma; Sapienza Università di Roma, Rome, Italy

42: Also at University of Belgrade, Faculty of Physics and Vinca Institute of Nuclear Sciences, Belgrade, Serbia
43: Also at Scuola Normale e Sezione dell'INFN, Pisa, Italy
44: Also at National and Kapodistrian University of Athens, Athens, Greece
45: Also at Riga Technical University, Riga, Latvia
46: Also at Institute for Theoretical and Experimental Physics, Moscow, Russia
47: Also at Albert Einstein Center for Fundamental Physics, Bern, Switzerland
48: Also at Istanbul University, Faculty of Science, Istanbul, Turkey
49: Also at Gaziosmanpasa University, Tokat, Turkey
50: Also at Istanbul Aydin University, Istanbul, Turkey
51: Also at Mersin University, Mersin, Turkey
52: Also at Cag University, Mersin, Turkey
53: Also at Piri Reis University, Istanbul, Turkey
54: Also at Adiyaman University, Adiyaman, Turkey
55: Also at Izmir Institute of Technology, Izmir, Turkey
56: Also at Necmettin Erbakan University, Konya, Turkey
57: Also at Marmara University, Istanbul, Turkey
58: Also at Kafkas University, Kars, Turkey
59: Also at Istanbul Bilgi University, Istanbul, Turkey
60: Also at Rutherford Appleton Laboratory, Didcot, United Kingdom
61: Also at School of Physics and Astronomy, University of Southampton, Southampton, United Kingdom
62: Also at Instituto de Astrofísica de Canarias, La Laguna, Spain
63: Also at Utah Valley University, Orem, USA
64: Also at Beykent University, Istanbul, Turkey
65: Also at Bingol University, Bingol, Turkey
66: Also at Erzincan University, Erzincan, Turkey
67: Also at Sinop University, Sinop, Turkey
68: Also at Mimar Sinan University, Istanbul, Istanbul, Turkey
69: Also at Texas A&M University at Qatar, Doha, Qatar
70: Also at Kyungpook National University, Daegu, Korea